University of Florence

International Doctorate in Structural Biology

Cycle XX (2005-2007)

Title

Structural genomic studies to unravel the function of proteins involved in copper translocation

Ph.D. thesis of

Shenlin Wang

Tutor	Coordinator
Prof. Lucia Banci	Prof. Claudio Luchinat

S.S.D. CHIM/03

This thesis has been approved by the Universityof Florence, the University of Frankfurt and the Utrecht University

Contents

1

INTRODUCTION

1.1 The role of copper in biological functions

Metal ions are essential for the biological function of many proteins. Thus, at least one-third of all proteins encoded in the human genome appear to contain metal ions or need metal ions to perform their function [1]. Metal ions are used either as a structural component or as a catalytic co-factor [2]. The metals are implicated in various biological processes such as electron transfer reactions, oxygen transport, and in a large variety of catalytic processes.

Metals are sometimes referred to as trace elements, but from the point of view of the cell, this is a misnomer. Studies of transition metal quotas of *Escherichia coli*, for instance, reveal that individual bacteria concentrate Zn and Fe by several orders of magnitude relative to the concentration in a typical growth medium until they achieve a quota of about 2×10^5 atoms per cell, which is equivalent to a total concentration of about 0.1 mM [1]. Metals such as Cu and Mn are maintained in the 10 to 100μM range. Other metals are also concentrated by the *E. coli* cell to a narrow, fixed, total concentration as follows: K and Mg, 10^8 atoms per cell, >10 mM; Ca, Zn, and Fe, 10^5 atoms per cell, ~0.1 mM; Cu, Mn, Mo, and Se, 10^4 atoms per cell, ~10 μM; V, Co, and Ni, low abundance [1].

Copper, as one of the abundant metal ions in living systems, has two oxidation states: cuprous Cu(I) and cupric Cu(II). Cu(II) is fairly soluble, whereas the solubility of Cu(I) is in the sub-micromolar range. A considerable number of enzymes in human cells use the redox property of copper for their functions. For example:

i) Ceruloplasmin (CP)

Ceruloplasmin is the primary copper carrier in serum. It is also a potent ferroxidase, capable of oxidizing Fe(II) to Fe(III) in the presence of molecule oxygen and accelerating the binding of iron by apotransferrin [3]. Oxidation of iron is important for its binding to transferrin. The latter oxidation step is critical for iron release from cells. In the case of copper deficiency, iron remains in the liver and upon addition of copper containing ceruloplasmin, iron is immediately released from liver into the blood [4,5].

ii) **Cytochrome *c* Oxidase (CcO)**

It is the terminal enzyme in respiratory chain, whose function is the conversion of O_2 to water. This enzyme anchors on the inner membrane of mitochondria. A number of metal cofactors are needed for its function. The metal binding sites includes two copper specific sites, Cu_A in Cox2 subunit and Cu_B in Cox1 subunit [6]. Cu_A is a binuclear, mixed valent center (one Cu(II) state and one Cu(I) state), located in the inner membrane space (IMS) of

mitochondria[7] . Cu_A site receives one electron from reduced cytochrome *c*, thus switching Cu(II) form to Cu(I) form. The electron is further transferred to the Cu_B center via two heme centers. Cu_B is located in the inner membrane of mitochondria, where O_2 is reduced. Since the formation of two water molecule from O_2 consumes four protons, a proton gradient is generated between IMS and the matrix. The energy stored by the proton gradient is subsequently utilized for ATP synthesis. The copper co-factors in this enzyme are critical for electron transfer and the overall catalytic reactions.

iii) Cu/Zn superoxide dismutase

Cu/Zn-SOD (SOD1) is a member of the SOD enzyme family, which. catalyzes the disproportionation reaction turning two molecules of superoxide into one molecule of O_2 and one of H_2O_2 [9]. The mechanism can be described as a cycling 'ping-pong':

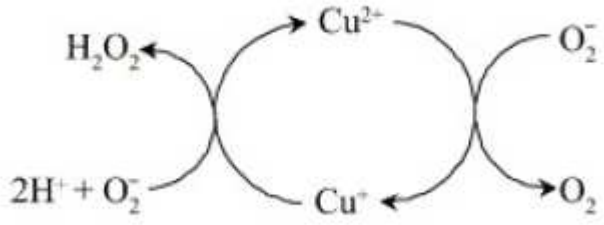

SOD1 is a homodimer that is largely localized in intracellular cytoplasmic spaces, but it is present also in the IMS [9].

iv) Metallothioneins (MT)

The primary purpose of this group of proteins is to sequester metal ions when they are present in excess [10]. Metallothioneins can bind Cu, Zn, Cd, Hg, Ag, or Ni [10]. However, Cu has the highest apparent affinity and can displace other metal ions [11]. It has been reported that metallothioneins with bound copper possess some SOD activity [11].

v) Lysyl oxidase

Lysyl oxidase plays an important role in development of connective tissues as it is required for cross-linking collagen and elastin [9,12]. In Menkes disease, connective tissue development is altered due to failure of lysyl oxidase [13, 14]. Due to reduced functionality of lysyl oxidase, patients show hyperelastic skin, hernias, and aortic aneurysms among other connective tissue related abnormalities [12, 15].

vi) Other copper associated proteins and enzymes

Copper is found in other enzymes, where it plays a role ranging from structural support to a redox active center, include tyrosinase, dopamine-β-monooxygenase, α-amidating enzyme, diamine oxidase, angiogenin, some matrix metalloproteinases such as

secreted protein acidic and rich in cysteine (SPARC), and blood clotting factors V and VIII[9,16]. Disruption of copper homeostasis can have effects on all of these enzymes and their activities as well as the development of toxic levels of the metal and reactive oxygen species.

1.2 Copper trafficking in human cell

Although copper is a kind of nutrient metal ion, it is also toxic for both eukaryotes and prokaryotes. Free copper ions contribute to produce reactive oxygen species (ROS). Furthermore, oxidative stress carried out by reactive oxygen species (ROS), could be amplified by copper reactivity, leading to the impairment of essential molecules such as lipids, proteins and DNA [17]. Thus biological systems have developed various copper homeostasis systems, ranging from copper storage to translocation, controlled by specific proteins. Free copper concentration in cell is indeed lower than 10^{-18}M [8].

Some homeostasis and translocation system for copper cargo in eukaryotic cells have been characterized. Copper is transported inside the eukaryotic cell by the protein family, called CTR. In *Saccharomyces cerevisiae,* depending on extracellular copper concentrations, copper is transported by two high-affinity copper transporters Ctr1 and Ctr3 (Km for copper ~1–5 μM), or by a low-affinity Cu/Fe-transporter Fet4 (Km for copper ~35μM)[19]. Prior its uptake, copper, which is present in the extracellular space in the Cu(II) form, is thought to be reduced to Cu(I) by one or more cell-surface Fe(III)/Cu(II) reductases encoded by the FRE1 genes [20]. The mechanism for cupric ion reduction prior to uptake remains unknown. Unlike other high affinity metal transporters (such as ATP7A and ATP7B), Ctr1 proteins do not require ATP for copper import [21].

The delivery of copper to target enzymes depends on specific and continuous complex systems (**Fig.1**). One of these copper translocation pathways was consisted of a small copper chaperone, called HAH1 or Atox1, and its partners. HAH1 transfers copper cargo to gene product of *ATP7A* (MNK protein) or *ATP7B* (WLN protein), both of which are important protein for copper homeostasis (also see section 1.4)

The second copper chaperone, CCS, is a protein required for the delivery of copper to SOD (**Fig.1**). CCS is a homodimer with 35-kDa subunits and 3 functional domains. Domain II is highly homologous to SOD, and heterodimer pairs of SOD and CCS subunits were observed, which could form to facilitate copper transfer [22]. Domain I contains the copper-binding site, but essential cysteines in domain III are involved in the transfer of copper to apo-SOD.

Copper translocation in mitochondria requires quite complex process (**Fig.1**). Several proteins are indeed involved in the correct copper binding of CcO, including Cox17, Sco1, Sco2, Cox11, Cox19 and Cox23. Cox17, which is only a 69-residue protein, acts as the copper chaperone in mitochondria. The overall fold of Cox17 is composed of two helixes and a flexible N-terminus [23]. *In vitro* studies showed that Cox17 is able to bind up to 4 copper ions by six Cys residues [24]. Cox17 is encoded by nucle DNA and leads to be imported into IMS by the TOM protein, located in the outer membrane of mitochondria. In cytosol, all six Cys resides of Cox17 are in the reduced state, since a large amount of reduced glutathione (GSH) is present. In mitochondria, four Cys residues of Cox17 are specifically oxidized by Mia40 to form two disulphide bonds. The remaining two reduced Cys residues are able to bind one copper ion. Because Cox17 is imported to mitochondria in the apo form, the mechanism by which copper was transported into mitochondria is still unknown.

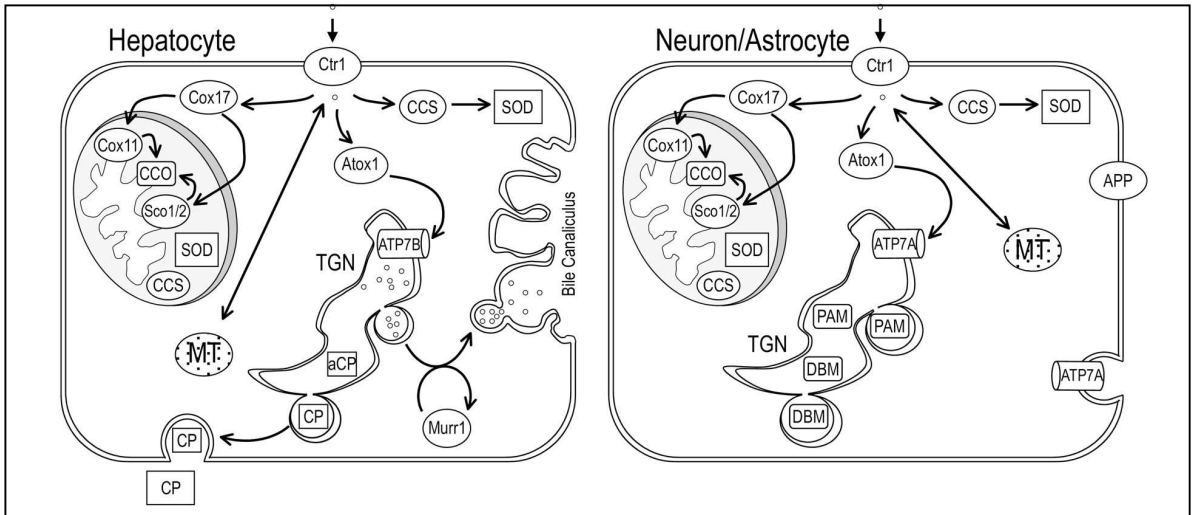

Fig 1: *Copper transport in hepatocytes, neurons, and astrocytes.* Reprinted from Prohaska, J. R. et al. J. Nutr. 2004

1.3 Copper and diseases

The alteration of copper homeostasis leads to errors of metabolism and damage to cells, resulting in pathological conditions. Such conditions are well exemplified by two inherited diseases of copper metabolism in humans, Menkes and Wilson syndromes: in both cases, the impairment by mutation of two homologous copper transport ATPases, ATP7A and ATP7B, which are selectively expressed in different tissues, leads either to the decrease or to the overload of copper in the cells.

Menkes disease (MD) is a fatal X-linked copper deficiency disorder. About one in 200,000 males are born with this devastating genetic disorder. Its symptoms include

profound mental retardation, and connective tissue (collagen) abnormalities that result in soft bones and cartilage and weakened artery walls [12,13,25]. The pathophysilogy of this disease are mutations on the ATP7A gene (MNK). The latter defect creates a systemic copper deficiency since MNK is primarily responsible for absorbing copper through diet. The copper content is particularly low in the brain of the patients with mutated ATP7A, because this protein is also expressed at the blood-brain barrier [26,27]. The current treatment of Menkes disease is administration of copper-histidine to the patient. Individuals affected by MD usually die in early childhood.

Wilson's disease (WD) is an autosomal recessive hereditary disease, with an incidence of about 1 in 30,000 in most parts of the world and a male preponderance. Symptoms usually appear around the ages of 10 to 21 years. The mutant form of ATP7B expressed in people with Wilson's disease inhibits the release of copper into bile, leading to liver failure as a result of the very high concentrations of copper accumulated in this organ. The disease is treated with lifelong use of chelating agents such as D-penicillamine or trienine hydrochloride, drugs that help remove copper from tissue. Patients will also need to take vitamin B6 and follow a low-copper diet, which means avoiding mushrooms, nuts, chocolate, dried fruit, liver, and shellfish [27].

Disorders due to respiratory chain deficiency determine also fatal diseases, leading to death at an early age as well. Isolated CcO deficiency represents one of the most commonly recognized causes of respiratory chain defects in humans associated with a wide spectrum of clinical phenotypes, primarily affecting those organs with high-energy demand such as the brain, skeletal, muscle and heart [28]. A number of mutations in genes encoding CcO assembly factors (Sco1, Sco2, Cox15, Cox10, Surf) have been described as a frequent cause of CcO deficiency and have been assigned with specific clinical symptoms.

Moreover, the imbalance of copper homeostasis have been linked to some neurodegenerative diseases as Alzheimer's disease (AD) [29], Creutzfeldt-Jakob disease, Parkinson's disease (PD)[30] and Amyotrophic Lateral Sclerosis disease (ALS)[31].

It is probable that aberrant reactivity of copper is a major source of production of ROS, which in turn is responsible for the more global oxidative stress parameters observed in these diseases. These disorders may all be classified as "conformational" in that they all show, as hallmarks, conformationally altered proteins, which precipitate, form aggregates, and may be responsible of cell damage. Direct interaction between copper and the proteins that are the pathological hallmark of these diseases has been reported, and thus, redox activity of the metal may also be involved in the process of protein misfolding. The

molecular mechanisms leading to neurodegeneration in all these diseases are still unknown. However, metal-mediated oxidative stress could induce a cascade of events, including mitochondrial dysfunction that may be responsible for cell death.

1.4 The functional and structural components of MNK and WLN

As described in section 1.2, the gene products of *ATP7A* (MNK) and *ATP7B* (WLN) are involved in one of the major intracellular copper translocating pathway. Moreover, these two proteins are also essential for copper homeostasis regulation in the body. An adult need 1mg copper per day. The dietary copper is absorbed in intestine. Protein Ctr1 imports the copper to the intestinal cells by passing the apical membrane. Copper is exported from the intestinal epithelium into the blood by MNK **(Fig.2)** in a process that involves trafficking of the transporter towards the basolateral membrane [32,33]. In other tissues, MNK and WLN are also responsible for copper homeostasis. But the expression patterns of *ATP7A* and *ATP7B* are somewhat complementary, with *ATP7A* expressed in the majority of tissues except for the liver, and *ATP7B* expressed primarily in the liver, but also in the kidney and placenta, and at lower levels in brain, heart and lungs. The excess copper is excreted into bile **(Fig.2)**. Thus, in Wilson disease patients, copper release into the bile is greatly impaired, resulting in marked accumulation of copper in the liver while the mutations in *ATP7A* induces copper deficiency on other tissues like brain.

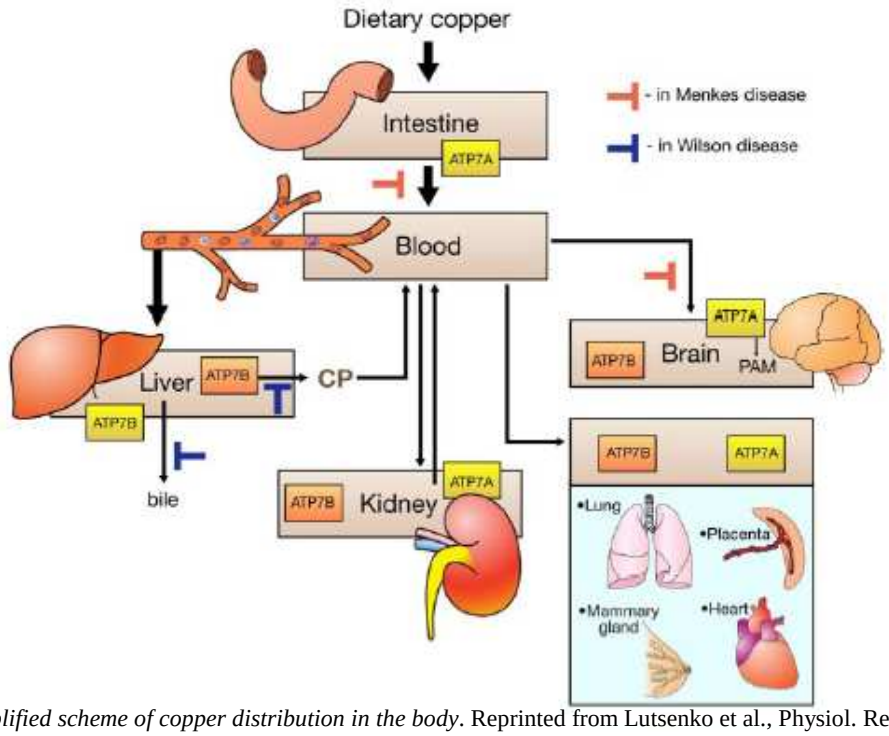

Fig. 2 *Simplified scheme of copper distribution in the body*. Reprinted from Lutsenko et al., Physiol. Rev. 2006

Inside the cells, both these two proteins reside at the trans Golgi-network, where copper is transported for incorporation into copper-dependent enzymes such as lysyl oxidase in fibroblasts (mediated by MNK) or ceruloplasmin in hepatocytes (mediated by WLN) **(Fig.1)**. When intracellular copper levels rise, the proteins are redistributed to different vesicular compartments close to the plasma membrane and excess copper are excreted. Both MNK and WLN proteins are large membrane proteins, composed by about 1500 amino acids. They are highly similar proteins, with significant primary sequence homology (50–60% identity). Recent studies have already established that both MNK and WLN are P-type ATPases, which use energy of ATP hydrolysis to transport copper ion across the membrane [34]. **Fig.3** shows the general architecture of MNK and WLN and their domains. The proteins are composed of eight trans membranes and several soluble domains, all of which extended into cytosol.

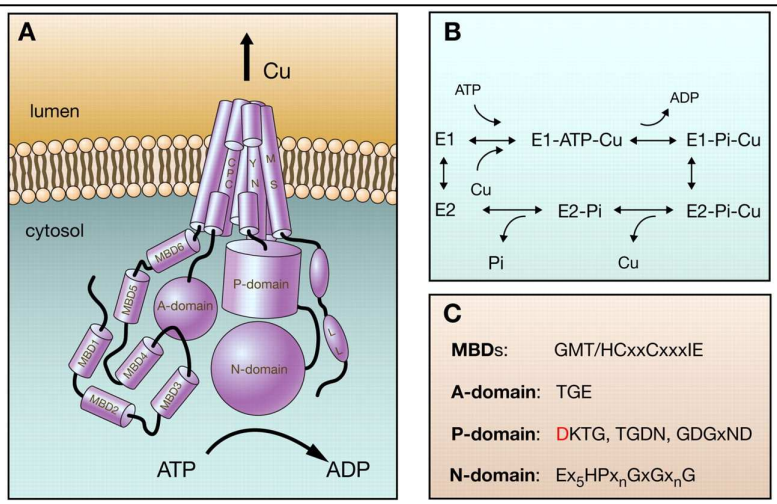

Fig. 3 *Domain organization and catalytic cycle of human Cu-ATPases.* Reprinted from Lutsenko et al., Physiol. Rev. 2006

In the N-terminal part, there are six soluble metal binding domains (MBDs), each harboring the sequence motif GMT/HCxxCxxxIE **(Fig.3C)**. Each of six MBDs can bind one reduced copper ion via two Cys residues in this motif. Structural information shows that the overall fold of individual MBDs is organized in a "ferredoxin"-like $\beta_\alpha\beta\beta_\alpha\beta$-fold. Though *in vitro* studies showed that all the six MBDs could bind one copper ion, the functional properties of each MBDs are not equal. Recent studies suggested that the MBD5 and MBD6, the closest to the membrane, are important for the copper incorporation in the TGN [35]. Indeed, it was believed that one of these two domains transfer copper ions to the CPC motif in the trans membrane helices. *In vitro* studies showed that MBD5-6 of WLN protein are unable to receive any copper ion from HAH1, but MBD4 and MBD1 are the copper downstream mediated by HAH1 [36]. This data suggest that the copper transferring chain is starting from MBD1 or MBD4 to MBD5-6, CPC motif receiving copper ion from

MBD5-6 and, finally, supplying the target enzymes in TGN. However, recent studies on MBD1-6 of Menkes protein indicate that MBD6 can be metallated by Cu(I)HAH1 directly [64]. The copper transfer still takes place after the Cys residues of domains 1 to 4 are mutated to alanine [64]. However, the function of all the MBDs is not well understood yet. It is predicted that copper binding and consequent changes in domain-domain interactions allow MNK or WLN to adopt specific conformations and/or interact with proteins necessary for the intracellular trafficking of these transporters [37].

Like the other ATPases, the activity of WNK and WLN is most likely mediated through coordinated action of the A-domain and the ATP-binding domain **(Fig.3B and 3C)**. The latter domain consists of two portions: N-domain and P-domain. The site of catalytic phosphorylation and the signature motifs for the P-type ATPase (DKTG, TGDN, GDGxND) reside in the P-domain and N-domain, respectively. A-domain contains the TGE sequenct motif, which is essential for enzymatic function of P-type ATPase. Several mutations in this region of *ATP7A* were linked to the Menkes disease phenotype. The COOH terminal tail contains 80-100 residues. In a recent study, it was shown that this domain is necessary for protein stability [38]. But the precise function of this domain is not yet understood.

1.5 Copper delivery to Cytochrome c oxidase

As mentioned in section 1.1, Cytochrome c oxidase (CcO) is the terminal enzyme in the energy transducing respiratory chain. This enzyme is located in the inner mitochondrial membrane, where it catalyses reduction of molecular oxygen to water and pumps protons across the membrane [39,40,41]. The energy stored by the proton gradient is subsequently utilized for ATP synthesis. Human CcO is composed of 13 subunits **(Fig 4)**, 10 of which are encoded by nuclear genes [42,43]. Two of the nuclear subunits (VIa and VIIa) have tissue-specific isoforms. The three mtDNA-encoded subunits (Cox1-Cox3) form the catalytic core of the enzyme. Beside the two copper sites, it also has two hemes (a and a3), one magnesium and one zinc ion [7]. It has been reported that more than 30 proteins are important for the assembly of CcO [44]. The function role of these accessory factors in the assembly of CcO can be classified to the assembly of subunits, the formation and insertion of heme A, the delivery and insertion of metal ions to the CcO in the mitochondria, and final maturation of the complex. Several proteins are important for the assembly of metal ions. Little is known about the delivery of Zn and Mg ions to the mitochondrion or whether specific accessory factors are necessary for the insertion of these ions into CcO.

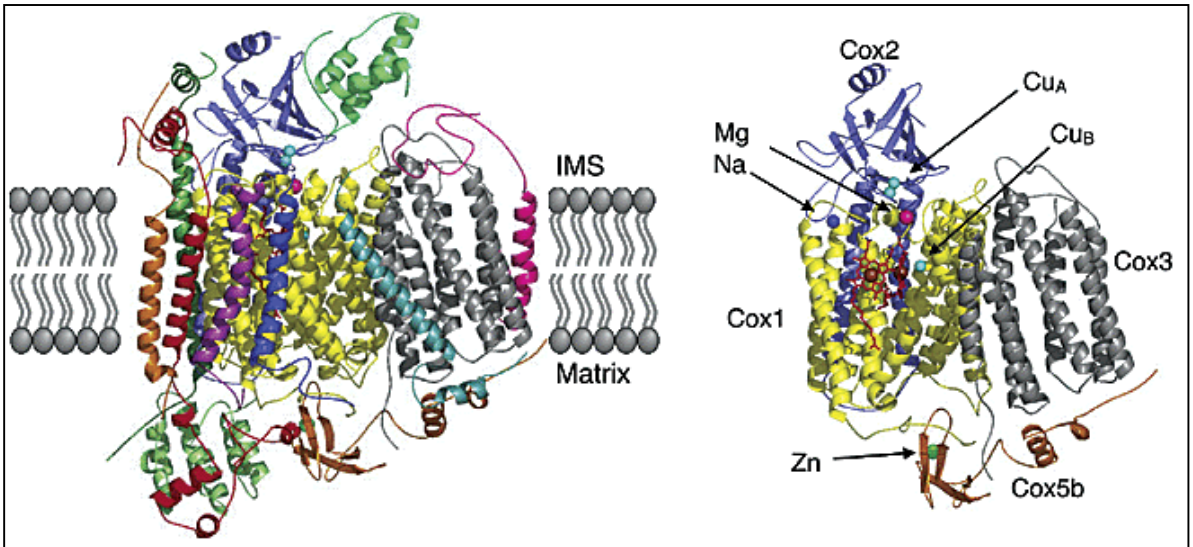

Fig.4 *The structure of bovine CcO and the metal cofactors.* Reprinted from Carr H. and Winge DR., Acc. Chem. Res.2003

In the eukaryotic cell, four proteins (Cox11, Cox17, Sco1 and Sco2) have been implicated in the copper ion loading of CcO. Cox17 has been supposed to be the key mitochondrial copper ion shuttle, whereas Cox11 and Sco1 function downstream. Yeast lacking *COX17* (*COX17*Δ yeast) are respiratory-deficient due to a complete lack of CcO activity [45]. It can be restored by the addition of 0.4% copper salts to the growth medium. This result is consistent with Cox17 functioning in copper delivery to CcO. The simple prediction was that Cox17 would shuttle Cu(I) into the IMS to be used in the assembly of CcO. This theory was strengthened by the observation that Cox17 is a copper binding protein [61]. However, Cox17 tethered to the mitochondrial inner membrane by a fusion to the transmembrane domain of the inner membrane protein Sco2 was able to reverse the respiratory defect of cox17Δ cells and restored normal CcO activity [62]. These results suggest that the function of Cox17 is confined to the mitochondrial intermembrane space[63].

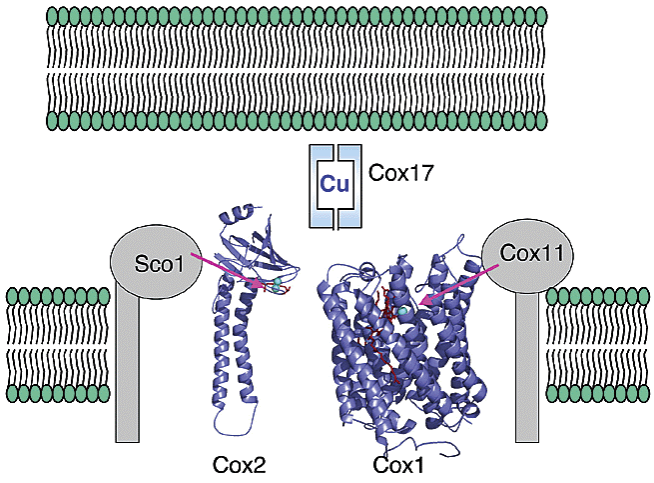

Fig.5 *Scheme of Cu metalation of Cox1 and Cox2 mediated by Cox11 and Sco1, respectively.* Reprinted from Carr H. and Winge DR., Acc. Chem. Res.2003

Sco1 was suggested to function in copper delivery to CcO **(Fig.5)** by the observation that the respiratory deficient phenotype of a *COX17-Δ* strain could be suppressed by over expression of *SCO1* or a related gene designated *SCO2* [45]. Yeast strains lacking *SCO1* also are respiratory deficient, and an excess of copper and or overexpression of either Cox17 or Sco2 cannot compensate for the Sco1-associated CcO deficiency [45]. The absolute requirement of Sco1 in the activation of CcO indicates that Sco1 functions downstream from Cox17 in the delivery of copper to CcO. Indeed, *in vitro* Sco1 can receive copper from the copper chaperone Cox17 [46]. It also appeared that Sco1 is important for formation of the Cu_A site in Cox2. Yeast Sco1 was shown to interact with Cox2 [47].

Sco1 and Sco2 are highly similar proteins. Both proteins contain a single trans membrane helix in the N-terminal segment of the proteins, anchoring of these two proteins to the inner mitochondrion while the C-terminal segment of Sco proteins is soluble and extended into IMS. A highly conserved CXXXC motif and a conserved His have been proposed to be the copper ligands. Mutation of any one of these conserved residues in Sco1 abrogates function, resulting in a nonfunctional CcO complex, which means that the function of Sco1 correlates with Cu(I) binding. Although Sco2 is highly similar to Sco1, studies with immortalized fibroblasts from Sco1 and Sco2 patients suggest that human Sco1 and human Sco2 have nonoverlapping but cooperative functions in CcO assembly [48]. Recently, it was shown that human Sco2 is also the downstream mediator of the balance between the utilization of respiratory and glycolytic pathways and has a regulatory role in the maintenance of cellular copper homeostasis [49].

Cox11 is the co-metallochaperone for the Cu_B site **(Fig.5)**. Recently, Hiser et al. demonstrated that the Cu_B site is absent in CcO purified from Rhodobacter sphaeroides lacking *COX11* gene [50]. Moreover, Tzagoloff et.al. [51] have shown that some Cox11 mutants lack CcO activity; however, RNA and protein synthesis of the core subunits I and II are normal, suggesting that Cox11 functions post-translationally to generate active CcO[51].

Yeast Cox11 is a 34kDa protein that resembles Sco1, with a single transmembrane helix of about 24 aminoacids just downstream of the N-terminal mitochondrial anchored targeting sequence. The C-terminal domain protrudes into the inner membrane space and, as with the soluble C-terminal domain of Sco1, binds a Cu(I) ion. Recently, the first structure of Cox11 family has been solved [52]. The fold of C-terminal domain of Cox11 is

organized into a novel type of Immunoglobulin-like Fold. The protein binds one copper atom per molecule.

Similar to eukaryotic cell, a number of proteins are essential for the assembly of metal cofactors of CcO of prokaryotic cell. A genome-wide search in all prokaryotic genomes combined with genomic context reveals that only Sco and Cox11 have orthologs in prokaryotes, whereas Cox17 orthologs are found only in eukaryotes[65]. As predicted from genomic contexts analysis, a protein of unknown function, called Hyp1, has been suggested to have a role of copper trafficking in prokaryotes. The latter is a soluble protein mostly occurring in the periplasm of Gram-negative bacteria, and consisting of about 150 amino acids. All Hyp1 sequences share a conserved Hx14Mx21HxM consensus motif, which could bind copper(I) ion. Recently, the first structure of Hyp1 protein from *Deinococcus radiodurans* (DR1885) showed that the fold of this class of proteins organizes in cupredoxin-like fold, which is similar to more studied protein CopC, involved in copper homeostasis[66].

Although Sco proteins are widespread proteins found in many prokaryotic organisms, it appears that the physiological function of Sco proteins goes beyond assembly of the Cu_A cofactor. Extensive analysis of completely sequenced prokaryotic genomes reveals that 18% of them contain either Sco proteins but not CuA-containing proteins or vice versa. In addition, in several cases, multiple Sco-encoding genes occur even if only a single potential Sco target is encoded in the genome[67].

1.6 CcO deficiency linked to HSco1/2 pathogenic mutations

Mutations in human *SCO1* and human *SCO2* genes cause severe, tissue-specific CcO deficiencies owing to a failure in CcO assembly: Human Sco2 (HSco2) mutations are predominately associated with early-onset hypertrophic cardiomyopathy and encephalopathy [53-55], whereas one missense mutation (P174L) in HSco1 is founds to be associated with fatal infantile hepatoencephalomyopathy [56], a progressive neonatal disorder predominantly affecting the liver. Pro174, adjacent to the conserved CXXXC motif of HSco1, is completely conserved in eukaryotes. It has been shown that the pathogenicity of the mutant does not result from its instability, but rather from an impaired function [57].

In HSco2, the E140K pathogenic mutation is adjacent to the postulated CXXXC conserved hypothetical copper binding motif. Also S225F pathogenic mutation is adjacent to the conserved His224, while the R171W mutation is close to a DXXXD conserved motif,

which is also spatially close to CXXXC motif. These observations suggest that the mutations probably impair the copper binding on HSco2 and/or the copper transfer process. On the other hand, using a policonal antibody against HSco2, severely decreased level of HSco2 in fibroblast and myoblast from patients with different Sco2 mutations were observed suggesting an unstable gene product [55]. Both HSco1 and HSco2 are ubiquitary expressed and the reason for "tissue specificity" in the disorders is unknown. Remarkably, CcO deficiency in cells from patients with HSco2 mutations [58,59] can be rescued by the addition of copper to the growth medium, but the mechanism by which this rescue occurs is unknown.

1.7 Aims and topics of the research

During the three years of PhD my research was focused on the investigation of the function of the proteins involved in the copper homeostasis and CcO assembly pathway, particularly, focusing on the proteins related to the diseases induced by copper disorder. My focus was on two systems: one was the sixth soluble copper binding domain of Menkes protein (MNK6), the other was the functional role of HSco1 and HSco2 in CcO assembly.

MNK6 is the closest domain to membrane, so it could be responsible to transfer copper to CPC motif in the trans membrane helix. One pathogenic mutation A629P in the last β-strand of MNK6 is linked to the Menkes disease and this is the only missense mutation in all the six soluble domains of MNK. Therefore, the aim of our research was to investigate the molecular reason of the pathogenic mutation, by comparing the structures and dynamic properties between wild type and its mutated protein.

The other interesting topic was the function role of HSco1 and HSco2 in CcO assembly. Copper incorporation in Cox2 is mediated by HSco1 and HSco2. However, it is still not clear yet about their specific functional role. Totally, six pathogenic mutations in this two proteins are linked to the CcO deficiency disease. All these six mutations are spatially close to the CXXXC motif based on structural model derived from the known similar fold. Thus, CcO deficiency induced by these mutations could be linked to copper binding properties. Therefore, the aim of this project is to investigate the function of HSco1/2 protein and discern the mechanism by which pathogenic mutations causes fatal diseases, by solving the solution structures of HSco1 and HSco2 and of a HSco1 related mutant (P174 HSco1) in different forms, i.e. apo and copper ion loaded, and studying their dynamics properties. Investigations of interaction of these two proteins with chaperone

Cox17, of their copper binding affinity and of their redox properties have been characterized to understand the functional aspects of these proteins.

1.8 Reference list

(1) Finney, L.A. & O'Halloran, T.V. (2003) *Science* 300, 931-936.

(2) Lander, E.S.; Linton, L.M.; Birren, B.; Nusbaum, C.; Zody, M.C. (2001) *Nature* 409 860-921.

(3) Sarkar, J.; V. Seshadri, N.A.; Tripoulas, M.E.; (2003) *J. Biol. Chem.* 278 45 44018-24

(4) Osaki, S.; Johnson, D.A. (1969) *J. Biol. Chem*. 244 20 5757-8

(5) Harris, Z.L.; Durley A.P.; Man T.K.; Gitlin J.D. (1999) *Proc Natl Acad Sci* 96 19 10812-7

(6) Ferguson-Miller, S.;. Babcock G.T. (1996) *Chem. Rev.* 96 7 2889-2908

(7) Yoshikawa S, Shinzawa-Itoh K, Nakashima R, Yaono R, Yamashita E, Inoue N, Yao M, Fei MJ, Libeu CP, Mizushima T, Yamaguchi H, Tomizaki T, Tsukihara T.; (1998) *Science*. 280(5370) 1723-9

(8) Rae, T.; Schmidt, P.J.; Pufahl, R.A.; Culotta, V.C. & O'Halloran, T.V. (1999) *Science* 284, 805-808.

(9) Zelko, I.N.; Mariani, T.J.; Folz, R.J. (2002) *Free Radic Biol Med* 33 3 337-49

(10) Cousins, R.J. (1985) *Physiol Rev* 65 2 238-309

(11) Kang, Y.J. (1999) *Proc Soc Exp Biol Med* 222 3 263-73

(12) Mercer, J.F. (1998) *Am J Clin Nutr* 67 5 Suppl 1022S-1028S

(13) Rucker, R.B.; Kosonen, T.; Clegg, M. S.; Mitchell, A. E.; Rucker, B. R.; Uriu-Hare, J.Y.; Keen C.L. (1998) *Am J Clin Nutr* 67, 5 Suppl, 996S-1002S

(14) Tang, C.; Klinman, J. (2001) P. *J. Biol. Chem*. 276 33 30575-8

(15) Kuivaniemi, H.; Peltonen, L.; Palotie, A.; Kaitila, I.; Kivirikko, K.I. (1982) *J Clin Invest* 69 3 730-3

(16) Sage, E.H.; Reed, M.; Funk, S.E.; Truong, T.; Steadele, M.; Puolakkainen, P.; Maurice, D.H.; Bassuk, J. A. (2003) *J. Biol. Chem.* 278 39 37849-57

(17) Rotillio, G.; Rossi, L.; De Martino, A.; Da Costa Ferreira,A.M.; Ciriolo, M.R. *J.Braz.Chem.Sco.* 6 221-227.

(18) Solioz, M.; Stoyanov, J.V. (2003) *FEMS* 27 183-195

(19) Hassett, R.; Dix, D.R.; Eide, D.J.;Kosman, D.J. (2000) *Biochem. J.* 15 351 Pt2:477-84.

(20) Hasset, R.; Kosman, D.J. (1995) *J. Biol. Chem.* 270 128-34.

(21) Lee, J.; Pena, M.M.; Nose, Y.; Thiele, D.J (2002) *J. Biol. Chem.* 277 4380–4387.

(22) Field, L. S.; Luk, E.; Culotta, V. C. (2002) *J. Bioenerg. Biomembr* 34 373-379

(23) Arnesano, F.; Balatri, E.; Banci, L.; Bertini, I.; D.R. Winge; (2005) *Structure.* 13 713-22

(24) Palumaa, P.; Kangur, L.; Voronova, A.; Sillard, R. (2004) *Biochem J.* 382 (Pt 1) 307-14

(25) Tang, C.; Klinman, J.P.; (2001) *J. Biol. Chem.* 276 33 30575-8;

(26) Pase, L.; Voskoboinik, I.; Greenough, M.; Camakaris (2003) *J. Biochem J* Pt; 39.

(27) Sarkar, B (1999) *Chem Rev* 99 9 2535-44

(28) Shoubridge, EA. (2001) *Am J Med Genet*. 106 46-52

(29) Waggoner, D.J.; Bartnikas, T.B.; Gitlin, J.D. (1999) *Neurobiol.Dis*. 6 221-230.

(30) Rotilio, G.; Ciriolo, M. R.; Carri, M. T.; Rossi, L. (2002) *Handbook of Copper Pharmacology and Toxicology*, Humana Press, Totowa, NJ. 277–96.

(31) Valentine, J.S.; Hart, P.J. (2003) *Proc. Natl. Acad. Sci.* USA 100, 3617–22

(32) Monty, J.F.; Llanos, R.M.; Mercer, J.F.; Kramer, D.R. (2005) *J. Nutr.* 135 2762–66,

(33) Ravia, J.J.; Stephen, R.M.; Ghishan, F.K.; Collins, J.F. (2005) *J. Biol. Chem.* 280: 36221–27

(34) Mercer, J.F.; Barnes, N.; Stevenson, J.; Strausak, D.; Llanos, R.M.; (2003) *Biometals* 16 175–184

(35) Rice, W.J.; Kovalishin, A.; Stokes, D.L. (2006) *Biochem Biophys Res Commun* 348 124–131

(36) Achila, D.; Banci, L.; Bertini, I.; Bunce, J.; Ciofi-Baffoni, S.; Huffman, D.L. (2006) *Proc Natl Acad Sci* U S A. 103 5729-34

(37) Tsivkovskii, R.; MacArthur, BC.; Lutsenko, S. (2001) .*J Biol Chem* 276 2234–42

(38) His, G.; Cullen, L.M.; Moira Glerum D; Cox, DW (2004) *Genomics* 83 473-481

(39) Wikstrom, M. (1984) *Nature* 308 558-560.

(40) Wikstrom, M. (1998) *Curr.Opin.Struct.Biol.* 8 480-488.

(41) Michel, H.; Behr, J.; Harrenga, A.; Kannt, A. (1998) *Annu.Rev.biophys.biomol.Struct.*27 329-356

(42) Capaldi, R. A. (1990) *Annu. Rev. Biochem.* 59 569–596.

(43) Poyton, R.O.; McEwen, J.E. (1996) *Annu. Rev. Biochem.* 65 563–607

(44) Tzagoloff, A.; Dieckmann, C. L; (1990) *Microbiol. Rev.* 54 211–225

(45) Glerum, D. M.; Shtanko, A.; Tzagoloff, A.; (1996) *J. Biol. Chem.* 271 20531–20535

(46) Horng, Y. C.; Cobine, P. A.; Maxfield, A. B.; Carr, H. S.; Winge, D. R.; (2004) *J. Biol. Chem.* 279, 35334–35340

(47) Lode, A.; Kuschel, M.; Paret, C.; Rodel, G. (2000) *FEBS Lett* 485, 19-24

(48) Leary, S.C.; Kaufman, B.A.; Pellecchia, G.; Guercin, G.H.; Mattman, A.; Jaksch, M.; and Shoubridge, E.A.; (2004) *Hum. Mol. Genet.* 13 1839–184

(49) Matoba, S.; Kang, J.G.; Patino, W.D.; Wragg, A.; Boehm, M.; Gavrilova, O.; Hurley, P.J.; Bunz, F.; Hwang, P.M. (2006). *Science* 312 1650–1653.

(50) Hiser, L.; Di Valentin, M.; Hamer, A.G.; Hosler, J.P. (2000) *J.Biol.Chem.* 275 619-623

(51) Tzagoloff, A.; Capitanio, N.; Nobrega, M.P.; Gatti, D. (1990) *EMBO J.* 9 2759-2764

(52) Banci, L.; Bertini, I.; Cantini, F.; Ciofi-Baffoni, S.; Gonnelli, L.; Mangani, S.; *J.Biol.Chem.*(2004) 279, 34833-9

(53) Papadopoulou, L.C.; Sue, C.M.; Davidson, M.M.; Tanji, K.; Nishino, I.; Sadlock, J.E.; Krishna, S.; Walker, W.; Selby, J.; Glerum, D. M.; Van Coster, R.; Lyon, G.; Scalais, E.; Lebel, R.; Kaplan, P.; Shanske, S.; De Vivo, D.C.; Bonilla, E.; Hirano, M.; DiMauro, S.; Schon, E.A (1999) *Nat. Genet.* 23, 333-337.

(54) Jaksch, M.; Ogilvie, I.; Yao, J.B.; Kortenhaus, G.; Bresser, H.G.; Gerbitz, K.D.; Shoubridge, E.A. (2000) *Hum. Mol. Genet.* 9, 795-801.

(55) Jaksch, M.; Paret, C.; Stucka, R.; Horn, N.; Muller-Hocker, J.; Horvath, R.; Trepesch, N.; Stecker, G.; Freisinger, P.; Thirion, C.; Muller, J.; Lunkwitz, R.; Rödel, G.; Shoubridge, E. A.; Lochmuller, H. (2001) *Hum. Mol. Genet.* 10, 3025-3035

(56) Valnot, I.; Osmond, S.; Gigarel, N.; Mehaye, B.; Amiel, J.; Cormier-Daire, V.; Munnich, A.; Bonnefont, J.P.; Rustin, P.; and Rötig, A. (2000) *Am. J. Hum. Genet.* 67, 1104-1109

(57) Williams, J. C., Sue, C., Banting, G. S., Yang, H., Glerum, D. M., Hendrickson, W. A.; Schon E. A. (2005) *J. Biol. Chem.* 280, 15202-15211

(58) Nittis, T.; George, G.N.; Winge, D.R. (2001) *J.Biol.Chem.* 276, 42520-42526

(59) Lode, A.; Kuschel, M.; Paret, C.; Rodel, G. (2000) *FEBS Lett* 485, 19-24

(60) Horng, O.C.; Cobine, P.A.; Maxfield, A.B.; Carr H.S.; Winge, D.R. (2004) *J. Biol. Chem.* 279, 35334–35340

(61) Heaton, D.N.; George, G.N.; Garrison, G.; Winge, D.R. (2001) *Biochem* 40, 743–751.

(62) Maxfield, A.B.. Heaton, D.N.; Winge, D.R. (2004) *J. Biol. Chem.* 279, 5072–5080.

(63) Horng, O.C.; Cobine, P.A.; Maxfield, A.B.; Carr H.S.; Winge, D.R. (2004) *J. Biol. Chem.* 279, 35334–35340.

(64) Banci, L.; Bertini, I.; Cantini, F.; Della-Malva, N.; Migliardi, M.; Rosato A.; (2007) *J. Biol. Chem.* 282,23140-6.

(65) Arnesano, F.; Banci, L.; Bertini, I.; Martinelli, M.; (2005) *J. Proteome Res.*, 4 , 63 –70.

(66) Banci, L.; Bertini, I.; Ciofi-Baffoni, S.; Katsari, E.; Katsaros, N.; Kubicek, K.; Mangani, S.; (2005) *Proc Natl Acad Sci* U S A. 102 3994-9

(67) Banci, L.; Bertini, I.; Cavallaro, G.; Rosato, A.; (2005) *J. Proteome Res.*, 6 , 1568-79

2

METHODOLOGICAL ASPECT

Obviously, NMR spectroscopy has already been one of the most important tools for protein structure determination. Up to now, about 15% structures, deposited in protein structure database, are solved by NMR spectroscopy. Considering that body fluids such as blood, stomach liquid and saliva are protein solutions where these molecules perform their physiological functions, NMR has obvious advantage to closely mimic a given physiological fluid.

Furthermore, in addition to protein structure determination, NMR applications include investigations of dynamic features of the molecular structures (see section 2.2), as well as studies of structural, thermodynamic and kinetic aspects of interactions between proteins and other solution components [1-4]. Here, this work will focus on the discussion of structure determination, dynamic properties studies and the characterization of protein-metal interaction by NMR spectroscopy.

2.1 Structure determination by NMR spectroscopy

The standard protocol for NMR structure determination includes the preparation of a homogeneous protein solution, the recording and handling of the NMR datasets, the structural interpretation of the NMR data. Typically, uniformly ^{13}C and ^{15}N labelled proteins are used for structure determination. Triple labelled sample, ^{2}D, ^{13}C and ^{15}N, is necessary for protein with larger size (more than 30kDa). The protocol of resonance assignments of double (^{15}N and ^{13}C) labelled proteins using 3D experiments is based on a number of experiments where show cross peaks among these relative nuclei of the backbone or the side chain [5].

2.1.1 Sample preparation

The first critical parameter for obtaining good quality NMR spectra is the amount of sample available. Typically, a molar concentration of 0.5mM is close to a minimal requirement for structural characterizations. Several techniques for protein expression and purification have improved dramatically in the past decade. Currently, the *E. coli* expression system is the most widely used for NMR purpose, which requires the production of high yield of labeled ^{15}N and ^{13}C samples. Considerable efforts are also underway to make alternative hosts more accessible and affordable, and eukaryotic systems including mammalian, yeast and insect cell expression are becoming easier and less

expensive to be used. In this work, all the proteins were expressed in *E.coli* system, by using competent E.coli BL21-Gold (DE3) cells. The ^{15}N-labeled and ^{15}N ^{13}C-labeled proteins were obtained by growing cells in minimal medium (M9) containing 3g/l ^{13}C-Glucose and 1g/l ^{15}N-$(NH_4)_2SO_4$ whereas LB medium was used for the non-labelled protein.

Copper proteins, in many cases, bind copper ion by Cys residues. In this work, Sco family proteins bind copper ions via CXXXC motif and one highly conserved His residue. The sixth soluble domain of Menkes protein (MNK6) binds copper ions via CXXC motif. When these samples were exposed into air, SH groups of Cys residues are easily to be oxidized by O_2, forming disulphide bonds. Moreover, the re-oxidation of the Cys residues could also induce unspecific intra-molecular disulfide bonds formation, which could induce protein aggregation and precipitation. Therefore, it is necessary to perform disulphide reduction on the sample prior to NMR measurement on the apo form and as well to the metallation of the sample. The reducing agent applied in this work is dithiothreitol (DTT). Glutathione and ascrobic acid are also widely used reducing agents. Protein reduction and metallation were carried out under nitrogen atomophere in an anaerobic chamber to prevent re-oxidation of the Cys residues. The excess DTT were removed by using PD-10 desalting column. All the NMR samples were prepared in Pi 50mM pH=7.2 buffer.

In order to obtain Cu(I) and Ni(II) metallated protein, progressive titration, monitored by UV-vis or ^{1}H-^{15}N HSQC experiments were performed, using the metals respectively in the $[Cu(I)(CH_3CN)_4]PF_6$ and $NiCl_2$ forms. The titration was performed using a maximum protein concentration of 0.2mM, in order to avoid the unspecific binding of metal ions on the protein surface. Excess metal ions were removed by dialysis overnight prior to the sample concentration.

2.1.2 Resonance assignments

After acquiring spectra on a protein sample, the peaks of the spectra have to be identified. Off diagonal peaks, called cross peaks, correspond to an interaction between two or more nuclei. The interaction is mainly of two different types: through space interactions and interactions through chemical bonds. **Table 1** listed the pulse sequences used for the backbone assignments and side chain assignments in this thesis.

Backbone assignment experiments	Side chain assignment experiments
HNCA	HBHA(CBCACONH)
HN(CO)CA	hCCH-TOCSY
CBCA(CO)NH	^{2}J ^{1}H-^{15}N HSQC
HNCACB	
HNCO	
HNHA	

Table 1. NMR experiments performed for backbone and side chain assignments.

The assignment usually starts with the identification of the HN-N pairs in the backbone of the amino acid residue sequence of the protein. After identification of the HN-N pairs, spectra from different sequential experiments are used to sequentially connect one with the other. After amino acid residues have been connected into chains, the chains are placed into amino acid sequence. Placing on the chain on the amino acid sequence is usually base on the chemical shifts of Cα and Cβ, which are dependent on amino acid type. Side chain nuclei are usually identified using TOCSY type experiments, correlating the side chain nuclei to the already known backbone nuclei in the same residues. In principle, all the nuclei should be assigned, but line-broadening effect induced by chemical exchange phenomenon could make the resonance too weak to be identified, such as N-terminal residues and residues located in flexible loops.

In the case of proteins with a molecular weight larger than 30 kDa, the use of TROSY-type experiments is necessary. TROSY experiments can reduce the signal loss [6], which is the direct consequence of the slower correlation tumbling of large molecules that results in faster relaxation and consequently broader lines in the NMR spectrum.

TROSY uses constructive interference between different relaxation mechanisms and works best at the highest available magnetic field strengths in the range of 700 to 900 MHz proton resonance frequencies. With TROSY the molecular size of proteins accessible for detailed NMR investigations has been extended several fold. The TROSY technique benefits a variety of triple resonance NMR experiments as the 3D HNCA and HNCOCA [7] and the TROSY-based NOESY experiments [8] for the collection of structural constraints are also available. CRINEPT-TROSY is another recently developed technique for even larger proteins. By combining INEPT with cross-correlated relaxation-induced polarization transfer, CRINEPT-TROSY can yield a further significant gain in sensitivity for molecular sizes above 200kDa[9,10]. The best magnetic field strengths for CRINEPT-TROSY are in

the range 900-1000MHz proton resonance frequencies.

2.1.3 Conformational constrains

Protein structure determination using NMR is mostly based on local distance and angle constrains, which could be derived from experimental data. Distance constrains are acquired from NOE spectroscopy (NOESY). Angle information is mainly obtained from chemical shifts and spin-spin interaction through bonds.

2.1.3.a Distance constrains

The NOE reflects the transfer of magnetization between spins coupled by the dipole-dipole interaction. The intensity of a cross peak in NOESY spectrum is mainly proportional to the distance between nuclei to the two power of minus six. The intensity is also dependent on the global and internal motions of the molecule. It is generally assumed that there exists a single rigid conformation that is compatible with all NOE data simultaneously, provided that the NOE data are interpreted in a conservative semi-quantitative manner.

Because the intensity of the cross peaks are also affected by motions of the molecule, NOE data are usually treated as upper bounds (UPL) on inter atomic distances instead of precise distance restraints. For the same reason, the absence of an NOE is in general not interpreted as a lower bound on the distance between the two interacting spins.

2.1.3.b Angle restrains

The structure quality will be much improved, if performed with additional torsion angle restraints beside distance restraints. Two techniques are widely used to obtain backbone angle constraints: **Chemical Shift Index (CSI)** [11] and **^{3}J coupling constants** [12].

CSI method relies on the fact that the chemical shifts of the different nuclei in the protein backbone are related both to the type of amino acid and to the nature of the secondary structure they are located in. By comparing the actual chemical shift for a nucleus in a specific amino acid with a reference value, it is possible to predict in what secondary structure element the nucleus resides. Several programs are available for the prediction of the secondary structure elements, such as TALOS [13] and PREDICTOR [14], by using a complete set of backbone chemical shifts for all H^{α}, C^{α}, C^{β} and CO resonances. In the latter program, the χ_1 angle could be also predicted.

Vicinal scalar coupling constants, $^3\boldsymbol{J}$, can also be used for torsion angle prediction,

according to Karplus equations [15]. ^3J H^NH^α coupling constants are obtained from the ratio between the intensity of the diagonal peak and that of the cross peak of the H^NH^α map. The Karplus equations are periodic, and thus more than one angle could be possible for a certain scalar coupling. The angular information is therefore included in the structure calculation as favored and less favored region instead of specific angles.

2.1.4 Structure calculation

After convert the experimental data to NMR conformation restraints, structures calculations are usually done with either one of three methods, simulated annealing [16,17], distance geometry [18] or torsion angle dynamic [19]. A number of programs are also available for automatically assignment and structure calculation either staring from chemical shifts and integrated peaks, such as AUTOSTRUCTURE [20], and CANDID [21], or starting from chemical shifts and NOESY spectra, such as ATNOS-CANDID [22]. The efficiency of structure determination was largely improved by the latter kind of programs, since the most time consuming work could be performed by program automatically. In this thesis, all the calculation works have been done by DYANA-1.5 or ATNOS-CANDID coupled with CYANA-2.0 by using torsion angle dynamics algorithm. In this algorithm, the molecular dynamics simulation uses torsion angles as degree of freedom, while bond lengths, angles, and backbone peptide plane angles are fixed. During the integration time steps, the favored conformation was searched by minimizing the deviation between constrains and obtained conformations. Compared with other algorithms, torsion angle dynamics provides at present the most efficient way to calculate NMR structures.

2.1.5 Structure refinement

At the end of the structure calculation, an important question is whether the structure calculation was “successful”. There are two important features, i) whether the calculated structures fulfill the given restraints, ii) whether the calculations are converged. The first feature could be described by statistical report of the target function. In each calculation, 20 or 30 conformers, among 200 or 350 conformers, with lowest final target functions were chosen to represent the solution structures. The average values of target function of the represent structures should be smaller than $1Å^2$ and each single violation should be smaller than $0.3Å^2$. The second feature was judged by RMSD (root mean square deviation) between these models. Only the family structure with backbone RMSD values close or less than 1 Å will be considered as “good”.

The "good" structures obtained from torsion angle dynamics finally should be refined in AMBER program [23]. In the final refinement, force field parameters are also considered. The refinement in explicit water box after the refinement *in vacuum* makes the structure qualities further improved.

2.1.6 Structure validation

The solved structures could be flawed or present a wrong fold, even though RMSD and target function values are accepted. The defect could be induced by only a few wrong assigned NOEs or other local constraints. Thus the validation protocol is critical to understand the quality of the structures. The validation of protein structures contains two aspects: 1) validation of coordinate data and 2) validation of experimental data.

2.1.6.a Validation of coordinate data

The validation of coordinate data measures the match between many aspects of the geometry and the expected range of permissible values for each geometric parameter. In this thesis, all the validation works of coordinate data were performed by using programs PROCHECK [24], PROCHECK_NMR [25] and WHAT IF [26]. In WHAT IF package, output files contains two classes of Z-scores: structure Z-scores and RMS Z-scores **(Table2** as an example**)**. RMS Z-scores check many stereochemical properties of proteins, including bond lengths, bond angles, tetrahedral geometry and planar group. Since these properties, are implemented in structure refinement programs as constraints, these scores are always good in practice. The only parameter that should be checked carefully for each residue is the chirality of individual group, which is not implemented in the refinement programs.

Structure Z-scores, positive is better than average:	
1st generation packing quality	: -2.774
2nd generation packing quality	: -2.213
Ramachandran plot appearance	: -2.996
chi-1/chi-2 rotamer normality	: -2.651
Backbone conformation	: -2.375
RMS Z-scores, should be close to 1.0:	
Bond lengths	: 0.668
Bond angles	: 1.215
Omega angle restraints	: 1.595 (loose)
Side chain planarity	: 1.308
Improper dihedral distribution	: 0.970
Inside/Outside distribution	: 1.052

Table2: Output of WHAT IF on Cu(I)HSco2 structure after refinement in water box.
Typically, Z-scores below –3 were considered poor,
those below –4 were considered bad

Structure Z-scores from WHAT IF package check dihedral-angle preference and

packing of structures. These scores are important to check the quality of the structures. Typically, Z-scores below –3 were considered poor, those below –4 were considered bad. Among these values, Ramachandran plot appearance checks backbone dihedral angels, ϕ and φ, whose combinations should represent in the theoretically allowed angle ranges. Similarly, PROCHECK_NMR also constructs dihedral angles mapping in defined four areas based on a great number of observations from high-quality of structures: most favoured, additionally allowed, generously allowed, and disallowed. For a good structure, the total percentage of residues occurring in the most favoured and additionally allowed should be more than 90%. In addition to backbone dihedral angles, χ_1/χ_2 rotamor normality scores are indicators for quality of side chain conformations. And scores of packing qualities could evaluate the packing qualities of atoms, thus, possibly, finding bad contacts.

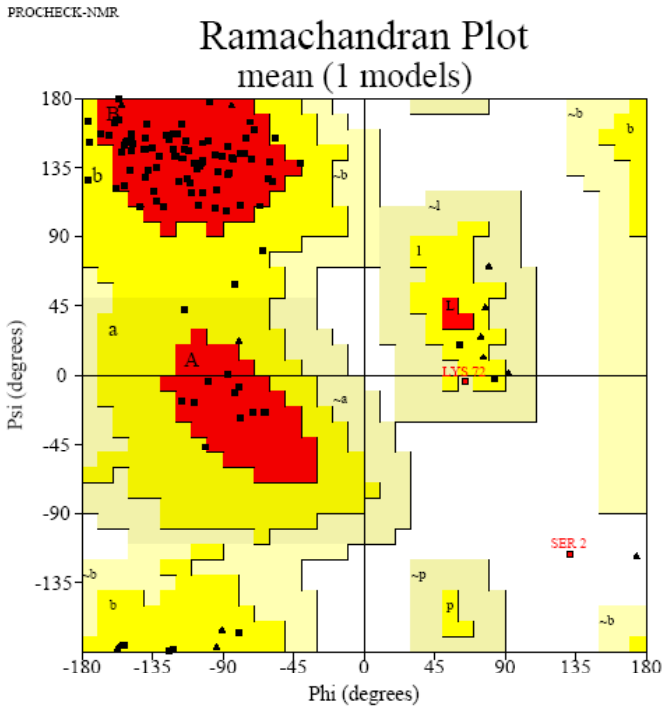

Fig 6. Ramachandran plot of the minimized mean structure of Cu(I)TTHA1943
81.7% residues occurs in the most favored region
16.1% in additional allowed region
1.1% in generally allowed region
1.1% in disallowed region.

Since the determination of solution structures are mainly based on distance restrains which are derived from NOESY spectrum, sometimes, it is unlikely to get well-defined local conformations when chemical exchange phenomenon is present, resulting in severely line broadening. Those residues, whose backbone assignments were missing or the number of NOEs was much less than other residues, were excluded in the statistics data.

2.1.6.b Validation of experimental data

The validation of experimental data consists two parts: NOE violations and NOE completeness. As discussed in section 2.1.5, single violation should be smaller than 0.3 $Å^2$. Large NOE violation could indicate a wrong assignment and the assignment to

corresponding cross peaks should be checked. In some cases, average values of target function of family structures are very small. In that situation, the scaling constant used for calibration of NOESY spectrum should be checked again. That value could be overestimated so that the NOE restrains are too loose to define a tight structure.

The completeness of the NOEs is another important parameter to understand whether experimental data is enough to define a high quality structure. In this thesis, all the NOE completeness work has been done via online AQUA program [27] (http://www.nmr.chem.uu.nl/users/jurgen/Aqua/server/). The input files of AQUA program consist of a NOE constrain file and a structure file. Theoretical NOE constrains will be predicted from the structures combined with user defined maximal observable distance, which is usually set to 4.0 or 5.0 Å. The average completeness for maximum distances of 4.0 and 5.0 Å for NMR protein structures was 48 +/- 13 and 26 +/- 9 %, respectively.

2.2 Dynamic properties characterization by NMR on different time scales

Function in biological systems is exquisitely dependent on spatial and temporal changes in proteins. Innumerable biological processes ultimately rely on transduction of information through conformational changes in proteins associated with folding and assembly, ligand binding and molecular recognition, and catalysis. A central problem in understanding biological processes at a molecular level is the elucidation of how the active conformation of proteins is achieved on time scales necessary for function. NMR spectroscopy has a unique capacity to investigate dynamic properties of molecules over a range of different time scales.

Interpretation of relaxation parameters of $\boldsymbol{R_1}$, $\boldsymbol{R_2}$ and **NOE** data of ^{15}N nuclei in protein is the most widely used technique to characterize the dynamic properties of protein, because local motions on both ps-ns and μs-ms time scale can be studied. Other techniques, such as Hydrogen/Deuterium exchange rate (H/D exchange rate) [28], scalar coupling constants [29], and residual dipole coupling constants [30], are also well established for the investigation of exchange phenomenon. In this thesis, interpretation of relaxation parameters and H/D exchange rate are used to investigate the dynamic properties of protein.

2.2.1 the nature of ^{15}N relaxation parameters

Relaxation rate constants for nuclei in proteins depend upon a large number of factors, including: overall rotational correlation times, internal motions, the geometrical

arrangement of nuclei, and the relative strengths of the applicable relaxation mechanisms. For spin 1/2 nuclei (^{1}H, ^{13}C and ^{15}N) in protein molecules, the dominant relaxation mechanisms are the magnetic dipolar and anisotropic chemical shift (CSA) mechanisms [31]. Other relaxation mechanisms, such as quadrupolar, scalar coupling interactions and so on [31], are of minor importance. If the overall correlation time and the three-dimensional structural coordinates of the protein are known, relaxation rate constants can be calculated in a relatively straightforward manner using *redfield* relaxation matrix approach. This approach introduces the spectral density function, ***J(ω)***, which represents the relative intensities at which a given frequency is contained within the full spectrum of random magnetic background oscillations. The ^{15}N relaxation parameters of a ^{15}N spin of an HN amide bond in protein can be obtained by following equations [32]:

$$R_1 = \frac{d^2}{4}[J(\omega_H - \omega_N) + 3J(\omega_N) + 6J(\omega_H + \omega_N)] + c^2 J(\omega_N) \qquad \textbf{(1)}$$

$$R_2 = \frac{d^2}{8}[4J(0) + J(\omega_H - \omega_N) + 3J(\omega_N) + 6J(\omega_H) + 6J(\omega_H + \omega_N)] + \frac{c^2}{6}[4J(0) + 3J(\omega_N)] \qquad \textbf{(2)}$$

$$\mathrm{NOE} = 1 + \frac{d^2}{4} \times \frac{\gamma_N}{\gamma_H}[6J(\omega_H + \omega_N) - J(\omega_H - \omega_N)] \times T_1 \qquad \textbf{(3)}$$

Where

$$d = \frac{\mu_0 h \gamma_N \gamma_H}{8\pi^2} < r_{HN}^{-3} > \qquad \textbf{(4)}$$

$$c = \frac{\Delta\sigma\omega_N}{\sqrt{3}} \qquad \textbf{(5)}$$

$$J(\omega) = \frac{2}{5}\left[\frac{\tau_c}{1 + \omega^2 \tau_c^{\,2}}\right] \qquad \textbf{(6)}$$

In eqs. (4) and (5), $\boldsymbol{\mu_0}$ = 4π × 10^{-7} kg m s^{-2} A^{-2}, $\boldsymbol{h}$ = 6.6262 × 10^{-34} erg • s, where h is Planck's constant; $\boldsymbol{\gamma_H}$ and $\boldsymbol{\gamma_N}$ are the gyromagnetic ratios of ^{1}H and ^{15}N respectively (2.6753 × 10^8 rad • s^{-1} • T^{-1} and -2.71 × 10^7 rad • s^{-1} • T^{-1}); $\boldsymbol{\omega_H}$ and $\boldsymbol{\omega_N}$ are the Larmor frequencies; $\boldsymbol{\Delta\sigma}$ is the anisotropy of the chemical shift tensor of the ^{15}N spin (160ppm or 170ppm); $\boldsymbol{r}_{HN}$ is the length of the HN bond (1.02 × 10^{-8} cm); $\boldsymbol{\tau_c}$ is the correlation time for molecular tumbling. In general, $\boldsymbol{\tau_c}$ is proportional to the molecular weight.

2.2.2 determination of overall correlation time

The first step in data interpretation is the determination of $\boldsymbol{\tau_c}$. In general, the apparent

$\tau_{c,app}$ for a given spin could be calculated from the ratio of R_2/R_1. In the case of isotropic tumbling, R_2/R_1 values are, approximately, proportional to $\omega_N^2\tau_c^2$. Ideally, the molecular correlation time τ_c could be obtained from averaging over relaxation data from all the resolved residues. However, the $\tau_{c,app}$ value for a single spin could be much higher or smaller than the overall correlation time by two factors: i) the presence of fast local motions (ps-ns) will make $\tau_{c,app}$ smaller than overall correlation time; ii) the line broadening contribution to R_2 (R_{ex} in μs-ms time scale) will make τ_c overestimated. Therefore residues whose internal mobility is not negligible are excluded to the measurement of τ_c, by two criteria:

i) the ^{15}N relaxation data of all the residues with a ^{15}N-NOE significantly below the maximum (usually with values < 0.65) should be removed from the calculation lists;

ii) residues with values of [(<R_2>- R_2) / < R_2> - (<R_1>- R_1) / < R_1>] > 1.5 times the std. should be removed from the calculation lists

In the case of anisotropic tumbling, R_2/R_1 ratio is also affected by the shape of globular proteins. A 3×3 diffusion tensor D could be fitted together with 3D-coordination structures, instead of a single τ_c value. In this thesis, the anisotropic diffusion tensors of proteins are calculated by using TENSOR2 program [33].

2.2.3 internal motions determined by reduced spectra density mapping

Relaxation rate constants are linear combinations of $J(\omega)$ sampled at the given frequencies of the spin system. Consequently, discrete values of $J(\omega)$ can be obtained by inverting the systems of Eqs. (1-3). However, three measurable relaxation parameters are insufficient to determine uniquely the values of the spectral density function at the five frequencies (0, ω_H-ω_N, ω_H +ω_N, ω_H, ω_N). In practice, the linear combinations of $J(\omega_H-\omega_N)$, $J(\omega_H)$ and $J(\omega_H+\omega_N)$ first order by a single term of the form $\alpha J(\beta\omega_H)$, in which α and β are constants [34-36]. This approach is called reduced spectral density mapping. In such manner, Eqs.(1-3) could be derived to:

$$R_1 = \frac{d^2}{4}[3J(\omega_N) + 7J(\beta_1\omega_H)] + c^2 J(\omega_N) \qquad \textbf{(7)}$$

$$R_2 = \frac{d^2}{8}[4J(0) + 3J(\omega_N) + 13J(\beta_2\omega_H)] + \frac{c^2}{6}[4J(0) + 3J(\omega_N)] \qquad \textbf{(8)}$$

$$\mathrm{NOE} = 1 + \frac{5d^2\gamma_N J(\beta_3\omega_H)T_1}{4\gamma_H} \qquad \textbf{(9)}$$

There are several ways for further approximation on the constant β_1, β_2 and β_3 in

order to obtain the spectra density function. The works in this thesis applied the approach by neglecting ω_N terms ($\beta_1=\beta_2=\beta_3=1$). Consequently, the reduced spectral density function values at the frequencies of interest are given by

$$J(\omega_H) = \frac{4(\mathrm{NOE}-1)R_1\gamma_H}{5d^2\gamma_N} \qquad \textbf{(10)}$$

$$J(\omega_N) = \frac{R_1 - 7J(\omega_H)}{\frac{3}{4}d^2 + c^2} \qquad \textbf{(11)}$$

$$J(0)_{eff} = \frac{R_2 - (\frac{3}{8}d^2 + \frac{1}{2}c^2)J(\omega_N) - \frac{13}{8}d^2J(\omega_H)}{\frac{1}{2}d^2 + \frac{2}{3}c^2} \qquad \textbf{(12)}$$

$\boldsymbol{J(0)}$ values obtained could be overestimated, if contributions to $\boldsymbol{R}_2$ from chemical exchange process, which arises from μs-ms time scale, are present. Thus, from sequential plot of the $\boldsymbol{J(0)_{eff}}$, spins with conformational exchange could be identified by the much higher values than average. Similarly, much higher $\boldsymbol{J(\omega_H)}$ values than average ones indicate fast local motions (ps-ns) on those residues.

The above approximation makes the data analysis easier and convenient to reveal the local motions. The limitation for this approach is the fact that the global shape of globular protein is always supposed to be spherical. In some systems, the wrong "interpreted motions", in fact, are the consequence of anisotropic tumbling.

2.2.4 internal motions determined by MODEL free approach

A different approach is called MODEL free approach introduced by Lipari and Szabo[37]. Given a protein with isotropic overall rotaional correlation time, the form of the corresponding MODEL free spectra density function is a Lorentzian:

$$J(\omega) = \frac{2}{5}[\frac{S^2\tau_c}{1+\omega^2{\tau_c}^2} + (1-S^2)\frac{\tau_e}{1+\omega^2{\tau_e}^2}] \qquad \textbf{(13)}$$

In the anisotropic rotation case, the J(w) can be written in the form

$$J(\omega) = \frac{2}{5}\sum_{i=-2}^{2} A_i[\frac{S^2\tau_c}{1+\omega^2{\tau_c}^2} + (1-S^2)\frac{\tau_e}{1+\omega^2{\tau_e}^2}] \qquad \textbf{(14)}$$

where $\boldsymbol{\tau_c}$ is the overall correlation time. Furthermore, it is assumed that the correlation function for the internal motion can be approximated by a single decaying exponential with a time constant of $\boldsymbol{\tau_e}$ and decays to a value of $\mathbf{S}^2$. The generalized order parameters $\mathbf{S}^2$ can be interpreted as a measure of the spatial restriction of the internal motion, and the effective correlation time $\boldsymbol{\tau_e}$ as a measure of the timescale of the internal motion. It satisfies

the inequality $0<\mathbf{S}^2<1$ and lower values indicate larger amplitudes of internal motions.

Furthermore, it is occasionally necessary to invoke motion on two widely-separated time scales to adequately fit the data, resulting in the so-called "extended model-free" spectral density of Clore et al [38]. In this thesis, MODEL free approach was applied to analysis the internal motion of protein TTHA1943 and its copper adduct (result 3.5). The calculations are performed by TENSOR2 program.

2.2.6 Cross-correlated relaxation rates combined with R_2 values provide another hints for conformational exchange.

Undoubtedly, data interpretation of $\boldsymbol{R_1}$, $\boldsymbol{R_2}$ and **NOE** of ^{15}N nucleus of the isolated HN vectors in protein, by different approaches, is the most powerful tool to unravel the local motions. There are several convenient programs, such as TENSOR2 and MODEL free, by which one can perform detailed analysis ^{15}N relaxation parameters, obtain diffusion tensors and get internal dynamic information in different time scales. One can also predict $\boldsymbol{\tau_c}$ value and relaxation rates from the known 3D-coordination structure by the programs, like HYDRONMR [39], by using rigid body assumption. However, these approaches are good only for the rigid system coupled with localized motion, for example, only a few residues in the sequence are flexible while the rest residues are rigid. In some unusual cases, which is really rare, proteins are fluctuating among all the peptide sequence [40]. In the latter cases, conformational exchange ($\boldsymbol{R}_{ex}$) contributes significantly to $\boldsymbol{R}_2$ values among the whole sequence. Thus, the determined $\boldsymbol{\tau_c}$ values are overestimated if following the above approaches. Moreover, it is incorrect to interpret data by reduced spectra density mapping or MODEL-free approach, since $\boldsymbol{R}_{ex}$ terms could be different from residue to residue.

In order to determine the $\boldsymbol{\tau_c}$ and estimate $\boldsymbol{R}_{ex}$ values, one can perform experiments for measuring the cross-correlated relaxation rate, $\boldsymbol{\eta}_{xy}$. As described above, the dominant mechanisms of ^{15}N relaxation in proteins are the dipole-dipole interaction and anisotropic chemical shift (CSA)[41]. Beside the single spin relaxation rate, for instance, Nz ($\boldsymbol{R_1}$) and Nx ($\boldsymbol{R_2}$), and cross relaxation rate (**NOE**), these two mechanisms are also the dominant mechanisms for the relaxation rates of the coupled spin state, for instance, HzNz, HzNx, HxNz and HxNx, and cross correlated relaxation rate Nx-NxHz as well. Different from single spin relaxation rate, the transverse cross correlated relaxation rates, $\boldsymbol{\eta}_{xy}$, are not affect by conformational exchange. Similarly, $\boldsymbol{\eta}_{xy}$ values could be obtained by *redfield* relaxation matrix, with given $\boldsymbol{\tau_c}$ and three-dimensional structure, according to the following equation:

$$\eta_{xy} = \rho\sigma_N[4J(0) + 3J(\omega_N)](3\cos^2\theta - 1) \qquad \textbf{(15)}$$

where

$$\rho = \frac{\mu_0 \gamma_H \gamma_N h}{16\sqrt{2}\pi^2 < r_{HN} >^3} \qquad \textbf{(16)}$$

$$\sigma_N = \frac{\gamma_N B_0 \Delta N}{3\sqrt{2}} \qquad \textbf{(17)}$$

where θ is the angle between the unique axes of the CSA and dipolar tensors; ΔN is the difference of the two principal components of the axially symmetric ^{15}N chemical shift tensor.

The quantitative measurement of cross correlation relaxation rates was performed by using the pulse scheme designed by Tjadra et al [42]. The $\boldsymbol{\eta}_{xy}$ values of well resolved residues were also extracted by following the approach in the same article. From the fitted $\boldsymbol{\eta}_{xy}$ value, $\boldsymbol{\tau_{c,app}}$ for each residues could be obtained by Eqs. (15). The θ values in this work were uniformly assumed to be 17°; and ΔN values were assumed to be 160ppm. These correlation times are independent from the conformational exchange. Consequently, the $\boldsymbol{R}_{2,calc}$ values could be back calculated according to Eqs. (8), assuming no chemical exchange contributes to the $\boldsymbol{R}_2$ values. The difference of $\boldsymbol{R}_{2,calc}$ and $\boldsymbol{R}_{2,expt}$ is the value of $\boldsymbol{R}_{ex.}$

Since $\boldsymbol{\tau_{c,app}}$ for each residues could be obtained independently from motions, this approach has an advantage in characterization the dynamic properties of wholly fluxional system. But the drawback of this approach resides in that several assumptions have to be used for data fitting and the sensitivity of the experiments is quite less than the classical $\boldsymbol{R}_1$, $\boldsymbol{R}_2$ and **NOE** measurements.

2.2.6 H/D exchange

Hydrogen/Deuterium exchange technique can also be used to study protein stability and dynamic properties. For a protein that is dissolved in D_2O, the H/D exchange can be described as in Eqs. (18) [43],

$$\text{H-Protein}_{\text{close}} \underset{k_{\text{cl}}}{\overset{k_{\text{op}}}{\rightleftarrows}} \text{H-Protein}_{\text{open}} \xrightarrow{k_{\text{rc}}} \text{D-Protein}_{\text{close}} \qquad \textbf{(18)}$$

where $\boldsymbol{k_{op}}$ and $\boldsymbol{k_{cl}}$ are the rate constants for opening and closing events in the protein, and $\boldsymbol{k_{rc}}$ is the rate constant for the H/D exchange at the amide group.

Under conditions favoring the folded state (i.e., $\boldsymbol{k_{cl}} >> \boldsymbol{k_{op}}$), the observed exchange

rate, k_{ex}, is given by

$$k_{ex} = \frac{k_{op} k_{rc}}{k_{cl} + k_{rc}} \qquad \textbf{(19)}$$

Depending on the ratio of k_{rc} to k_{cl}, the following two limiting conditions may be encountered:

(i) If $k_{cl} << k_{rc}$, each opening fluctuation leads to an isotope exchange, and Eqs. 19 simplifies to

$$k_{ex} = k_{op} \qquad \textbf{(20)}$$

In this case, the exchange is limited by the opening rate, k_{op}. Obviously, HN exchange measurements under these conditions provide readily interpretable data that can be correlated with a key feature of internal protein motility.

(ii) If $k_{cl} >> k_{rc}$, the intrinsic exchange is the rate-limiting step, and Eqs. 19 reduces to

$$k_{ex} = K_{op} k_{rc} \qquad \textbf{(21)}$$

Here, $K_{op} = k_{op} / k_{cl}$ is the equilibrium constant for the conformational transition between the folded and the unfolded states. In this case, the rate of H/D exchange is slow enough to detect the k_{ex} values. By following the intensities of resonances in ^{1}H-^{15}N HSQC spectra in different time, k_{ex} can be described by

$$k_{ex} = -\frac{1}{t} \ln \frac{I}{I_0} \qquad \textbf{(22)}$$

where I is the peak intensity at time t, and I_0 is the initial intensity when t is equal to 0. It has already been well established to investigate folding and unfolding equilibrium by using k_{ex} values. In this thesis, this technique was applied to study the stability of β-sheet of A629P MNK6. It was found that the k_{ex} values of the residues in the last β-strand of A629P MNK6, where mutant residue reside, and the residues in the first β-strand, which forming H-bonds net work with the last one, are two folder faster or more than those of wild type one. This indicates that the stability of the secondary elements is much decreased due to the mutation.

2.3 Investigating the metal binding of proteins by NMR spectroscopy

Identification of the metal-binding sites in proteins and mapping the structural and dynamic changes upon metal binding are important for our understanding of the biological function of metal-dependent proteins.

2.3.1 monitoring metal ion binding in protein by NMR

The binding of diamagnetic metal ions to proteins can be studied by chemical shift perturbation caused by the metal ion binding. This approach is also called “chemical shift mapping”. The chemical shift perturbations can be followed in titration experiments, where the concentration of the diamagnetic metal ion is increased gradually.

If the exchange rate between metal free and metal bound form are much smaller than the chemical shift difference between two forms, two separate peaks will be detected during titration experiments. This phenomenon is called “slow exchange”. On the contrary, if the exchange between the metal-free and the metal-bound form of the protein is fast compared to the chemical shift difference between the two forms, a single exchange-averaged signal is observed [44]. The chemical shift of the exchange-averaged signal will depend on the metal ion concentration. In this thesis, MNK6 protein, Sco family proteins and TTHA1943 bind copper ion in a process of slow exchange. The residues, whose chemical shifts are significantly different (> 0.2ppm) between apo and holo form, are ones close to the binding sites. To consider the chemical shift change on both ^{1}H and ^{15}N dimensions, composite chemical shifts are used in the mapping according to Eqs. 23. **Fig 7** shows an example of chemical shift variation between apo and copper form of TTHA1943.

$$\delta(HN) = \sqrt{\frac{\Delta\delta H^2 + (\Delta\delta N / 5)^2}{2}} \qquad \textbf{(23)}$$

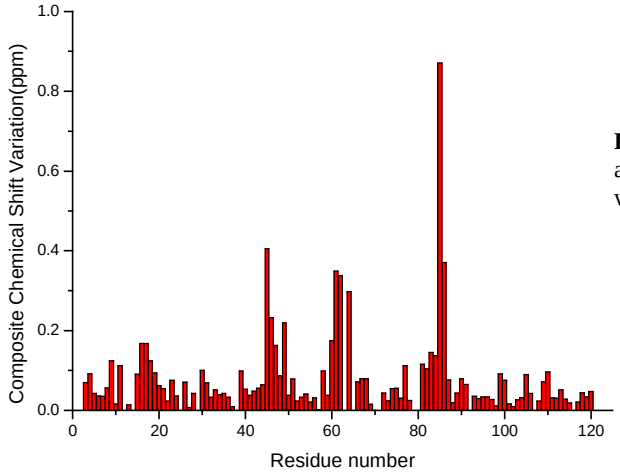

Fig 7: combined chemical shift variation between apoTTHA1943 and Cu(I)TTHA-1943. Copper ion was bound to His 46, Met 59, His 85 and Met 85

In addition to sulfur atom of Cys residues, nitrogen atom of the aromatic side chain of His residues and sulfur atom of Met residues are also potential copper binding ligands. Typically, if copper ion is bound to the sulfur atom of Met residues, chemical shift

variation of methyl group (Cε) should be detected in the ^{1}H-^{13}C HSQC. The chemical shift changes of His side chains could be followed by a ^{1}H-^{15}N HSQC experiments tailored to the detection of ^{2}J ^{1}H-^{15}N coupling. In the latter spectra, three or four patterns represent one aromatic side chain of His residues.

2.3.2 Measuring copper binding affinity

Since the change of signal intensities or positions for the residues around the metal binding sites is easily followed in the ^{1}H-^{15}N HSQC with different metal/protein ratio, NMR is also a good technique to determine the dissociation constant ($\boldsymbol{K_D}$). But sometimes the metal binding affinity is so high that the $\boldsymbol{K_D}$ value is unlikely to detect directly with the titration between metal and protein. In the slow exchange process, dissociation constant is in nM range, with a few exceptions. In this thesis, the $\boldsymbol{K_D}$ values of copper proteins were measured by copper competition experiments between copper load form of protein and copper chelator (DTT). Since copper exchange between protein and DTT is also in a process of slow exchange, peak intensities, which represent the same residues in apo and copper loaded form, are followed in different DTT/protein ratio. Provided that the reaction is in the equilibrium:

$$\mathrm{Cu(I)Protein + DTT} \rightleftharpoons \mathrm{apoProtein + Cu(I)DTT}$$

The equilibrium constant

$$K_{eq} = \frac{[Cu(I)DTT][apo\,\mathrm{Pr}\,otein]}{[DTT][Cu(I)\,\mathrm{Pr}\,otein]} \qquad \textbf{(24)}$$

can be fitted according to following equations:

$$y = \frac{-(1-x) - \sqrt{(1-x)^2 + \frac{4x}{K_{eq}}}}{2x} \qquad \textbf{(25)}$$

where $\boldsymbol{y}$ is the ratio of peak intensities of a residue between copper loaded form and apo form ($\boldsymbol{y}$=[Cu(I)Protein]/[apoProtein]) and $\boldsymbol{x}$ is the ratio between total concentration of DTT and total concentration of protein. $\boldsymbol{K_D}$ values of protein can be extracted by

$$K_D = K_{eq} \times K_{D(DTT)}$$

where $\boldsymbol{K}_{D(DTT)}$ is 6.31×10^{-12} M [45]

If the exchange process of metal binding is very fast, there is, even during the titration, only a single set of resonances whose chemical shifts are the fractionally weighted average

of the free and bound chemical shifts. Here the resonances of nuclei close to the binding sites move in a continuous fashion during the titration. It is often observed for weaker interactions (in μM range), when the interaction is in the process of fast exchange. Within the latter range, K_D values can be determined directly by fitting chemical shift in different metal/protein ratio. Provided a protein binds one diamagnetic metal according to the following equilibrium:

$$\text{apo-protein} + \text{Me} \rightleftharpoons \text{Me-protein}$$

K_D values can be fitted according to following equations:

$$\Delta\delta = \Delta\delta_{\infty}(-B - \sqrt{B^2 - 4ab})/(2a) \qquad \textbf{(26)}$$

where

$$B = -(a + b + K_D) \qquad \textbf{(27)}$$

and **a** and **b** are the total concentrations of protein and metal ion, respectively. **Δδ** is the chemical shift change of a protein residue upon addition of metal ion, and $\Delta\delta_{\infty}$ is the estimated chemical shift change for the state where $b/a \rightarrow \infty$.

2.4 Reference list

(1) van Tilborg, P.J.; Czisch, M.; Mulder, F.A.; Folkers, G.E.; Bonvin, A.M.; Nair, M.; Boelens, R.; Kaptein, R. (2000) *Biochemistry* 39 (30) 8747-57

(2) Ishima, R.; Wingfield, P.T.; Stahl S.J.; Kaufman J.D.; Torchia, D.A. (1998) *J. Am. Chem. Soc.* 120 10534

(3) Lee, AL.; Kinnear, SA; Wand, AJ. (2000) *Nat Struct Biol.* 7(1) 72-7

(4) Ottiger, M.; Zerbe, O.; Güntert, P.; Wüthrich, K.; (1997) *J Mol Biol.* 272 64 64-81

(5) Wüthrich, K. (2001) *Nat. Stru. Biol.* 8 923-925

(6) Pervushin, K.; Riek, R.; Wider, G.; Wüthrich, K. (1997) *Proc. Natl. Acad. Sci.* 94 12366-12371

(7) Salzmann, M.; Pervushin, K.; Wider, G.; Senn, H.; Wüthrich, K. (1999) *J Biomol NMR.* 14:85-8

(8) Pervushin, K.V.; Wider, G.; Riek, R.; Wüthrich, K. (1999) *Proc. Natl. Acad. Sci.*. 96 9607-12

(9) Riek, R.; Wider, G.; Pervushin, K.; Wüthrich, K. (1999) *Proc. Natl. Acad. Sci.* 96 4918-23

(10) Rudiger, S.; Freund, SM.; Veprintsev, D.B.; Fersht, A.R. (2002) *Proc. Natl. Acad. Sci.* 99 11085-90

(11) Mielke, S.P.; Krishnan, V.V. (2004) *J. Biomol. NMR* 30 143-53

(12) Wang, A. C.; and Bax, A.; (1996) *J. Am. Chem. Soc.* 118, 2483-2494.

(13) Cornilescu, G.; Delaglio, F.; Bax A. (1999) *J. Biomol. NMR* 13, 289-302

(14) Berjanskii1, MV.; Neal, S.; Wishart, DS.; (2006) *Nucleic Acids Res* 34(Web Server issue):W63-9.

(15) Karplus, M.; (1963) *J. Am. Chem. Soc.*85 2870-1

(16) Brünger, AT; (1992) *X-PLOR, Version 3.1. A System for X-ray Crystallography and NMR,* Yale University Press, New Haven, USA.

(17) Brünger, A.T.; Nilges, M. (1993) *Quart. Rev. Biophys.* 26, 49-125.

(18) Havel, T. F.; Wüthrich, K. (1984) *Bull. Math. Biol.* 46 673-698

(19) Güntert, P.; Mumenthaler, C.; Wüthrich, K. (1997) *J. Mol. Biol.* 273 283-298

(20) Huang, YJ.; Moseley, HN.; Baran, MC.; Arrowsmith, C.; Powers, R.; Tejero, R.; Szyperski, T.; Montelione, GT; (2005) *Methods Enzymol.*394 111-41

(21) Herrmann, T.; Güntert, P.; Wüthrich, K. (2002) *J Mol Biol.* 319 209-27

(22) SHerrmann, T.; Güntert, P.; Wüthrich, K. (2002) *J Biomol NMR.* 24 171-89

(23) Case, D.A.; Darden, T.A.; Cheatham, T.E.; Simmerling, C.L.; Wang, J.; Duke, R.E.; Luo, R.; Merz, K.M.; Wang, B.; Pearlman, D.A.; et al. (2004) *AMBER 8 (computer program)*. University of California, San Francisco.

(24) Laskowski, R. A., Rullmann, J. A. C., MacArthur, M. W., Kaptein, R.; Thornton, J. M. (1996) *J. Biomol. NMR* 8, 477–486.

(25) Laskowski, R. A., MacArthur, M. W., Moss, D. S.; Thornton, J. M. (1993) *J. Appl. Crystallogr.* 26, 283–291.

(26) Vriend, G. (1990). *J. Mol. Graph.* 8, 52–56.

(27) Doreleijers, J.F.; Raves, M.L.; Rullmann J.A.C.; Kaptein, R.; (1999) *J. Biomol. NMR* 14, 123-132

(28) Hernandez, G.; LeMaster, D. M.; (2001) *Biochemistry* 40, 14384

(29) Chou, J. J.; Case, D. A.; Bax, A.; (2003) *J. Am. Chem. Soc.* 125, 8959

(30) Tolman, J.R. (2002) *J. Am. Chem. Soc.* 124, 12020

(31) Cavanagh, J.; Fairbrother, W.J.; Palmer, A.G.; Skelton, N.J. (1996) *Protein NMR spectroscopy: Principles and practice*, Academic Press; San Diego, CA

(32) Abragam, A. (1961) *Principles of Nuclear Magnetism*; Clarendon Press; Oxford, U.K.

(33) Dosset, P.; Hus, JC.; Blackledge, M.; Marion, D.; (2000) *J. Biomol, NMR* 16, 23-8

(34) Farrow, N.A.; Zhang, O; Szabo,A.; Torchia,D.A.; Kay,L.E. (1995) *J. Biomol, NMR* 6 153-62

(35) Ishima, R.; Nagayama, K. (1995) *J.Magn.Reson.*, Ser. B, 108 73

(36) Peng, J.W.; Wagner, G. (1995) *Biochemistry* 34 16733-52

(37) Lipari, G.; Szabo, A. (1982) *J. Am. Chem. Soc.* 104, 4546-59

(38) Clore, G.M.; Szabo, A.; Bax, A.; Kay, L.E.; Driscoll, P.C.; Gronenborn, A.M. (1990) *J. Am. Chem. Soc.* 112 4989-91.

(39) García de la Torre J, Huertas ML, Carrasco B. (2000) *J. Magn. Reson.* 147 138-46

(40) Bertini, I.; Cowan, J.A.; Del Bianco, C.; Luchinat, C.; Mansy, S.S. (2003) *J. Mol. Biol.* 331 907-24

(41) Halla, J.B.; Dayieb, K.T.; Fushman D. (2003) *J..Biomol. NMR* 26 181–6

(42) Tjandra, N.; Szabo, A.; Bax, A. (1996) *J. Am. Chem. Soc.*, 118,6986–91

(43) Kjellsson, A.; Sethson, I.; Jonsson, BH.; (2003) *Biochemistry*, 42, 363-374

(44) Zuiderweg, ER; (2002) *Biochemistry* 41, 1-7

(45) Krezel, A.; Lesniak, W.; Jezowska-Bojczuk, M.; Mlynarz, P.; Brasun, J.; Kozlowski, H.; and Bal, W. (2001) *J. Inorg. Biochem.* 84, 77–88

3

RESULT

During the three years of the PhD course, I mainly focused my work on protein structures determination, protein dynamic properties characterization, metal binding affinity measurements and metal mediated protein-protein interactions. All these work have been performed by NMR spectroscopy. All the structures mentioned in this thesis have been deposited in RCSB PDB. Specifically:

As discussed in the introduction section, Menkes disease is a fatal disease that can be induced by various mutations in the *ATP7A* gene. One of the disease causing mutations, A629P, occurs in the last of the six copper(I) binding soluble domains (MNK6). In order to understand why this apparently minor amino acid replacement is pathogenic, solution structures of MNK6 and A629P-MNK6 were determined in both apo and copper(I) loaded forms. Totally, four structures were obtained. The structure difference induced by mutation is subtle. Comparing H/D exchange rates of wild type and mutant proteins, it was shown that A629P mutation makes the protein β-sheet more solvent accessible, possibly resulting in an enhanced susceptibility of ATP7A to proteolytic cleavage and/or in reduced capability of copper(I)-translocation. A small reduction of the affinity for copper(I) was also observed. Detailed results were reported in result section 3.1

In order to understand the function role of HSco1 in CcO assembly, solution structures of apo, Cu(I), and Ni(II) human Sco1 have been determined. The protein passes from an open and conformationally mobile state to a closed and rigid conformation upon metal binding as shown by NMR data. The metal binding ligands are two Cys residues of the CXXXCP motif and one highly conserved His residue. Crystals of the Ni(II) derivative were also obtained with the Ni(II) ion bound to the same His residue and to the two oxidized Cys residues of the CPXXCP motif (The work about crystal structure of Ni(II)HSco1 has been done by Dr. Vito Calderone). From the various structures solved, two functional roles could be assigned to HSco1 protein: i) copper chaperone for CcO and ii) thioredoxin function. Detailed discussions were reported in result section 3.2.

Mutant P174L of HSco1 The pathogenic mutant (P174L) of human Sco1 produces respiratory chain deficiency associated with CcO assembly defects. The position of this mutant is the proline residue of CXXXCP binding motif. In order to compare with the wild type structure, I solved the solution structure of Cu(I)-P174L-HSco1. It is shown that Leu-174 prevents the formation of a well packed hydrophobic region around the metal-binding site and causes a reduction of the affinity of copper(I) for the protein. $\mathbf{K}_D$ values for Cu(I)WT-HSco1 and Cu(I)P174L-HSco1 are ~10^{-17} M and ~10^{-13} M, respectively. The

latter value for copper donor to HSco1, $Cu(I)_1Cox17_{2S\text{-}S}$, is ~$10^{-15}$ M, indicating that Cox17 has higher copper affinity than mutant HSco1 but lower than that of WT-HSco1. Thus we could conclude that mutant P174L induces less well packed hydrophobic region, decreases the copper binding affinity, thus impairs the copper transfer from Cox17 to HSco1. Detailed works were shown in result section 3.3.

The solution structure of copper(I) loaded human Sco2 (Cu(I)HSco2) has also been determined. Although the overall fold of Cu(I)HSco2 is highly similar to HSco1 homolog, the dynamic properties and the conformational disorder are quite different when the apo forms and the copper(I)-loaded forms of the two proteins are compared separately. Comparing $\boldsymbol{R}_2$ values and $\boldsymbol{\eta}_{xy}$ values of Cu(I)HSco2, it was shown that certain degree of fluxionality is present through all the peptide sequence. This property is absent in HSco1 protein. Such different are accounted for in terms of the different physicochemical properties in strategic protein locations. Detailed description was shown in result section 3.4.

As discussed in introduction section, the physiological function of Sco proteins in prokaryotes go beyond assembly of the Cu_A of CcO and could be different from organism to organism, although Sco proteins are widespread proteins found in many prokaryotic organisms. And a new protein, called Hyp1, has been suggested to have a role of copper trafficking in prokaryotes. In order to unravel the function of Hyp1 protein and Sco protein in different prokaryotic organisms, the solution structures of Hyp1 protein in T. thermopiles, the gene product of TTHA1943, were solved by NMR in both apo and copper(I) binding forms. Copper binding affinity was also determined by competition experiments, showing a dissociation constant of $\mathbf{K}_D$=2.2 ± 0.6×10^{-13}M. Protein-protein interactions with Sco protein of *T. Thermophillus* (TTSco) and Cu_A have been also performed. From various protein-protein interaction data, it is suggested that TTSco might function as a thioredoxin, instead of copper chaperone, whereas TTHA1943 is a copper(I) chaperone for Cu_A site. This work has not been published yet and the paper is in preparation. Detailed works were shown in section 3.5.

doi:10.1016/j.jmb.2005.07.034 J. Mol. Biol. (2005) 352, 409–417

JMB

Available online at www.sciencedirect.com

SCIENCE DIRECT®

ELSEVIER

An Atomic-level Investigation of the Disease-causing A629P Mutant of the Menkes Protein, ATP7A

Lucia Banci[1,2,3], Ivano Bertini[1,2]*, Francesca Cantini[1,2] Manuele Migliardi[1,2], Antonio Rosato[1,2] and Shenlin Wang[1]

[1]*Magnetic Resonance Center (CERM), University of Florence Via L. Sacconi 6, 50019 Sesto Fiorentino, Italy*

[2]*Department of Chemistry University of Florence, Via della Lastruccia 3, 50019 Sesto Fiorentino, Italy*

[3]*FiorGen OnLus, Via L. Sacconi 6, 50019 Sesto Fiorentino Italy*

**Corresponding author*

Menkes disease is a fatal disease that can be induced by various mutations in the ATP7A gene, leading to unpaired uptake of dietary copper. The ATP7A gene encodes a copper(I)-translocating ATPase. Here the disease-causing A629P mutation, which occurs in the last of the six copper(I)-binding soluble domains of the ATPase (hereafter MNK6), was investigated. To understand why this apparently minor amino acid replacement is pathogenic, the solution structures and dynamics on various time-scales of wild-type and A629P-MNK6 were determined both in the apo- and copper(I)-loaded forms. The interaction *in vitro* with the physiological ATP7A copper(I)-donor (HAH1) was additionally studied. The A629P mutation makes the protein β-sheet more solvent accessible, possibly resulting in an enhanced susceptibility of ATP7A to proteolytic cleavage and/or in reduced capability of copper(I)-translocation. A small reduction of the affinity for copper(I) is also observed. Both effects could concur to pathogenicity.

Keywords: copper; Menkes disease; ATP7A; metal homeostasis; hydrogen exchange

Introduction

Copper is an essential heavy metal involved in various cellular processes, being required as a cofactor in several enzymes. Although essential, copper is toxic when it accumulates beyond an acceptable level. Since dietary copper intake generally exceeds the trace amount required, organisms have evolved mechanisms for the absorption, delivery, and removal of copper to achieve homeostasis.[1–3] The occurrence of human disorders that disrupt copper homeostasis demonstrates the need for stringent regulation of intracellular copper levels: Menkes disease (MD)[1] is a disorder associated with tissue copper deficiency, often leading to death in the first decade of life, whereas Wilson disease (WD) results from copper overload and is more treatable than MD with patients often seeking the first medical advice between the second and the third decade of life.

MD is an X-linked copper deficiency syndrome, first characterized in 1962.[4] It has been shown that MD is caused by mutations in the gene ATP7A.[5–7] This gene encodes a 1500 amino acid residue copper-translocating P-type ATPase, which is an integral membrane protein with various soluble domains, including a long N-terminal cytosolic tail containing six putative metal-binding domains. Copper(I) is delivered to the N-terminal metal-binding domains of the ATPase for subsequent translocation by a small protein, HAH1, which functions as a so-called metallochaperone.[8] Each of the six N-terminal domains of ATP7A can bind a single copper(I) ion by coordinating it to two cysteine side-chains.[9] ATP7A is expressed in most tissues, including heart, lung, skeletal muscle, skin, colon, lymphoblasts, fibroblasts, and, at a low level, pancreas, kidney and stomach (see expression profile at UniGene†). ATP7A has two important cellular functions: (i) to facilitate the export of copper from non-hepatic tissues and its absorption

Abbreviations used: MD, Menkes disease; WD, Wilson disease; HGMD, Human Gene Mutation Database; WT, wild-type; MNK2, second binding domain of Menkes protein; MNK5, fifth binding domain of Menkes protein; MNK6, sixth binding domain of Menkes protein; HSQC, heteronuclear single quantum coherence spectroscopy.

E-mail address of the corresponding author: ivanobertini@cerm.unifi.it

† http://www.ncbi.nlm.nih.gov/UniGene/ESTProfileViewer.cgi?uglist=Hs.496414

0022-2836/$ - see front matter

into circulation, and (ii) to deliver copper to the secretory pathway for incorporation into copper-dependent enzymes.[10] To carry out both functions, ATP7A must be correctly localized within distinct subcellular compartments, which is achieved through a copper-dependent trafficking of the polypeptide within the cell.[11] Under low copper conditions, ATP7A is localized within the trans-Golgi network; copper stimulation results in the redistribution of ATP7A to the plasma membrane for copper transport into circulation.

The clinical features of MD can be attributed to the malfunctioning of one or more copper-requiring enzymes,[12] such as lysyl oxidase, cytochrome *c* oxidase, and dopamine β-hydroxylase, caused by the copper deficiency resulting from the absence of ATP7A activity.[13] The clinical features of the disease are hypopigmented hair and pili torti (kinky hair syndrome), resulting from reduced keratin cross-linking, connective tissue fragility (aortic aneurysms, fragile bones) and severe neurological defects. On the other hand, the mechanisms accounting for the prenatal cerebral and cerebellar degeneration remain unknown, implying the existence of as yet unidentified copper-requiring enzymes, which play an essential role in neuronal growth and differentiation in the developing human fetus.[13] ATP7A mutations leading to MD show great variability. In particular, point mutations have been reported in a number of patients, (see the Human Gene Mutation Database (HGMD)†, and His & Cox[14]). The various types of point mutations are represented almost equally among ATP7A mutations (deletions/insertions 39.1%, missense and nonsense mutations 37.9%, splice-site mutations 23%). The large majority of the mutations result in truncation of the protein. Gross genomic deletions of ATP7A have also been reported.[15] There are very few point mutations within the N-terminal metal-binding domains causing MD, with only one missense mutation reported in the HGMD. This is the Ala629Pro mutation,[16] which is located in the last strand of the β-sheet of the sixth domain of ATP7A (MNK6 hereafter). A comparison between the disease-causing mutations of ATP7A and its human paralog ATP7B (leading to WD) reveals some differences in their distribution throughout the two genes.[14] In particular, mutations in the region between MNK6 and the first trans-membrane helix are found in many MD patients, compared with only 3% of WD patients.[14] Notably, mutagenesis of the ATP7B gene shows that its sixth metal-binding domain is sufficient but not essential for function.[17] These data suggest that the integrity of the boundary between the cytoplasmic tail and the trans-membrane region, which has been proposed to be important for proper interaction between the soluble copper-binding domains and the remainder of the ATP7A protein chain,[18] may be critical for MD. It is however quite likely that there is not a single mechanism by which amino acid substitutions cause MD (or WD), as different disease-causing variants may show or not changes in ATP7A localization[19] as well as may retain or not copper(I)-translocation capabilities.[20] Indeed, the mutation investigated here is partly functional when inserted in a yeast strain lacking the copper(I)-transporting ATPase Ccc2.[21] The present investigation thus contributes to the accumulating evidence that amino acid substitutions may lead to pathological states by means of very subtle changes in the behaviour of a protein in solution rather than by means of disruption of protein structure or of abrogation of catalytic activity.[22–25] Such effects are difficult to predict also with respect to their effect on the phenotype. In this respect it is worth noting that MD is characterized by a poor correlation between mutations and phenotype.[19,26]

† www.hgmd.org

Results

Protein characterization and structural calculations

Wild-type (WT) and A629P-MNK6 bound one copper(I) ion per protein molecule, and were monomeric in solution in both the apo and copper(I) forms. Backbone assignments were obtained using standard strategies based on triple resonance experiments (Supplementary Data, Table S1) and are given in the Supplementary Data (Tables S2–S5). The resonances of the amide moieties of residues 2 and 16–17 (residues have been numbered from 1 to 76, rather than starting from 561, for the sake of simplicity; with this numbering, the mutated position 629 corresponds to 69) were not detectable. Combined chemical shift variations between the apo and copper(I) forms of WT and A629P-MNK6 are highly similar and localized around the metal-binding loop (Figure S1). Combined chemical shift differences between WT and A629P-MNK6 (Figure 1(a) and (b)) show that the mutation affects mainly residues 4–6, 9–11, 37, 43, 48, 58, 62–64, 67–68, 70 in the apo form and residues 4–6, 10–11, 48, 62, 67–68, 70 in the copper(I) form (taking as significant a variation of at least 0.1 ppm). Residue 11 is in both forms the most affected by the mutation. In apo-MNK6, these residues map mainly to the strands β1 and β4, and the C-terminal part of helix α2 (Figure 1(c)). However, perturbations extend also to strand β3, which is H-bonded to β1, and to one residue in β2.

The restraints used in the four structure calculations performed are in Tables S6–9. Backbone RMSD values were in all cases around 0.65($\pm$0.10) Å. Target function values were satisfactory in all cases (see Supplementary Data), with no distance constraint violation above 0.30 Å. The percentage of residues in the most favourable regions of the Ramachandran plot was about 80%. An analysis of various features of the structures obtained is given

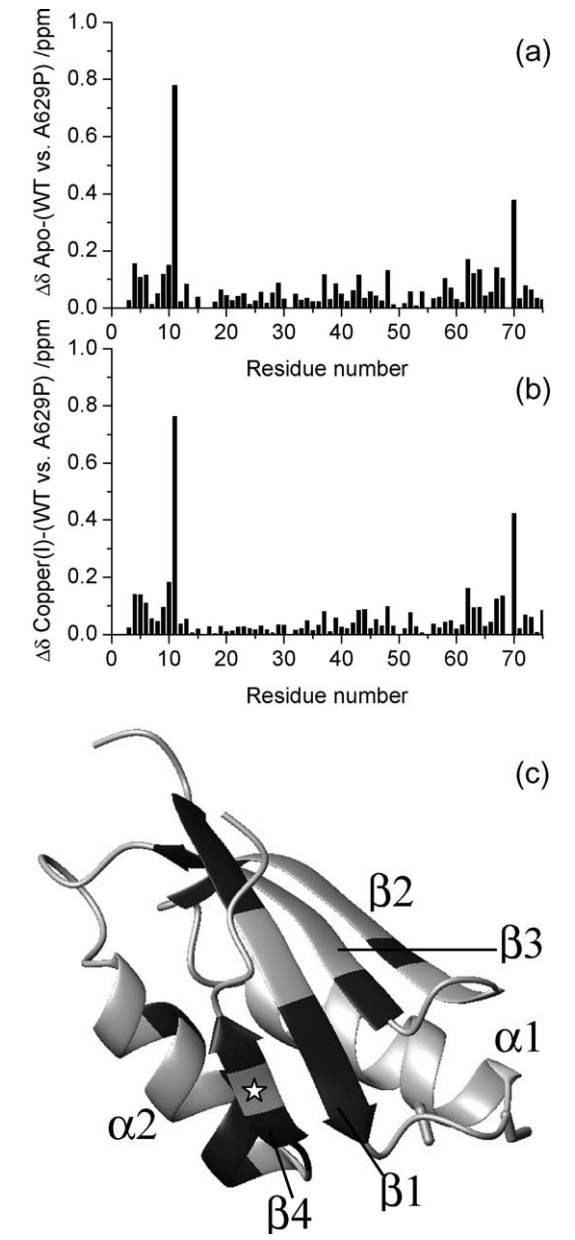

Figure 1. Combined chemical shift variations of backbone amide moieties between WT and A629P-MNK6 for both the apo (a) and copper(I) forms (b) of the protein. The mutation is located at position 69 in the present numbering scheme. (c) Structure of apo-WT-MNK6 colour-coded to highlight residues whose backbone amide moieties experience combined chemical shift variations of at least 0.1 ppm (in black). The mutated residue 69 is identified by a white star. The side-chains of the metal-binding cysteine residues are also shown.

in Tables S6–9. Table S10 reports the secondary structures elements identified by PROCHECK.[27] Figure 2 shows a comparison of the four structures. It appears immediately that the mutation does not affect the fold of the protein, and in particular the structure of the β-sheet within which the mutated residue is located (being the last-but-one residue in the fourth strand). An analysis of the superposition of the mean structures identifies only the loop region (residues 49–54) between the third β-strand and the second α-helix as a stretch with some difference between the WT and mutant structures. This region, which is distant from the mutation, has the higher local RMSD in all structures, suggesting that the small difference observed is not significant. The structure of the metal-binding loop region is instead essentially unaffected by the mutation, even though residue 16 is not involved in helix α_1 in some structures of apo-A629P-MNK6. Indeed, variations in the geometry and structural features, e.g. H-bond patterns, of this loop between apo and copper(I)-MNK6 are relatively small and do not follow a defined trend. The same is true when comparing the structures of A629P-MNK6 and WT-MNK6.

The temperature dependence of CD and heteronuclear single quantum coherence (HSQC) spectra is similar for WT and A629P-MNK6. CD spectra are for both systems only marginally altered between 293 K and 363 K, indicating that the fraction of unfolded protein is very small even at the highest temperature. Instead, A629P-MNK6 is slightly more easily denatured by guanidinium chloride than WT-MNK6, as qualitatively demonstrated in Figure 3, which shows that at 3.5 M [guanidinium] A629P-MNK6 is completely unfolded, while WT-MNK6 is still partly folded. Indeed in the spectrum of the latter, peaks from both the folded and the unfolded protein are detected, while the spectrum of the former contains only peaks from the unfolded protein (Figure 3).

Protein dynamics

^{15}N relaxation measurements show that the protein dynamics on the sub-nanoseconds as well as microseconds–milliseconds time-scales is essentially the same in all four systems studied here. The N and C termini are quite flexible on the sub-nanosecond time-scale, while mobility on the μs–ms time-scale is observed in the metal-binding loop region and for the loop between the first α-helix and the second β-strand, similarly to MNK2.[28]

The kinetics of H/D exchange up to 20 h has been measured for the apo and copper(I)-forms of WT and A629P-MNK6. For both proteins, the variation in the kinetics of H/D exchange between the apo and copper(I) forms is small all over the sequence, with the exception of residues 22–23, 65 and 67, which are in contact and form a small hydrophobic cluster. On the other hand, residues in the mutated protein exchange as fast as or faster than the corresponding residues in the WT protein. In strand β4, where the A629P mutation is located, only residue 68, which precedes in sequence the mutation, can be compared, as Ser70 exchanges too fast to be detected in all four systems. Residue 68 in A629P-MNK6 exchanges so fast that its signal in the first ^{1}H–^{15}N HSQC, taken immediately after dissolving the sample in $^{2}H_2O$, is already not detectable, while the corresponding signal in WT-MNK6 decays with a half-life of the order of

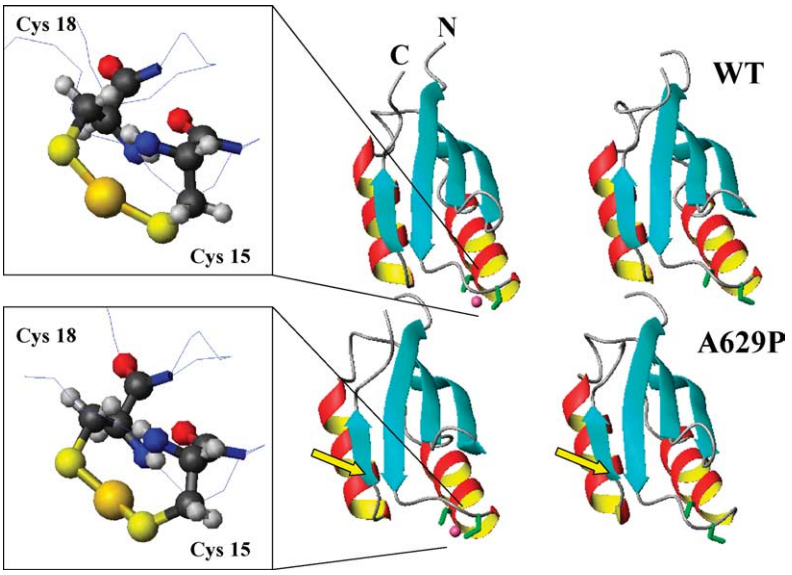

Figure 2. Comparison of the structures of apo (right) and copper(I) (left) WT-MNK6 (top) and A629P-MNK6 (bottom). The metal site is shown (cysteine bonds in green; copper(I) ion in pink). The yellow arrow indicates the position of the mutation. The N and C termini are also labelled, only for copper(I)-WT-MNK6. The metal coordination is shown in the insets.

10–15 min. The same behaviour is also observed only for residue 11 (Figure 4), which is H-bonded to residue 68. The other residues featuring significant (i.e. a twofold or more) variations of their kinetic constants with respect to the WT-MNK6 are mainly located in strands β1 and β3, and in part in strand β2 (Figure 5 and Table S11).

Interaction with HAH1

The interaction of WT and A629P-MNK6 with HAH1 was studied by titrating the ^{15}N-enriched apo-protein with unlabelled copper(I)-HAH1. The process was followed through ^{1}H-^{15}N HSQC spectra. No variation in the chemical shifts of the amide signals in MNK6 could be observed at any stage of the titration. Instead, the intensities of apo-protein signals decreased with increasing HAH1 concentration. Concomitantly, signals corresponding to copper(I)-MNK6 (Met13, Thr14, Cys15, Ser17, Cys18, Val19 and His20, which are the only ones clearly distinguishable between the apo and the copper(I) forms) appeared and increased in intensity along the titration (Figure S2 of Supplementary

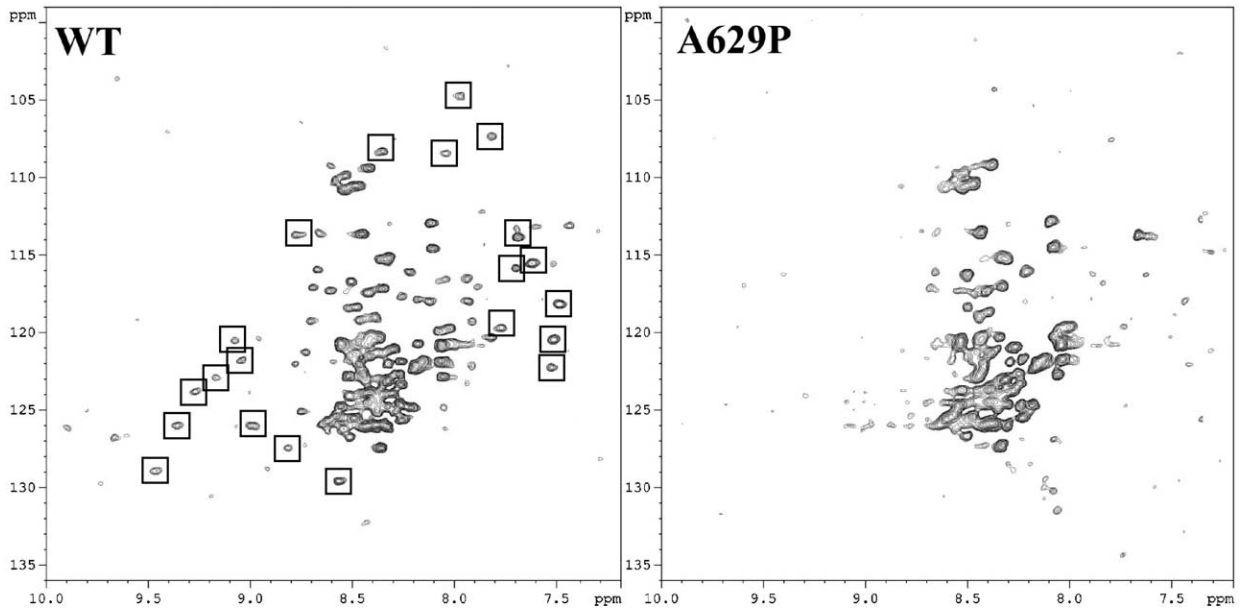

Figure 3. Comparison of the ^{1}H–^{15}N HSQC spectra of apo-A629P- (right) and WT-MNK6 (left) in the presence of 3.5 M guanidium chloride, showing that A62P-MNK6 is completely unfolded, while well-dispersed signals from the folded protein are still observable for WT-MNK6. The residues boxed in the ^{1}H–^{15}N HSQC of WT-MNK6 belong to the folded protein, while no signals from the folded protein can be observed in the case of A629P-MNK6. Only well-resolved peaks from folded apo-WT-MNK6 have been boxed (i.e. there are other peaks from the folded protein that have not been boxed because they are very close to or in overlap with the signals of the unfolded protein).

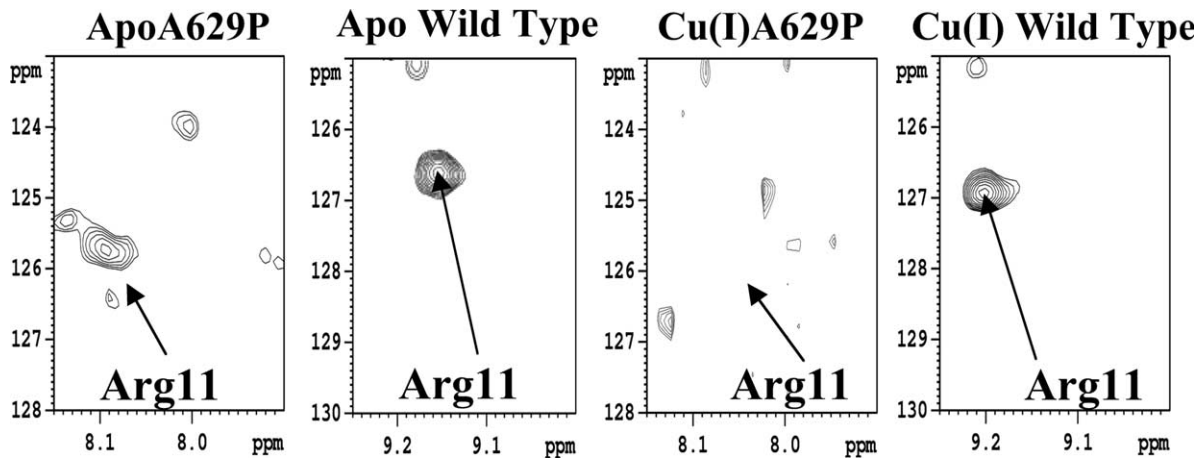

Figure 4. Comparison of the first ^{1}H–^{15}N HSQC spectrum taken after dissolving in $^{2}H_2O$ (from left to right) apo-A629P and WT-MNK6, and copper(I)-A629P and WT-MNK6.

Data). No additional signals from a possible intermediate could be detected. These results are analogous to those observed for the MNK2 and MNK5 domains.[29]

The above data thus indicate that there is no formation of an adduct between MNK6 and HAH1 at detectable concentration, while copper(I) is transferred between the two proteins. The latter process is slow on the chemical shift time-scale, setting an upper limit for the equilibration rate around 10^2–10^3 s^{-1}. The molar fraction of apo and copper(I)-MNK6 as a function of the MNK6:HAH1 molar ratio can be fitted with an equilibrium constant for the transfer of copper(I) from HAH1 of 8.7($\pm$2.6) for WT-MNK6 and 6.5($\pm$1.1) for A629P-MNK6, similar to MNK2 and MNK5.[29]

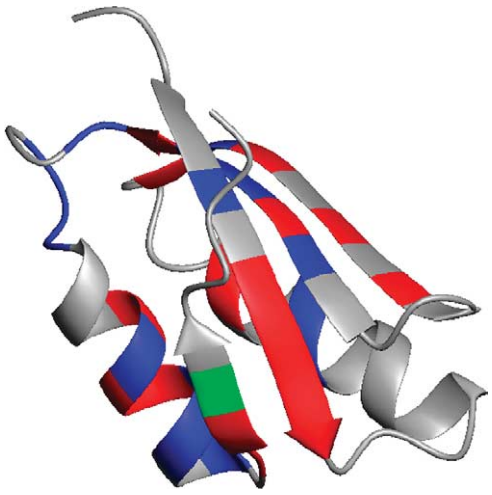

Figure 5. Average solution structure of apo-WT-MNK6 coloured as a function of the variation in H/D exchange rates between apo-WT-MNK6 and apo-A629P-MNK6. Residues in grey exchange too fast in both systems to be detected in HSQC experiments. Residues in blue have the same exchange rates, within error, in the two proteins, while residues in red feature at least a twofold variation in exchange rate. The mutated residue A629P is in green.

To define the relative affinity for copper(I) of WT and A629P-MNK6, an equimolar mixture of apo-WT-MNK6 and copper(I)-A629P-MNK6 was prepared. The interaction between apo-WT-MNK6 and copper(I)-A629P-MNK6 is slow on the time-scale of the NMR chemical shift, and reaches equilibrium within a few minutes from mixing (i.e. the system is already at equilibrium in the first HSQC spectrum). The ratio of the integrals of selected amino acids displaying well-resolved peaks for the apo and copper(I)-forms, indicates that the apparent ratio between the two copper(I) binding constants' affinity for copper(I) of WT-MNK6 and A629P-MNK6 is 1.3($\pm$0.2) (WT/A629P). Note that this value matches the value expected from the ratio of the equilibrium constants for the transfer of copper(I) from HAH1 to MNK6 (8.7/6.5 = 1.34). The latter constants have been independently measured in separate experiments, giving confidence in the observed, albeit small, effect.

Discussion

The structural properties of MNK6 are not significantly altered by the disease-causing A629P mutation. The same is true for its dynamic properties on the sub-nanosecond and μs–ms time-scales. A number of examples have accumulated where disease-causing mutations are found to marginally affect the global fold of the protein. In mutants of superoxide dismutase causing familial amyotrophic lateral sclerosis (fALS), such as G93A, G37R, the tertiary structure of the enzyme is essentially conserved.[23] Some small differences have been detected in protein dynamics.[23] Other seemingly similar subtle mutations associated with fALS still do not change the fold but induce protein polymerization, resulting in the formation of fibres containing an essentially correctly folded protein.[25] This is similar to what is observed in sickle cell disease, where a mutation of the β-subunit of hemoglobin induces the formation of fibres

involving hemoglobin tetramers, which can be rescued by the interaction with chains containing other mutations.[30,31] Finally, in the case of Wilson disease, it has been proposed that the fold of the common H1069Q mutant (His1069 is located in the nucleotide-binding domain of ATP7B) is the same as that of the WT protein at the level of resolution provided by CD spectroscopy.[32] Nevertheless, the H1069Q mutant has been shown to be degraded more rapidly than the WT protein.[33]

Here, a significant difference between WT-MNK6 and A629P-MNK6 is observed for the kinetics of H/D exchange, both in the apo and copper(I) forms. Under non-denaturing conditions, the mechanism for H/D exchange in well-folded proteins involves an equilibrium between a so-called closed state (which is not competent for exchange) and an open state (which is the one allowing the amide proton to exchange). H/D exchange takes place from the open state, with an intrinsic kinetic constant that depends only on the primary sequence and the pH of the solution.[34] The experimental kinetic constant is equal to the product of the equilibrium constant and the intrinsic kinetic constant. The opening reaction for each residue can be interpreted as a folding/unfolding equilibrium involving that particular residue.[34,35] Coordinated opening of more than a single amide group is often detected, leading to the concept of the existence of "cooperative folding units" within proteins.[35]

Calculations of the intrinsic exchange rates with well-established methods[36] predict that, except for residue 70, they are not affected by the mutation. Consequently, the ratio of the H/D exchange kinetics constants measured for each backbone amide in WT and A629P-MNK6 is equal to the ratio of the corresponding equilibrium constants for the opening reaction. The experimental exchange rates in A629P-MNK6 are equal to or, particularly in the protein β-sheet (Figure 5), higher than the rates observed for WT-MNK6. Thus, it can be concluded that for the mutant protein the equilibria between folded and unfolded conformations are shifted towards the unfolded state(s), i.e. the β-sheet is more often transiently exposed to the bulk solvent. This is in agreement with the finding that denaturation by guanidinium is more easily induced for A629P-MNK6 than for WT-MNK6 (Figure 3). The most dramatic evidence for increased propensity towards unfolding is observed for residues 11 and 68 (Figure 4). In addition, several other residues mainly in the β-sheet are characterized by enhanced H/D exchange rate in the mutant (Figure 5), indicating that the weakening introduced in the connection between the first and the last strands makes the entire element of secondary structure more prone to opening, i.e. makes partially unfolded states more easily populated under native conditions. This is also suggested by inspection of Figure 1, showing that combined chemical shift variations, which can be taken as indicative of slight changes in inter-atomic contacts and/or H-bonds, are largest close (in space) to the mutation site, but extend through the β-sheet as well as helix α1. Comparison of Figures 1(c) and 5 additionally shows that residues experiencing variation in exchange rates often correspond to or are adjacent to residues whose amide moieties have combined chemical shift variations larger than 0.1 ppm.

From the structural point of view this is due to the mutation causing some minor rearrangements by affecting the packing of side-chains. Indeed, the impact of the mutation on the structure is expected to be small as the side-chain of the Ala in WT-MNK6 does not form close contacts with other residues. Therefore, given the similar polarity and size (the Pro side-chain volume is ca twice that of Ala), a Pro residue should be accommodated in the same position with relative ease. On the other hand, in the various soluble domains of ATP7A (and ATP7B as well), the position corresponding to Ala629 is always occupied by an alanine, but in the third domain. The small repacking associated with the mutation, while leaving essentially unaltered the protein fold, weakens significantly the H-bond pattern connecting strands β1 and β4, which then acts as a "nucleation seed" for enhanced transient unfolding of the β-sheet. As discussed at the beginning of this section, in fact subtle changes in interatomic contacts may affect significantly the behaviour in solution of various proteins, leading to or modulating the phenotype of pathological states.

The present data show that HAH1 is capable of transferring copper(I) to both WT and A629P-MNK6. The affinity for copper(I) of the protein is marginally lowered by the mutation, as competition experiments indicate that the WT has a binding constant 20–30% higher than that of the A629P protein. This is the only other observable difference, in addition to the loosening of the β-sheet discussed above, between WT and A629P-MNK6. The variation in copper(I) affinity observed is however well within the expected span of the affinity constants of each individual metal-binding domain, as suggested by data for human ATP7B.[37] The relative contribution of the other five soluble domains to transferring copper(I) from the cytoplasm to the binding site in the trans-membrane part of ATP7A is unknown, while for ATP7B it has been shown that a mutant in which the cysteine residues of the sixth domain only had been removed could deliver copper to Fet3p as well as normal ATP7B.[17]

It can be proposed that the mechanism by which the A629P mutation causes MD is linked to two factors. The first one is that the increased readiness of the sixth domain to expose its backbone might render the protein more susceptible to degradation, i.e. may increase the turn-over rate of the protein, ultimately leading to a decreased concentration on the membrane surface. Indeed, it is known that unstructured regions serve as the initiation site for degradation, being hydrolysed first, after which the rest of the protein is digested sequentially.[38] In agreement with the present proposal, degradation of the Wilson disease-causing H1069Q mutant is

faster than for the WT protein.[33] A second factor is a slightly decreased metal-binding ability of the sixth soluble domain, possibly leading to decreased efficiency in transporting copper(I) across the membrane. These two factors could actually work synergistically in causing MD, by making mutant ATP7A an enzyme that is both less efficient and more quickly recycled than the WT protein. Enhanced proteolysis of the ATP7B protein could play a role in the onset of Wilson disease, where various disease-causing missense mutations, mapped to the metal-binding domains 2, 5 and 6, have been reported.[14] A similar contention has been proposed for the H1069Q mutation.[33] Note that domain 2 in ATP7B is a proposed preferential entry point for copper(I) delivered by HAH1.[39,40]

Here, it is shown that the A629P mutation produces subtle effects on the properties of MNK6. This may be in agreement with the observation that A629P-ATP7A produces reduced (with respect to normal ATP7A) but still detectable levels of functional (i.e. copper-containing) Fet3p in yeast lacking Ccc2 (*ccc2*Δ) at variance with other two ATP7A mutants, P1001A and H1086Q, which are not able to restore copper incorporation into Fet3p.[21] Notably, the study in *ccc2*Δ-yeast[21] indicates that the onset of alterations in copper(I) homeostasis induced by the A629P mutation is not, or only partly, dependent on re-localization of ATP7A from the trans-Golgi network to the plasma membrane, because this process is absent in yeast. Note that the re-localization and transport properties of ATP7A can be uncoupled, leading to MD mutations retaining copper(I) transport function but with detective re-localization.[20] In particular, this has been demonstrated for a deletion of the sequence between Ser624 and Gln649, encoded in exon 8, which comprises the last β-strand of MNK6 and a part of the linker between MNK6 and the first trans-membrane helix.[20] This mutation responded well to copper replacement therapy.[20] On the other hand, incorrect localization is not necessarily the only molecular mechanism underlying MD.[19]

As in the case of other diseases (such as fALS, sickle cell anemia, and the related WD), mutations causing MD can induce a variety of different subtle effects at the molecular level leading to the pathological phenotype. In particular, protein structure as well as catalytic function may be little affected, and other factors such as propensity to aggregation or thermodynamic stability are determinant for the onset of disease. The relative importance of the effects induced is quite variable among the different mutations, even in the presence of similar phenotypes. The present data, together with available studies in *ccc2*Δ-yeast,[21] suggest that reduction in copper(I) affinity and, perhaps more importantly, enhanced protein turn-over are involved in the mechanism by which the A629P mutation induces MD.

Materials and Methods

The protocol adopted to express and purify WT-MNK6 and A629P-MNK6 was essentially the same as that previously used by us to produce MNK2.[28] The expression plasmid for WT-MNK6 was obtained as described for MNK2, while the expression plasmid for A629P-MNK6 was obtained from that of WT-MNK6 through the Quickchange (Stratagene) mutagenesis kit. The poly-His tag was removed from MNK6 protein samples used for assignments and structure calculations. Copper(I)-containing samples were prepared by incubating the apo-protein with a slight excess of the acetonitrile complex of copper(I). Recombinant protein characterization, NMR frequency assignments and solution structure determinations were carried out as done for MNK2.[28] A table summarizing the NMR experiments performed on WT-MNK6 and A629P-MNK6 is given in the Supplementary Data (Table S1).

Variations in the position of signals between apo and copper(I)-MNK6 are quantified through the combined chemical shift variation.[41] This is calculated from the experimental ^{1}H and ^{15}N chemical shift variations ($\Delta\delta(^{1}H)$ and $\Delta\delta(^{15}N)$, respectively) measured between corresponding peaks in the two forms, through the following equation:

$$\Delta\delta^{\text{combined}} = \sqrt{\frac{(\Delta\delta(^{1}H))^2 + \frac{1}{25}(\Delta\delta(^{15}N))^2}{2}}$$

HAH1 samples were produced as described, always without poly-His tag.[42] The procedure used to investigate the interaction between WT or A629P-MNK6 with HAH1 was the same as reported for the interaction between MNK2 and MNK5 with HAH1,[29] by adding copper(I)-HAH1 to apo-MNK6 directly in the NMR tube (under N2 atmosphere). Titrations were carried out up to MNK6:HAH1 ratios of 1:1.4, and could be fit to an equilibrium constant for copper(I) exchange, according to the following equation:

$$\text{copper(I)}{-}\text{HAH1} + \text{apo} - \text{MNK6} \leftrightarrows \text{apo} - \text{HAH1} + \text{copper(I)}{-}\text{MNK6}$$

To investigate the exchange of copper(I) between WT and A629P-MNK6, we prepared an equimolar solution of unlabelled copper(I)-A629P-MNK6 and ^{15}N labelled apo-WT-MNK6, and measured the relative intensities of signals in the ^{1}H-^{15}N HSQC spectrum of apo and copper(I)-WT-MNK6. The above procedure is equivalent to mixing one equivalent of each apo-protein with only one equivalent of copper(I).

The thermodynamic stability of apo, WT and A629P-MNK6 was determined (i) by titrating the proteins with guanidinium chloride (pH 7), up to 3.5 M, followed through ^{1}H–^{15}N HSQC spectra; (ii) through variable temperature CD experiments using a JASCO J-810 spectrometer and a Peltier temperature controller; (iii) through variable temperature ^{1}H–^{15}N HSQC spectra.

Protein Data Bank accession codes

The structures and NMR constraints have been deposited in the RCSB PDB (codes 1YJR, 1YJT, 1YJU, 1YJV).

Acknowledgements

We thank Stefano Carganico for help in A629P-MNK6 preparations. This work was supported by MIUR-COFIN 2003, Ente Cassa di Risparmio di Firenze (Project "PROMELAB"), the European Commission (contract-no. QLG2-CT-2002-00988).

Supplementary Data

Supplementary data associated with this article can be found, in the online version, at doi:10.1016/j.jmb.2005.07.034

The supplementary data comprise 11 Tables and two Figures.

References

1. O'Halloran, T. V. & Culotta, V. C. (2000). Metallochaperones: an intracellular shuttle service for metal ions. *J. Biol. Chem.* **275**, 25057–25060.
2. Harrison, M. D., Jones, C. E., Solioz, M. & Dameron, C. T. (2000). Intracellular copper routing: the role of copper chaperones. *Trends Biochem. Sci.* **25**, 29–32.
3. Puig, S. & Thiele, D. J. (2002). Molecular mechanisms of copper uptake and distribution. *Curr. Opin. Chem. Biol.* **6**, 171–180.
4. Menkes, J. H., Alter, M., Steigleder, G. K., Weakley, D. R. & Sung, J. H. (1962). A sex-linked recessive disorder with retardation of growth, peculiar hair, and focal cerebral and cerebellar degeneration. *Pediatrics*, **29**, 764–779.
5. Vulpe, C. D., Levinson, B., Whitney, S., Packman, S. & Gitschier, J. (1993). Isolation of a candidate gene for Menkes disease and evidence that it encodes a copper-transporting ATPase. *Nature Genet.* **3**, 7–13.
6. Chelly, J., Tumer, Z., Tonnesen, T., Petterson, A., Ishikawa-Brush, Y., Tommerup, N. *et al*. (1993). Isolation of a candidate gene for Menkes disease that encodes a potential heavy metal binding protein. *Nature Genet.* **3**, 14–19.
7. Mercer, J. F., Livingston, J., Hall, B., Paynter, J. A., Begy, C., Chandrasekharappa, S. *et al*. (1993). Isolation of a partial candidate gene for Menkes disease by positional cloning. *Nature Genet.* **3**, 20–25.
8. Pufahl, R., Singer, C. P., Peariso, K. L., Lin, S.-J., Schmidt, P. J., Fahrni, C. J. *et al*. (1997). Metal ion chaperone function of the soluble Cu(I) receptor Atx1. *Science*, **278**, 853–856.
9. Lutsenko, S., Petrukhin, K., Cooper, M. J., Gilliam, C. T. & Kaplan, J. H. (1997). N-terminal domains of human copper-transporting adenosine triphosphatases (the Wilson's and Menkes disease proteins) bind copper selectively *in vivo* and *in vitro* with stoichiometry of one copper per metal-binding repeat. *J. Biol. Chem.* **272**, 18939–18944.
10. Voskoboinik, I. & Camakaris, J. (2002). Menkes copper-translocating P-type ATPase(ATP7A): biochemical and cell biology properties, and role in Menkes disease. *J. Bioenerg. Biomemb.* **34**, 363–371.
11. Petris, M. J., Mercer, J. F., Culvenor, J. G., Lockhart, P. & Camakaris, J. (1996). Ligand-regulated transport of the Menkes copper P-type ATPase efflux pump from the Golgi apparatus to the plasma membrane: a novel mechanism of regulated trafficking. *EMBO J.* **15**, 6084–6095.
12. Danks, D. M., Campbell, P. E., Stevens, B. J., Mayne, V. & Cartwright, E. (1972). Menkes's kinky hair syndrome. An inherited defect in copper absorption with widespread effects. *Pediatrics*, **50**, 188–201.
13. Kodama, H. & Murata, Y. (1999). Molecular genetics and pathophysiology of Menkes disease. *Pediatr. Int.* **41**, 430–435.
14. Hsi, G. & Cox, D. W. (2004). A comparison of the mutation spectra of Menkes disease and Wilson disease. *Hum. Genet.* **114**, 165–172.
15. Tumer, Z., Birk Moller, L. & Horn, N. (2003). Screening of 383 unrelated patients affected with Menkes disease and finding of 57 gross deletions in ATP7A. *Hum. Mutat.* **22**, 457–464.
16. Tumer, Z., Lund, C., Tolshave, J., Vural, B., Tonnesen, T. & Horn, N. (1997). Identification of point mutations in 41 unrelated patients affected with Menkes disease. *Am. J. Hum. Genet.* **60**, 63–71.
17. Forbes, J. R., Hsi, G. & Cox, D. W. (1999). Role of the copper-binding domain in the copper transport function of ATP7B, the P-type ATPase defective in Wilson disease. *J. Biol. Chem.* **274**, 12408–12413.
18. Tumer, Z., Moller, L. B. & Horn, N. (1999). Mutation spectrum of ATP7A, the gene defective in Menkes disease. *Advan. Exp. Med. Biol.* **448**, 83–95.
19. Moller, L. B., Bukrinsky, J. T., Molgaard, A., Paulsen, M., Lund, C., Tumer, Z. *et al*. (2005). Identification and analysis of 21 novel disease-causing amino acid substitutions in the conserved part of ATP7A. *Hum. Mutat.*, 26.
20. Kim, B. E., Smith, K. & Petris, M. J. (2003). A copper treatable Menkes disease mutation associated with defective trafficking of a functional Menkes copper ATPase. *J. Med. Genet.* **40**, 290–295.
21. Payne, A. S. & Gitlin, J. D. (1998). Functional expression of the Menkes disease protein reveals common biochemical mechanisms among the copper-transporting P-type ATPase. *J. Biol. Chem.* **273**, 3765–3770.
22. Ivanova, M., Jasuja, R., Krasnosselskaia, L., Josephs, R., Wang, Z., Ding, M. *et al*. (2001). Flexibility and nucleation in sickle hemoglobin. *J. Mol. Biol.* **314**, 851–861.
23. Shipp, E., Cantini, F., Bertini, I., Valentine, J. S. & Banci, L. (2003). Dynamic properties of the G93A mutant of copper-zinc superoxide dismutase as detected by NMR spectroscopy: implications for the pathology of familial amyotrophic lateral sclerosis. *Biochemistry*, **42**, 1890–1899.
24. Levasseur, D. N., Ryan, T. M., Reilly, M. P., McCune, S. L., Asakura, T. & Townes, T. M. (2004). A recombinant human hemoglobin with anti-sickling properties greater than fetal hemoglobin. *J. Biol. Chem.* **279**, 27518–27524.
25. Antonyuk, S., Elam, J. S., Hough, M. A., Strange, R. W., Doucette, P. A., Rodriguez, J. A. *et al*. (2005). Structural consequences of the familial amyotrophic lateral sclerosis SOD1 mutant His46Arg. *Protein Sci.* **14**, 1201–1213.
26. Dagenais, S. L., Adam, A. N., Innis, J. W. & Glover, T. W. (2001). A novel frameshift mutation in exon 23 of ATP7A (MNK) results in occipital horn syndrome and not in Menkes disease. *Am. J. Hum. Genet.* **69**, 420–427.
27. Laskowski, R. A., MacArthur, M. W., Moss, D. S. &

Thornton, J. M. (1993). PROCHECK: a program to check the stereochemical quality of protein structures. *J. Appl. Crystallog.* **26**, 283–291.
28. Banci, L., Bertini, I., Del Conte, R., D'Onofrio, M. & Rosato, A. (2004). Solution structure and backbone dynamics of the Cu(I) and apo-forms of the second metal-binding domain of the Menkes protein ATP7A. *Biochemistry*, **43**, 3396–3403.
29. Banci, L., Bertini, I., Chasapis, C., Ciofi-Baffoni, S., Hadjiliadis, N. & Rosato, A. (2005). An NMR study of the interaction between the human copper(I) chaperone and the second and fifth metal-binding domains of the Menkes protein. *FEBS J.* **272**, 865–871.
30. Ivanova, M., Jasuja, R., Krasnosselskaia, L., Josephs, R., Wang, Z., Ding, M. *et al*. (2001). Flexibility and nucleation in sickle hemoglobin. *J. Mol. Biol.* **314**, 851–861.
31. Levasseur, D. N., Ryan, T. M., Reilly, M. P., McCune, S. L., Asakura, T. & Townes, T. M. (2004). A recombinant human hemoglobin with anti-sickling properties greater than fetal hemoglobin. *J. Biol. Chem.* **279**, 27518–27524.
32. Tsivkovskii, R., Efremov, R. G. & Lutsenko, S. (2003). The role of the invariant His-1069 in folding and function of the Wilson's disease protein, the human copper-transporting ATPase ATP7B. *J. Biol. Chem.* **278**, 13302–13308.
33. Payne, A. S., Kelly, E. J. & Gitlin, J. D. (1998). Functional expression of the Wilson disease protein reveals mislocalization and impaired copper-dependent trafficking of the common H1069Q mutation. *Proc. Natl Acad. Sci. USA*, **95**, 10854–10859.
34. Huyghues-Despointes, B. M., Pace, C. N., Englander, S. W. & Scholtz, J. M. (2001). Measuring the conformational stability of a protein by hydrogen exchange. *Methods Mol. Biol.* **168**, 69–92.
35. Bai, Y. W., Sosnick, T. R., Mayne, L. & Englander, S. W. (1995). Protein folding intermediates: native-state hydrogen exchange. *Science*, **269**, 192–197.
36. Bai, Y., Milne, J. S., Mayne, L. & Englander, S. W. (1993). Primary structure effects on peptide group hydrogen exchange. *Proteins: Struct. Funct. Genet.* **17**, 75–86.
37. Wernimont, A. K., Yatsunyk, L. A. & Rosenzweig, A. C. (2004). Binding of copper(I) by the Wilson disease protein and its copper chaperone. *J. Biol. Chem.* **279**, 12269–12276.
38. Prakash, S., Tian, L., Ratliff, K. S., Lehotzky, R. E. & Matouschek, A. (2004). An unstructured initiation site is required for efficient proteasome-mediated degradation. *Nature Struct. Biol.* **11**, 830–837.
39. Walker, J. M., Huster, D., Ralle, M., Morgan, C. T., Blackburn, N. J. & Lutsenko, S. (2004). The N-terminal metal-binding site 2 of the Wilson's disease protein plays a key role in the transfer of copper from Atox1. *J. Biol. Chem.* **279**, 15376–15384.
40. van Dongen, E. M., Klomp, L. W. & Merkx, M. (2004). Copper-dependent protein–protein interactions studied by yeast two-hybrid analysis. *Biochem. Biophys. Res. Commun.* **323**, 789–795.
41. Garrett, D. S., Seok, Y. J., Peterkofsky, A., Clore, G. M. & Gronenborn, A. M. (1997). Identification by NMR of the binding surface for the histidine-containing phosphocarrier protein HPr on the N-terminal domain of enzyme I of the *Escherichia coli* phosphotransferase system. *Biochemistry*, **36**, 4393–4398.
42. Anastassopoulou, J., Banci, L., Bertini, I., Cantini, F., Katsari, E. & Rosato, A. (2004). Solution structure of the apo-and copper(I) loaded human metallo-chaperone HAH1. *Biochemistry*, **43**, 13046–13053.

Edited by M. F. Summers

(Received 10 May 2005; received in revised form 8 July 2005; accepted 12 July 2005)
Available online 27 July 2005

A hint for the function of human Sco1 from different structures

Lucia Banci*, Ivano Bertini*†, Vito Calderone*, Simone Ciofi-Baffoni*, Stefano Mangani*‡, Manuele Martinelli*, Peep Palumaa§, and Shenlin Wang*

*Magnetic Resonance Center and Department of Chemistry, University of Florence, Via Luigi Sacconi 6, 50019 Florence, Italy; ‡Department of Chemistry, Università degli Studi di Siena, Via Aldo Moro 1, 53100 Siena, Italy; and §Department of Gene Technology, Tallinn University of Technology, Akadeemia tee 15, 12618 Tallinn, Estonia

Edited by Joan Selverstone Valentine, University of California, Los Angeles, CA, and approved April 12, 2006 (received for review February 17, 2006)

The solution structures of apo, Cu(I), and Ni(II) human Sco1 have been determined. The protein passes from an open and conformationally mobile state to a closed and rigid conformation upon metal binding as shown by electrospray ionization MS and NMR data. The metal ligands of Cu(I) are two Cys residues of the CPXXCP motif and a His residue. The latter is suitably located to coordinate the metal anchored by the two Cys residues. The coordination sphere of Ni(II) in solution is completed by another ligand, possibly Asp. Crystals of the Ni(II) derivative were also obtained with the Ni(II) ion bound to the same His residue and to the two oxidized Cys residues of the CPXXCP motif. We propose that the various structures solved here represent the various states of the protein in its functional cycle and that the metal can be bound to the oxidized protein at a certain stage. Although it now seems reasonable that Sco1, which is characterized by a thioredoxin fold, has evolved to bind a metal atom via the di-Cys motif to act as a copper chaperone, the oxidized form of the nickel-bound protein suggests that it may also maintain the thioredoxin function.

cytochrome *c* oxidase | NMR | x-ray | assembly factor

Sco is a family of proteins ubiquitous to all kingdoms of life. Ortholog and paralog genome browsing has shown that one or more representative of this class are present in most bacterial and eukaryotic genomes (1, 2). In the bacterial operons, Sco proteins often are associated with copper enzymes, suggesting that they are involved in the maturation or functioning of such enzymes (1). Eukaryotic genomes contain two paralogs, Sco1 and Sco2 (3, 4), both involved in copper-dependent assembly of cytochrome *c* oxidase (CcO) (5). CcO contains two functional copper ions located in the binuclear Cu_A site and one located in the binuclear Cu_B-heme a_3 site (6). CcO is a multimeric enzyme complex embedded in the inner mitochondrial membrane of all eukaryotes and in the plasma membrane of prokaryotes, and it functions as terminal enzyme of the respiratory chain (7). Sco1 was first suggested to be involved in copper ion delivery to the CcO complex based on the observation that, in the presence of high copper concentrations, overexpression of either Sco1 or the homologous Sco2 can restore the CcO activity of *Saccharomyces cerevisiae* strains lacking the gene of the mitochondrial copper chaperone Cox17 (8). Yeast strains lacking Sco1 also are respiratory deficient, and an excess of copper and/or overexpression of either Cox17 or Sco2 cannot compensate for the Sco1-associated CcO deficiency (8). The absolute requirement of Sco1 in the activation of CcO indicates that Sco1 functions downstream from Cox17 in the delivery of copper to CcO. Indeed, *in vitro* Sco1 can receive copper from the copper chaperone Cox17 (9).

Human Sco1 (HSco1) is a 301-residue polypeptide anchored through a single helix to the inner mitochondrial membrane of eukaryotes (10). The functional part of the Sco1 protein is composed of a single soluble domain, located in C-terminal region, whereas the N terminus contains a mitochondrial-targeting sequence followed by a transmembrane helix (11). The structure of the soluble domain was first resolved by NMR for apoSco1 from *Bacillus subtilis* (12). The structure revealed a potential metal binding site constituted by two Cys residues present in a conserved motif CPXXCP and a fully conserved His residue, in agreement with earlier extended x-ray absorption fine structure investigations of yeast Cu(I)Sco1 (13). Besides extended x-ray absorption fine structure data many other spectroscopic data on the human, yeast, and *B. subtilis* Sco proteins have confirmed that the protein binds Cu(I), Cu(II), and other metal ions (14–17). The fold of apoSco1 protein, which contains four α-helices and seven β-strands organized in two β-sheets (12), is atypical for a metal chaperone given that it resembles the fold of thioredoxins, which are enzymes specialized for the reduction of protein disulfides (18). Also, the x-ray structures of the apo forms of the *B. subtilis* Sco1 and HSco1 proteins have been determined (16, 19). Some crystals of *B. subtilis* apoSco1 contained Sco1 with S—S bonds, thus supporting a role of the protein in redox processes. In addition, it has been recently suggested on the basis of the extreme sensitivity of the yeast *sco1*-null mutant to hydrogen peroxide that HSco1 might function as a mitochondrial redox signaling molecule (19). Thus, the specific role of Sco1 in maturation of CcO, either as a copper chaperone or connected with redox processes, is still elusive.

To date there are no structures available for any metallated forms of Sco1 proteins. The structure of the metal adducts is, however, crucial for understanding the mechanism of Sco-mediated copper insertion into CcO. We have succeeded in preparing a human Cu(I)Sco1 derivative [hereafter referred to as Cu(I)HSco1] *in vitro* and have determined its solution structure through NMR. We also have investigated the structure of the Ni(II) derivative of HSco1 as a model for the binding of bipositive metal ions like Cu(II). We would like to stress that NMR solution structure determination of metalloproteins is a difficult challenge as far as the protein metal-binding mode is concerned because NMR does not provide direct information on protein–metal interaction. In contrast, it is also common that the crystallization procedures might provide derivatives different than the physiological ones. Still, these derivatives may be significant as models of transient species and for the mechanism of action. Indeed, the x-ray structure of human Ni(II)Sco1 [hereafter referred to as Ni(II)HSco1], also reported here, displays a completely different metal binding with respect to the solution structure, being the metal bound to the S—S bond of the oxidized HSco1. Structural information for different conformers of the same protein is extremely valuable because individual structures often mimic transient species, which enable elucidation of the mechanism of protein action.

Conflict of interest statement: No conflicts declared.

This paper was submitted directly (Track II) to the PNAS office.

Abbreviaions: CcO, cytochrome *c* oxidase; ESI, electrospray ionization; HSco1, human Sco1; HSQC, heteronuclear single quantum correlation.

Data deposition: The atomic coordinates, structural restraints, chemical shifts, and structural factors have been deposited in the Protein Data Bank, www.pdb.org [PDB ID codes 2GT5 and 2GVP for apoSco1; 2GQM and 2GT6 for Cu(I)Sco1; and 2GQK, 2GQL, and 2GGT for Ni(II)Sco1].

†To whom correspondence should be addressed. E-mail: bertini@cerm.unifi.it.

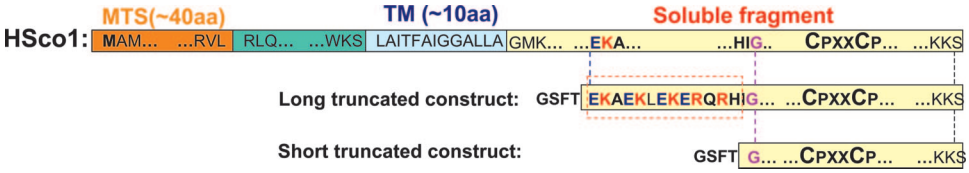

Fig. 1. Diagram of the protein sequence and cloned constructs of HSco1. The positions of the mitochondrial target sequence (MTS), transmembrane helix (TM), and the soluble fragment of HSco1 are orange, blue, and yellow, respectively. The N terminus of HSco1 protruding into the mitochondrial matrix is green. The soluble fragments used in the present study are named long and short truncated constructs. The truncates lack only the mitochondrial target sequence and transmembrane helix. The essential CPXXCP motif, the tobacco etch virus protease recognition site (GSFT), and the 14-aa segment (red dotted box) at the N terminus side are indicated in bold. The positively and negatively charged amino acids are represented in blue and red, respectively.

Here, we propose that the Cu(I)HSco1 species act as chaperones for copper ion delivery and that the specific oxidation of metal-ligating thiolates of HSco1 could have a role in the transfer of copper ions to CcO.

Results

Two truncated forms of the HSco1 gene have been engineered, both lacking the N-terminal mitochondrial targeting sequence and the single-transmembrane helix (Fig. 1). The two truncated forms differ by a 14-aa segment at the N-terminal side. This 14-aa segment is rich in positively and negatively charged residues and is predicted to be unstructured. Size-exclusion chromatography equipped with multiangle light scattering shows that the shorter apoHSco1 construct eluted in fractions corresponding to a monomeric state for the protein, whereas the longer construct eluted as a dimer (see Fig. 6, which is published as supporting information on the PNAS web site). This observation suggests that the residues separating the transmembrane helix from the folded domain are essential to promote dimerization. *In vivo* studies also have shown that this N-terminal region is crucial for yeast Sco1 function and cannot be replaced, even by its Sco2 counterpart (20).

For the structural and electrospray ionization (ESI)-MS characterization, the short construct of 170 aa (corresponding to residue segment 132–301) of the HSco1 gene was used. Additionally, this construct contains an additional 4-aa segment (GSFT), corresponding to the tobacco etch virus protease recognition site at the N terminus (Fig. 1), thus producing a final construct of 174 aa whose identity was confirmed by ESI-MS analysis. The ESI-MS spectrum of the oxidized apoWT-HSco1 showed two main peaks corresponding to +9 and +10 ions, and the deconvolution of the spectrum gave the expected molecular mass of 19,741.3 Da. Incubation of oxidized HSco1 with 1 mM DTT increased molecular mass by 2.3 Da (molecular mass = 19,743.9 Da), which indicates that the disulfide bridge in HSco1 could be reduced easily by 1 mM DTT.

Reconstitution of Fully Reduced HSco1 with Metal Ions. We are able to prepare HSco1 containing Cu(I) ions at 1:1, a ratio suitable for structural studies. Mass spectra of fully reduced HSco1 reconstituted at pH 7.5 with increasing concentrations of Cu(I) ions, are presented in Fig. 7, which is published as supporting information on the PNAS web site. Addition of one equivalent of Cu(I) ions to reduced HSco1 generates a new peak in MS spectrum, which corresponds to Cu_1HSco1 (Fig. 7). Addition of further equivalents of Cu(I) ions leads to a slight additional increase of the Cu_1HSco1 peak but does not induce metalloforms with higher metal stoichiometry (Fig. 7). We also showed that oxidized HSco1 does not form complex with Cu(II) ions in an ESI-MS experiment (Fig. 7), which indicates that such a complex, even if present in solution, is weak and dissociates during the ESI process. Accordingly, addition of Ni(II)Cl_2 to oxidized ^{15}N HSco1 does not affect the ^{1}H–^{15}N heteronuclear single quantum correlation (HSQC) spectrum. However, we have prepared the Cu(II) and Ni(II)HSco1 derivatives of reduced HSco1 in a 1:1 metal/protein ratio. The ultraviolet/visible (UV/VIS) and EPR spectra of Cu(II)HSco1 are identical to those recently reported (15). Similar UV/VIS spectra also were reported for bacterial Sco homologues (12, 14, 17) and Cu(II) nitrosocyanin (21, 22). In addition, the UV/VIS spectrum of Ni(II)HSco1 (Fig. 8, which is published as supporting information on the PNAS web site) is similar to that reported for the *B. subtilis* and *Rhodobacter sphaeroides* homologues (14, 17), with two weak bands at 380 and 540 nm, respectively, correlating with the two low-energy bands of the Cu(II)HSco1 spectrum although shifted to lower energy (Fig. 8). The intense thiolate-Ni(II) charge transfer band (23) is also red-shifted at 304 nm with respect to the Cu(II)HSco1 spectrum (Fig. 8).

The aggregation state and the conformational properties of the Cu(I) and Ni(II)HSco1 forms have been investigated by multiple techniques, including size-exclusion chromatography, ESI-MS, and NMR. In NMR, ^{15}N relaxation rates are modulated by the correlation time for the protein tumbling (τ_m), which is directly related to the molecular weight of the protein, thus monitoring its aggregation state (24). The correlation times of Cu(I)HSco1 and Ni(II)HSco1 proteins (at millimolar concentrations) are 14.5 ± 1.1 ns and 15.6 ± 1.2, respectively, as expected for a protein of this size in a monomeric state. These values also are similar to the τ_m of apoHSco1 (13.8 ± 1.6 ns), which reorients in solution as a monomeric protein as shown by size-exclusion chromatography and multiangle light scattering experiments. ESI-MS experiments conducted at a 1.8 μM concentration of protein did not detect any higher aggregates for apoHSco1 or Cu_1HSco1. ESI-MS spectra and, especially, the charge-state distribution of ions also can yield information about the conformational states of proteins under a variety of conditions (25). Upon the binding of Cu(I), the charge state distribution of Cu_1HSco1 species shifted toward ions with lower charges (+9 and +8), which indicates that binding of metal induces a conformation change of the protein to a more compact state (Fig. 7).

Cu(I), Ni(II), and apoHSco1 Solution Structures. The solution structures of Cu(I)HSco1 and Ni(II)HSco1 (Fig. 2) were determined by using distance and angle restraints as obtained from 2D and 3D heteronuclear NMR experiments (Table 1, which is published as supporting information on the PNAS web site). The overall fold of Cu(I)HSco1 and Ni(II)HSco1 structures is the same as that of the crystal structure of apoHSco1 (19) and contains four α-helices and nine β-strands organized into the thioredoxin fold. The solution structure of apoHSco1 also displays the same global thioredoxin fold. However, the β-hairpin present in the extended, solvent-exposed loop-8 region does not form anymore (Fig. 2).

Cu(I) is coordinated by the two Cys residues of the CPXXCP conserved motif, shared by the third loop and helix α1, and by the conserved His-260 (Fig. 2), located in the seventh β-strand, as shown by $^2J_{NH}$ coupling-based ^{1}H–^{15}N HSQC experiments

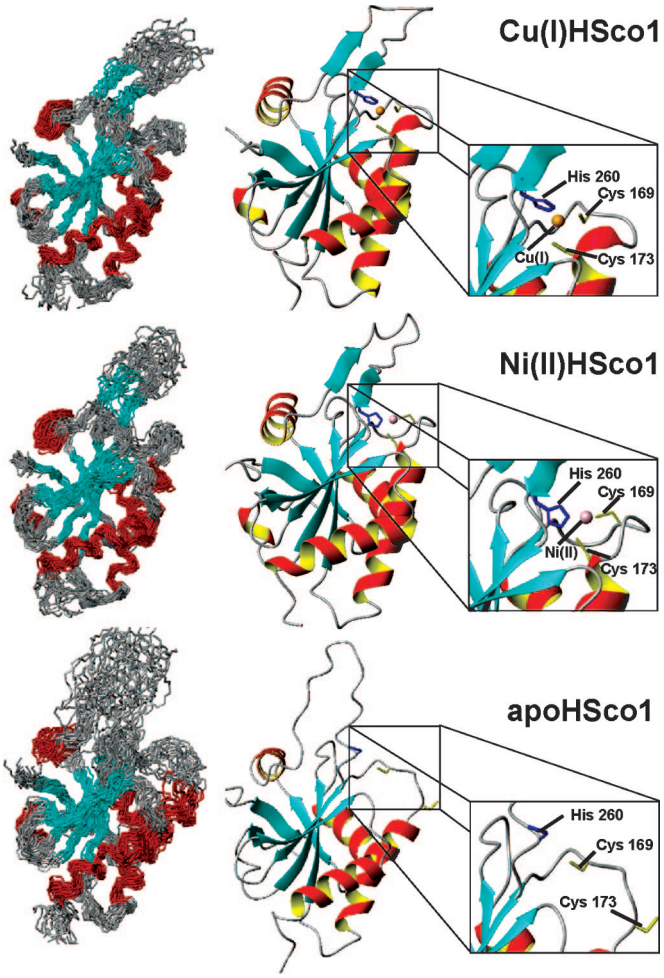

Fig. 2. Solution structures of human Cu(I), Ni(II), and apoSco1. (*Left*) The superimposition of 20 structures of Cu(I), Ni(II) and apoHSco1 are shown. α-helices and β-strands are colored in red and cyan, respectively. (*Right*) The average structures of the lowest energy ensemble are shown. The metal-binding residues Cys-169, Cys-173, and His-260 are shown in yellow and blue, respectively. Cu(I) and Ni(II) ions are depicted as orange and pink spheres, respectively.

(Fig. 9, which is published as supporting information on the PNAS web site). From these experiments, it appears that, in Cu(I)HSco1, His-260 acquires a preferential conformation where $N^{\delta 1}$ is protonated and $N^{\varepsilon 2}$ is coordinated to the metal ion. The involvement in the metal binding of residues from two different regions of the protein produces a compact state of protein with respect to the apo form, in agreement with observations in ESI-MS experiments. Backbone NH resonances of three regions comprising residues 166–180, 202–204, and 244–264 are indeed not detected in the ^{1}H–^{15}N HSQC spectrum of apoHSco1, although they are present in both Cu(I) and Ni(II)HSco1 spectra. These three regions comprise the CPXXCP metal-binding motif and the surrounding loops 5 and 8, the latter containing the third ligand, His-260. The inability to detect the backbone NH signals listed above is because of their fast exchange with the bulk solvent or because of the presence of multiple backbone conformations in the metal-binding area of apoHSco1, whereas the metal binding is able to "freeze" these regions in a more rigid conformation. In particular, the large conformational variability of the long loop 8 observed in the apoHSco1 solution structure (no long-range nuclear Overhauser effects are detected in loop 8) indicates that backbone structural

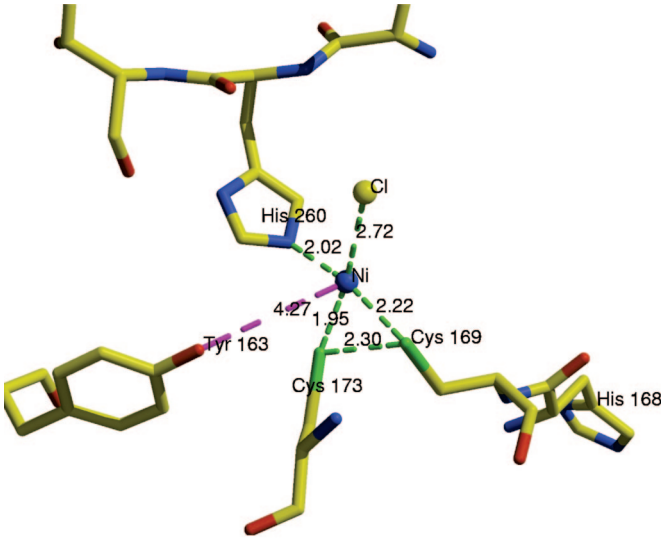

Fig. 3. The distorted square planar coordination of nickel as present in the x-ray structure of oxidized Ni(II)HSco1. Bonding distances between nickel and the coordinating moieties are shown in green along with the distance between the two Cys residues. The distance between the nickel ion and the OH oxygen of Tyr-163 is also shown in magenta, and it is too large to be considered a bonding interaction.

changes are necessary to locate the metal ligand His-260 in the vicinity of the other two ligands, Cys-169 and Cys-173 (Fig. 2). Analysis of backbone dynamics (Fig. 10, which is published as supporting information on the PNAS web site) also is in agreement with the latter picture and demonstrates that both metallated forms of HSco1 do not display extensive motions on both milli- to microsecond and/or nano- to picosecond time scales, with the exception of the C and N termini.

When reduced, HSco1 binds a divalent cation, as Ni(II), and the metal is still bound by the two Cys residues of the CPXXCP motif and by His-260 through the $N^{\varepsilon 2}$ atom (Fig. 2), as confirmed by ^{2}J ^{1}H–^{15}N HSQC NMR experiments. Because Ni(II) is expected to be at least four-coordinated, it is feasible that a forth ligand is completing its coordination sphere. This ligand could be a water molecule or a residue donated by the protein. The solution structure of Ni(II)HSco1 shows that two acidic groups (Asp-171 and Asp-259) could complete the Ni(II) coordination sphere, but our data do not allow discrimination between these two possibilities.

Ni(II)HSco1 Crystal Structure. Crystals of the Ni(II)HSco1 derivative also were obtained in aerobic conditions. The overall structure of the Ni(II)HSco1 complex is essentially superimposable with that of apoHSco1 [Protein Data Bank (PDB) ID code 1WP0] (19), which was used as the model in the molecular replacement. The main exception is the solvent exposed a region involving residues 240–260 (loop 8 and the β-hairpin), ending with the metal-binding His-260. This loop indeed acquires a more ordered conformation as a consequence of the metal binding, according to the behavior in solution; this greater stability is confirmed by the good quality of the electron density map in that region for both molecules in the asymmetric unit, which is indeed better than that observed in the apoHSco1 crystal structure (19). A further confirmation is the significantly lower temperature factors of the atoms belonging to the above-mentioned loop in the structure of Ni(II)HSco1 with respect to those of the crystal structure of apoHSco1 (19).

The coordination sphere of Ni(II) in the crystal structure of Ni(II)HSco1 is quite odd and unexpected. In this structure, the

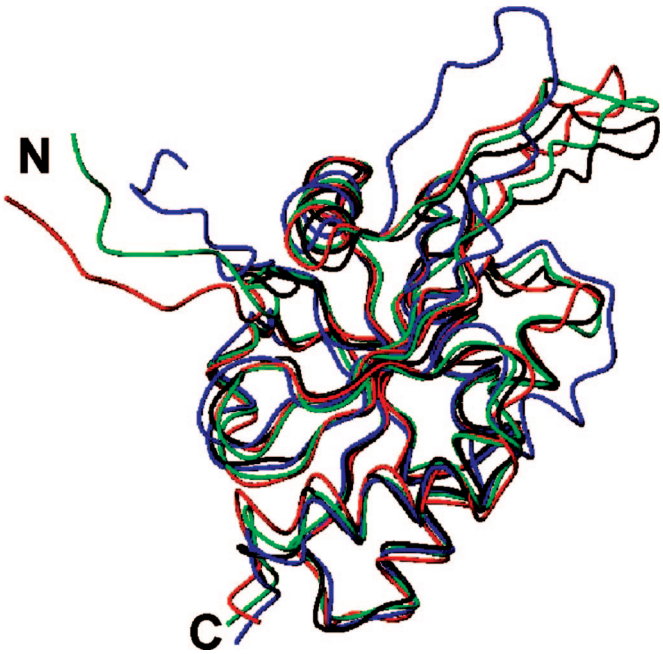

Fig. 4. Overlay of the backbone of apo (blue), Cu(I) (green), and Ni(II) (red) HSco1 solution structures and of Ni(II) (black) HSco1 x-ray structure.

two metal-binding Cys residues are oxidized and form a disulfide bond (Fig. 3; see also Fig. 11, which is published as supporting information on the PNAS web site) and therefore not capable of binding the Ni(II) ion as thiolates. Still, the metal ion remains in contact with the S—S bridge with a Ni—S distance of 2.0–2.2 Å, suggesting the formation of bonds with the available lone pairs of sulfur atoms (Fig. 3). The coordination sphere of Ni(II) is completed by His-260 ($N^{\varepsilon 2}$—Ni, 2.03–2.45 Å), in agreement with the solution structure of Ni(II)HSco1, and a water molecule or more likely an anion such as Cl^- arranged in a distorted square planar geometry.

We have been able to trace one case only in the PDB of a nickel ion coordinated to Cys residues (PDB ID code 1FRF) that are at bonding distance; in this case, the metal-binding site is dinuclear (iron and nickel) and is made of four Cys residues pointing toward two metal ions that are at a distance of 3.2 Å from each other. Cys-75 and Cys-546 are at interaction distance (2.4 Å), whereas Cys-72 and Cys-543 are farther apart (3.0 Å) (26). The distances between nickel and the four sulfur atoms are as follows: Cys-72–Ni, 2.15 Å; Cys-543–Ni, 2.11 Å; Cys-75–Ni, 1.61 Å; and Cys-546–Ni, 2.44 Å.

Discussion

The solution and crystal structures of the metal derivatives of HSco1 are completely superimposable along the entire amino acid sequence (Fig. 4) (backbone rms deviation to the new structure within 0.8 Å). These structures also are very similar to the solution structure of apoHSco1 with the exception of loop 8, which displays a different backbone conformation in apoHSco1, positioning the imidazole ring of His-260 at ≈10 Å from the sulfur atoms of the metal binding Cys residues (Fig. 4). In addition, helix $\alpha 2$, which encompasses the CPXXCP metal-binding site at its N terminus, is tilted in the apo solution structure with respect to the structure of the metallated HSco1 (Fig. 4). From the NMR structures, it appears that the apo form is highly disordered around the metal binding site, sampling more open conformations than in the metallated forms (Fig. 2). This observation also agrees with the results of conformation analysis by ESI-MS. In the x-ray structure of apoHSco1 (19), however, the protein is frozen in a specific conformation that does not reflect the real condition in solution. Therefore, metal binding is accompanied by a relatively large, albeit localized, effect on the protein structure, mainly involving loop 8: From an open conformation with local disorder, the structure converts into a well defined, compact state in which a metal ion is bound. In particular, the presence of the His ligand, suitably located in loop 8 to coordinate both divalent and monovalent metal ions, is important to modulate the order and disorder state of loop 8 observed in the metallated and apo forms, respectively. Also taking into account that disordered regions in protein structure often are engaged in protein–protein interactions (27), one may speculate that loop 8 modulates association–dissociation of HSco1 with its partner, the Cu(I) chaperone Cox17. For example, it is possible that, once Cu(I)Cox17 interacts transiently with apoHSco1 and donates its copper cargo to HSco1, loop 8 structurally rearranges and allows His binding and concomitant formation of the compact Cu(I)HSco1 structure, which might not exchange copper with Cox17. The formation of the stable, compact Cu(I)HSco1 state could thus constitute the important driving force of the copper transfer from Cox17 to HSco1.

Biological Context. The debate on whether HSco1 is a metalloprotein or a thioredoxin can significantly be advanced in light of the structural results presented here. HSco1 forms 1:1 complexes with the Cu(I) and Ni(II) ions by exploiting the same metal binding ligands, which confirms that HSco1 is suitable for binding both monovalent and divalent metal ions (15). Reduced HSco1 also can bind one equivalent of Cu(II); however, the reconstituted Cu(II)HSco1 complex shows two different coordination environments with different populations (15). Similar results on Cu(II)Sco1 complexes also were obtained for the *B. subtilis* and yeast proteins (12, 15). It is therefore reasonable to assign a copper chaperone role to HSco1, the metal ion being coordinated by two Cys residues and one His residue. A similar metal-binding site also is found in another copper chaperone, i.e., the ATX1 from *Synecocystis* (28). Similarly to the latter system, the metal-donating and the metal-receiving coordination sites are different, thus overcoming the condition that "donor" and "recipient" protein partners in metal transfer processes need metal-binding sites similar in structure, as recently suggested (29). The presence of three ligands, one of each being a "flexible" His residue, also makes the site suitable for the binding of divalent metal ions. Indeed, Cu(II), Ni(II), and, presumably, Zn(II) (14) can bind at the same site of HSco1. In the case of a divalent metals, the coordination can be completed by an additional exogenous ligand, e.g., H_2O, or by a protein carboxylate. The latter hypothesis is supported by the observation that the affinity of HSco1 for the Cu(II) ion is reduced if Asp-259 is mutated (15).

The fold of HSco1 is similar to that of redox-active proteins like thioredoxins and peroxiredoxins, with the metal-binding Cys residues located at the same positions as the conserved catalytic Cys residues in thioredoxins. This feature became apparent when the first structure of a Sco1 homolog was solved (12). Therefore, a thioredoxin fold has evolved as a metal chaperone to bind the metal atom via the di-Cys motif, and one may speculate that the thioredoxin function is still maintained. Indeed, apoHSco1 can be easily oxidized to form S—S bonds. In this research, we also have shown that, in the oxidized form, the protein has low affinity for metal ions because their addition did not affect the ^1H–^{15}N HSQC spectrum of oxidized apoHSco1, and no metal adduct has been detected by ESI-MS experiments. In the PDB, only one example of a metal ion bound to an oxidized S—S bond is reported (26). Therefore, it is feasible that the present crystal structure of the nickel derivative of oxidized HSco1 represents the transient copper-delivery complex, which might exist just before the copper is transferred to the Cu_A site of the COXII subunit. Indeed, biochemical and genetic studies on yeast Sco1

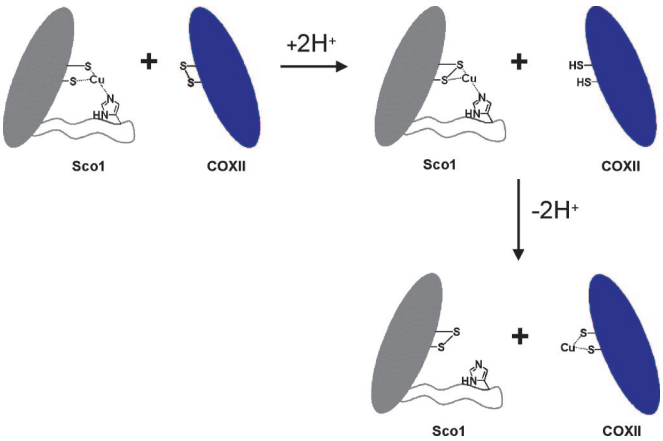

Fig. 5. Proposed mechanism for copper transfer from HSco1 to the COXII subunit of CcO. This model implies that HSco1 may form a transient species characterized by an oxidized S—S moiety still able to interact with a copper ion. This state might exist just before the copper is transferred to the Cu_A site of CcO. In the metal transfer mechanism, HSco1 also can work as a thioredoxin in the reduction of the Cys residues in the Cu_A site of COXII. At this stage, the oxidization state of copper during the metal transfer cannot be assessed. The Cu_A site of the COXII subunit can indeed accept both Cu(I) and Cu(II) ions from HSco1. Broken lines indicate the metal coordination bonds.

demonstrated its ability for direct interaction with the COXII subunit (30, 31). Because numerous proteins in the mitochondrial intermembrane space have disulfide bonds (32–34), the two Cys residues of the Cu_A site of COXII may also require reduction before metal transfer. The same requirement applies to the bacteria in which the COXII subunit is exposed to oxidizing periplasmatic or extracelluar environments. Therefore, it may be argued that Sco1 participates, along with metal transfer, in the reduction of the Cu_A site of COXII and its metal-transfer mechanism might include the following steps: (*i*) CuHSco1 interacts with the oxidized COXII and reduces the Cys residues of the Cu_A site as a thioredoxin, and (*ii*) the oxidized HSco1 protein transfers Cu to the reduced Cu_A site (Fig. 5). The oxidized apoHSco1 could be reduced before the next metal transfer and its reduction can be performed by another thioredoxin-like protein, such as HSco2, which is known to play a key role in Cu_A formation (35), or by cytochrome *c*, an electron-transfer protein that is found in the same operon of Sco1 homologs in some bacteria or is fused to some Sco1 paralog proteins (1). The copper delivery process therefore seems to involve several proteins in a complex molecular mechanism that requires further investigation. Interestingly, a dual functional role in the assembly mechanism of the copper enzyme superoxide dismutase has been similarly proposed for its copper chaperone CCS, which is, along with the copper donation, involved in the formation of an intramolecular disulfide essential for superoxide dismutase activity (36).

Concluding Remarks. We have succeeded in preparing Cu(I) and Ni(II) derivatives of HSco1 and determined their solution structures. The solution structure of apoHSco1 also has been determined. The structures confirm that the metal ions are bound by two Cys residues and one His residue, and they show the transition from a locally disordered apo protein to a compact metallated form, as confirmed by ESI-MS studies. We also obtained crystals of Ni(II)HSco1, which suggest the binding of the metal ion to the oxidized form of HSco1. This species may represent a transition state of the copper transfer from HSco1 to the Cu_A site of COXII. This transient species may present a missing link that integrates the metal transfer and thioredoxin functions already proposed for this fascinating protein. A similar mechanism of copper transfer also has been previously suggested for the bacterial Sco1 homologue PrrC from *Rhodobacter sphaeroides* (17).

Methods

Protein Preparation and Characterization. Long and short soluble domains of HSco1 (lacking the first 351 and 393 bp, respectively, corresponding to residues 1–117 and 1–131) were amplified by PCR, cloned into the Gateway Entry vector pENTR/tobacco etch virus/D-TOPO (Invitrogen), and subcloned into pETG-30A (European Molecular Biology Laboratory Protein Expression and Purification Facility) by Gateway LR reaction to generate N-terminal, His-GST fused proteins. The proteins were expressed in *Escherichia coli* BL21-Gold(DE3) cells (Stratagene), which were grown in LB and minimal medium [$(^{15}NH_4)_2SO_4$ and/or [^{13}C]-glucose] for the production of labeled samples. Purification was performed by using a HiTrap chelating HP column (Amersham Pharmacia Biosciences) charged with Zn(II). His-GST tag was cleaved with AcTEV, and separated from the C-terminal domain with a second purification step. After this purification, the protein preparations showed a single component by SDS/PAGE with <5% of copper bound to the protein, as checked through ESI-MS spectrometry. DTT was added to the apoprotein in a 10 mM concentration to reduce the Cys residues of the CPXXCP motif before metal reconstitution. The Cu(I), Cu(II), Ni(II) metallated forms were obtained by addition of stoichiometric amounts of the metal ions {as $[Cu(I)(CH_3CN)_4]PF_6$, $CuSO_4$, and $NiCl_2$} to diluted protein solutions in 50 mM phosphate buffer at pH 7.2, followed by protein concentration under nitrogen atmosphere. The metal content was finally determined by inductively coupled plasma MS.

Electronic spectra on the metal derivatives were recorded on a Cary 50 spectrophotometer (Varian). EPR spectra on Cu(II)HSco1 were recorded at 180 K on an Elexsys E500 spectrometer (Bruker) equipped with a X-band microwave bridge (microwave frequency, 9.45 GHz) and an ER 4131 VT unit for temperature control. To investigate the aggregation state of HSco1, 0.5–1 mM protein samples were run on a Superdex75 HR-10/30 size-exclusion column on an AKTA-FPLC system (Amersham Pharmacia Biosciences) connected with a multiangle light scattering (DAWN-EOS, Wyatt Technologies, Santa Barbara, CA) coupled with quasielastic light-scattering detectors.

Before ESI-MS experiments, purified apoHSco1 protein was brought into 50 mM ammonium acetate buffer (pH 7.5) by using a HiPrep26/10 desalting column (Amersham Pharmacia Biosciences). In MS experiments, 1.8 μM protein samples were infused by a syringe pump at 15 μl/min into an Ettan API ESI-TOF mass spectrometer (Amersham Pharmacia Biosciences). Mass spectra were recorded during 2–3 min at a capillary exit voltage of 150 V. apoHSco1 was reduced by addition of 0.5 or 1.0 mM DTT at 25°C. Reconstitution of apoHSco1 with copper was conducted as follows. First, Cu(II) acetate was dissolved at 150 μM concentration in argon-saturated 50 mM ammonium acetate, pH 7.5, and Cu(II) was reduced to Cu(I) by addition of 0.5 mM DTT. Different equivalents of freshly prepared Cu(I)DTT complex were added to the apoHSco1 samples (protein concentration, 1.8 μM), the mixture was incubated for 1 min at 25°C, and ESI-MS spectra were recorded as described above.

Solution Structures Determination. NMR spectral assignment and structure determination were obtained through the experiments listed in Table 1, which also indicates the magnetic fields at which they were collected. Overall, the resonances of 95% of carbon atoms, 97% of nitrogen atoms, and 90% of protons were assigned in Cu(I)HSco1 and Ni(II)HSco1 (deposited in the Protein Data Bank database). In the case of apo form, the resonances of 85% of carbon atoms, 80% of nitrogen atoms, and 80% of proton

atoms were assigned. The ^{1}H, ^{13}C, and ^{15}N resonance assignments of the apo, Cu(I), and Ni(II)HSco1 forms are reported, respectively, in Tables 2–4, which are published as supporting information on the PNAS web site. The His ring protons were assigned through a ^{1}H–^{15}N HSQC experiment tailored to the detection of ^{2}J ^{1}H–^{15}N couplings and from the analysis of the ^{13}C-NOESY-HSQC spectra. For all His residues, all of the nonexchangeable protons were assigned in Cu(I)HSco1 and Ni(II)HSco1. The exchangeable proton of the metal-binding ligand, His-260, also was detected in both metallated forms. R_1 and R_2 ^{15}N relaxation rates and ^{1}H–^{15}N nuclear Overhauser effects (with and without ^{1}H saturation) (Table 1) were measured at 298K on Avance 500 and 600 MHz Bruker spectrometers and then analyzed by using a standard procedure (37). After conversion of the NMR data in structural constraints [3,035, 2,776 and 2,066 meaningful proton–proton distances, together with 85 ψ and 83 ϕ angle constraints for Cu(I)HSco1, Ni(II)HSco1, and apoHSco1, respectively], the structures were calculated using the program DYANA (38). The best 30 structures of the DYANA family were then subjected to restrained energy minimization with AMBER 8.0 (39). The force-field parameters for the metal ions were adapted from similar systems (40, 41). The statistical analysis of the restrained energy minimization family of apoHSco1, Cu(I)HSco1, and Ni(II)HSco1 structures are reported, respectively, in Tables 5, 6, and 7, which are published as supporting information on the PNAS web site. The programs PROCHECK and PROCHECK-NMR (42, 43) were used in the evaluation of the quality of the structures. More than 90% of residues were located in the allowed regions of the Ramachandran plot.

Crystallization, Data Collection, and Structure Solution. Crystals of Ni(II)HSco1 grew at 20°C from a 0.1 M Tris·HCl/30% polyethylene glycol 6000 solution at pH 8.5 by the vapor diffusion technique. The final protein concentration was ≈10 mg/ml. The data set was collected by using synchrotron radiation at beamline ID-29 (European Synchrotron Radiation Facility, Grenoble, France) at 100 K, with the crystal cryocooled, in the presence of 10–15% of ethylen glycol. The Ni(II)HSco1 crystal diffracted up to 2.5-Å resolution and belongs to space group $P2_12_12_1$ (a = 51.46 Å, b = 52.44 Å, c = 136.41 Å) with two molecules in the asymmetric unit, a solvent content of 47.1%, and a mosaicity of 0.7°. The structure was solved by using the molecular replacement technique, with the structure of the apoHSco1 (PDB ID code 1WP0) as starting model.

The Ramachandran plot of the refined model shows that 97.5% of residues are in allowed regions of the plot, 2.5% of residues are in generously allowed, and no residues are in disallowed regions. Table 8, which is published as supporting information on the PNAS web site, reports the data collection and refinement statistics.

We thank Dr. Rannar Sillard (Karolinska Institute, Stockholm) for providing access to ESI-MS instruments. This work was supported by European Community "Structural Proteomics in Europe" Grant QLG2-CT-2002-00988, by Marie Curie Host Fellowship MEST-CT-2004-504391 for early stage research training ("NMR in Inorganic Structural Biology"), Estonian Science Foundation Grant 5635, and by Ente Cassa Risparmio di Firenze.

1. Arnesano, F., Banci, L., Bertini, I. & Martinelli, M. (2005) *J. Proteome Res.* **4,** 63–70.
2. Chinenov, Y. V. (2000) *J. Mol. Med.* **78,** 239–242.
3. Schulze, M. & Rodel, G. (1989) *Mol. Gen. Genet.* **216,** 37–43.
4. Smits, P. H., de Hann, M., Maat, C. & Grivell, L. A. (1994) *Yeast* **10,** 75–80.
5. Carr, H. S. & Winge, D. R. (2003) *Acc. Chem. Res.* **36,** 309–316.
6. Tsukihara, T., Aoyama, H., Yamashita, E., Tomizaki, T., Yamaguchi, H., Shinzawa-Itoh, K., Nakashima, R., Yaono, R. & Yoshikawa, S. (1996) *Science* **272,** 1136–1144.
7. Khalimonchuk, O. & Rodel, G. (2005) *Mitochondrion* **5,** 363–388.
8. Glerum, D. M., Shtanko, A. & Tzagoloff, A. (1996) *J. Biol. Chem.* **271,** 20531–20535.
9. Horng, Y. C., Cobine, P. A., Maxfield, A. B., Carr, H. S. & Winge, D. R. (2004) *J. Biol. Chem.* **279,** 35334–35340.
10. Buchwald, P., Krummeck, G. & Rodel, G. (1991) *Mol. Gen. Genet.* **229,** 413–420.
11. Beers, J., Glerum, D. M. & Tzagoloff, A. (2002) *J. Biol. Chem.* **277,** 22185–22190.
12. Balatri, E., Banci, L., Bertini, I., Cantini, F. & Ciofi-Baffoni, S. (2003) *Structure (London)* **11,** 1431–1443.
13. Nittis, T., George, G. N. & Winge, D. R. (2001) *J. Biol. Chem.* **276,** 42520–42526.
14. Andruzzi, L., Nakano, M., Nilges, M. J. & Blackburn, N. J. (2005) *J. Am. Chem. Soc.* **127,** 16548–16558.
15. Horng, Y. C., Leary, S. C., Cobine, P. A., Young, F. B., George, G. N., Shoubridge, E. A. & Winge, D. R. (2005) *J. Biol. Chem.* **280,** 34113–34122.
16. Ye, Q., Imriskova-Sosova, I., Hill, B. C. & Jia, Z. (2005) *Biochemistry* **44,** 2934–2942.
17. McEwan, A. G., Lewin, A., Davy, S. L., Boetzel, R., Leech, A., Walker, D., Wood, T. & Moore, G. R. (2002) *FEBS Lett.* **518,** 10–16.
18. Arner, E. S. & Holmgren, A. (2000) *Eur. J. Biochem.* **267,** 6102–6109.
19. Williams, J. C., Sue, C., Banting, G. S., Yang, H., Glerum, D. M., Hendrickson, W. A. & Schon, E. A. (2005) *J. Biol. Chem.* **280,** 15202–15211.
20. Lode, A., Paret, C. & Rodel, G. (2002) *Yeast* **19,** 909–922.
21. Arciero, D. M., Pierce, B. S., Hendrich, M. P. & Hooper, A. B. (2002) *Biochemistry* **41,** 1703–1709.
22. Basumallick, L., Sarangi, R., DeBeer George, S., Elmore, B., Hooper, A. B., Hedman, B., Hodgson, K. O. & Solomon, E. I. (2005) *J. Am. Chem. Soc.* **127,** 3531–3544.
23. Maroney, M. J., Choudhury, S. B., Bryngelson, P. A., Mirza, S. A. & Sherrod, M. J. (1996) *Inorg. Chem.* **35,** 1073–1076.
24. Bruschweiler, R. (2003) *Curr. Opin. Struct. Biol.* **13,** 175–183.
25. Eyles, S. J. & Kalatshov, I. A. (2004) *Methods* **34,** 88–99.
26. Rousset, M., Montet, Y., Guigliarelli, B., Forget, N., Asso, M., Bertrand, P., Fontecilla-Camps, J. C. & Hatchikian, E. C. (1998) *Proc. Natl. Acad. Sci. USA* **95,** 11625–11630.
27. Dyson, H. J. & Wright, P. E. (2005) *Nat. Rev. Mol. Cell. Biol.* **6,** 197–208.
28. Banci, L., Bertini, I., Borrelly, G. P. M., Ciofi-Baffoni, S., Robinson, N. J. & Su, X. C. (2004) *J. Biol. Chem.* **279,** 27502–27510.
29. Rosenzweig, A. C. (2001) *Acc. Chem. Res.* **34,** 119–128.
30. Lode, A., Kuschel, M., Paret, C. & Rodel, G. (2000) *FEBS Lett.* **485,** 19–24.
31. Dickinson, E. K., Adams, D. L., Schon, E. A. & Glerum, D. M. (2000) *J. Biol. Chem.* **275,** 26780–26785.
32. Hofmann, S., Rothbauer, U., Muhlenbein, N., Baiker, K., Hell, K. & Bauer, M. F. (2005) *J. Mol. Biol.* **353,** 517–528.
33. Field, L. S., Furukawa, Y., O'Halloran, T. V. & Culotta, V. C. (2003) *J. Biol. Chem.* **278,** 28052–28059.
34. Sturtz, L. A., Diekert, K., Jensen, L. T., Lill, R. & Culotta, V. C. (2001) *J. Biol. Chem.* **276,** 38084–38089.
35. Leary, S. C., Kaufman, B. A., Pellecchia, G., Guercin, G. H., Mattman, A., Jaksch, M. & Shoubridge, E. A. (2004) *Hum. Mol. Genet.* **13,** 1839–1848.
36. Furukawa, Y., Torres, A. S. & O'Halloran, T. V. (2004) *EMBO J.* **23,** 2872–2881.
37. Peng, J. W. & Wagner, G. (1992) *J. Magn. Reson.* **98,** 308–332.
38. Güntert, P., Mumenthaler, C. & Wüthrich, K. (1997) *J. Mol. Biol.* **273,** 283–298.
39. Case, D. A., Darden, T. A., Cheatham, T. E., Simmerling, C. L., Wang, J., Duke, R. E., Luo, R., Merz, K. M., Wang, B., Pearlman, D. A., *et al.* (2004) AMBER (Univ. of California, San Francisco), Version 8.0.
40. Poger, D., Fuchs, H. J. R., Nedev, H., Ferrand, M. & Crouzy, S. (2005) *FEBS Lett.* **579,** 5287–5292.
41. Banci, L., Bertini, I., Bruni, B., Carloni, P., Luchinat, C., Mangani, S., Orioli, P. L., Piccioli, M., Rypniewski, W. & Wilson, K. (1994) *Biochem. Biophys. Res. Commun.* **202,** 1088–1095.
42. Laskowski, R. A., Rullmann, J. A. C., MacArthur, M. W., Kaptein, R. & Thornton, J. M. (1996) *J. Biomol. NMR* **8,** 477–486.
43. Laskowski, R. A., MacArthur, M. W., Moss, D. S. & Thornton, J. M. (1993) *J. Appl. Crystallogr.* **26,** 283–291.

Corrections

IN THIS ISSUE, MEDICAL SCIENCES. For the "In This Issue" summary entitled "Mammary tumors arrested in mice by deleting Notch" appearing in issue 24, June 13, 2006, of *Proc. Natl. Acad. Sci. USA* (**103,** 8907–8908), the title of the summary appeared incorrectly and should read "Mammary tumors arrested in mice by deleting *Myc*."

www.pnas.org/cgi/doi/10.1073/pnas.0605124103

CHEMISTRY. For the article "A hint for the function of human Sco1 from different structures," by Lucia Banci, Ivano Bertini, Vito Calderone, Simone Ciofi-Baffoni, Stefano Mangani, Manuele Martinelli, Peep Palumaa, and Shenlin Wang, which appeared in issue 23, June 6, 2006, of *Proc. Natl. Acad. Sci. USA* (**103,** 8595–8600; first published May 30, 2006; 10.1073/pnas.0601375103), the authors note that, due to a printer's error, the first sentence of the *Discussion* on page 8598, "The solution and crystal structures of the metal derivatives of HSco1 are completely superimposable along the entire amino acid sequence (Fig. 4) (backbone rms deviation to the new structure within 0.8 Å)," should read: "The solution and crystal structures of the metal derivatives of HSco1 are completely superimposable along the entire amino acid sequence (Fig. 4) (backbone rms deviation to the mean structure within 0.8 Å)." This error does not affect the conclusions of the article.

www.pnas.org/cgi/doi/10.1073/pnas.0605020103

EVOLUTION. For the article "Naked corals: Skeleton loss in Scleractinia," by Mónica Medina, Allen G. Collins, Tori L. Takaoka, Jennifer V. Kuehl, and Jeffrey L. Boore, which appeared in issue 24, June 13, 2006, of *Proc. Natl. Acad. Sci. USA* (**103,** 9096–9100; first published June 5, 2006; 10.1073/pnas.0602444103), the caption for the issue cover image appeared incorrectly, due to a PNAS error. The online version has been corrected. The corrected cover caption appears below.

Cover image: Oral view of the naked coral *Discosoma* sp. (Cnidaria: Anthozoa: Hexacorallia: Corallimorpharia). This coral species inhabits shallow tropical waters in the Indo-Pacific Sea. Corallimorpharians like this one appear to be scleractinian stony corals that, during the Cretaceous period, lost the ability to precipitate a calcium carbonate skeleton. See the article by Medina *et al.* on pages 9096–9100. Image courtesy of Mónica Medina and David Keys (Joint Genome Institute, Walnut Creek, CA).

www.pnas.org/cgi/doi/10.1073/pnas.0604989103

MEDICAL SCIENCES. For the article "Anomalous levels of Cl^- transporters in the hippocampal subiculum from temporal lobe epilepsy patients make GABA excitatory," by E. Palma, M. Amici, F. Sobrero, G. Spinelli, S. Di Angelantonio, D. Ragozzino, A. Mascia, C. Scoppetta, V. Esposito, R. Miledi, and F. Eusebi, which appeared in issue 22, May 30, 2006, of *Proc. Natl. Acad. Sci. USA* (**103,** 8465–8468; first published May 18, 2006; 10.1073/pnas.0602979103), the authors note that the last sentence of the Abstract, "We conclude that the anomalous expression of both Cl^- transporters, KCC1 and NKCC2, in TLE hippocampal subiculum probably causes altered Cl^- transport in the 'epileptic' neurons, as revealed in the microtransplanted *Xenopus* oocytes, and renders GABA aberrantly 'exciting,' a feature that may contribute to the precipitation of epileptic seizures," should read: "We conclude that the anomalous expression of both Cl^- transporters, NKCC1 and KCC2, in TLE hippocampal subiculum probably causes altered Cl^- transport in the 'epileptic' neurons, as revealed in the microtransplanted *Xenopus* oocytes, and renders GABA aberrantly 'exciting,' a feature that may contribute to the precipitation of epileptic seizures." This error does not affect the conclusions of the article.

www.pnas.org/cgi/doi/10.1073/pnas.0604971103

MICROBIOLOGY. For the article "Two major classes in the M protein family in group A streptococci," by Paul O'Toole, Lars Stenberg, Marianne Rissler, and Gunnar Lindahl, which appeared in issue 18, September 15, 1992, of *Proc. Natl. Acad. Sci. USA* (**89,** 8661–8665), the author name Paul O'Toole should have appeared as Paul W. O'Toole. The online version has been corrected. The corrected author line appears below.

Paul W. O'Toole, Lars Stenberg, Marianne Rissler, and Gunnar Lindahl

www.pnas.org/cgi/doi/10.1073/pnas.0604596103

Human Sco1 functional studies and pathological implications of the P174L mutant

Lucia Banci*†, Ivano Bertini*‡, Simone Ciofi-Baffoni*, Iliana Leontari*, Manuele Martinelli*, Peep Palumaa§, Rannar Sillard§¶, and Shenlin Wang*

*Magnetic Resonance Center (CERM) and Department of Chemistry, University of Florence, Via Luigi Sacconi 6, 50019 Sesto Fiorentino, Florence, Italy; †FiorGen Foundation, Via Luigi Sacconi 6, 50019 Sesto Fiorentino, Florence, Italy; ¶Department of Medical Biochemistry and Biophysics, Karolinska Institutet, SE-171 77 Stockholm, Sweden; and §Department of Gene Technology, Tallinn University of Technology, Akadeemia tee 15, 12618 Tallinn, Estonia

Edited by Joan Selverstone Valentine, University of California, Los Angeles, CA, and approved October 30, 2006 (received for review July 21, 2006)

The pathogenic mutant (P174L) of human Sco1 produces respiratory chain deficiency associated with cytochrome *c* oxidase (CcO) assembly defects. The solution structure of the mutant in its Cu(I) form shows that Leu-174 prevents the formation of a well packed hydrophobic region around the metal-binding site and causes a reduction of the affinity of copper(I) for the protein. K_D values for Cu(I)WT-HSco1 and Cu(I)P174L-HSco1 are $\approx 10^{-17}$ and $\approx 10^{-13}$, respectively. The reduction potentials of the two apo proteins are similar, but slower reduction/oxidation rates are found for the mutant with respect to the WT. The mitochondrial metallochaperone in the partially oxidized $Cu_1(I)Cox17_{2S\text{-}S}$ form, at variance with the fully reduced $Cu_4(I)Cox17$, interacts transiently with both WT-HSco1 and the mutant, forming the Cox17/Cu(I)/HSco1 complex, but copper is efficiently transferred only in the case of WT protein. $Cu_1(I)Cox17_{2S\text{-}S}$ indeed has an affinity for copper(I) ($K_D \approx 10^{-15}$) higher than that of the P174L-HSco1 mutant but lower than that of WT-HSco1. We propose that HSco1 mutation, altering the structure around the metal-binding site, affects both copper(I) binding and redox properties of the protein, thus impairing the efficiency of copper transfer to CcO. The pathogenic mutation therefore could (*i*) lessen the Sco1 affinity for copper(I) and hence copper supply for CcO or (*ii*) decrease the efficiency of reduction of CcO thiols involved in copper binding, or both effects could be produced by the mutation.

cytochrome *c* oxidase | mass spectrometry | NMR | copper chaperone | respiratory chain deficiency

Cytochrome *c* oxidase (CcO) is the terminal enzyme of the respiratory chain, embedded in the inner mitochondrial membrane of all eukaryotes and in the plasma membrane of many prokaryotes. In eukaryotes, a large number of nuclear genes are required for the proper assembly and function of the CcO complex, among which at least six proteins (Cox17, Cox23, Cox19, Sco1, Sco2, and Cox11) are involved in the delivery and insertion of copper into the binuclear Cu_A and Cu_B-heme a_3 sites of CcO (1–3). Sco1 and Sco2, which are anchored to the inner mitochondrial membrane through a single transmembrane helix, are specifically implicated in the assembly of the Cu_A site of CcO (4–7). Sco1 and Sco2 are both metal-binding proteins capable to bind either copper(I) or copper(II) in the same metal-binding site (8, 9); mutations of the ligands that abrogate their copper-binding ability drastically compromise CcO activity (9, 10). The mitochondrial copper chaperone Cox17 is capable of donating copper(I) to Sco1 (11), implying that it might transfer copper to Sco1, which, in turn, inserts it into the Cu_A site. According to this mechanism, Sco1 was shown to interact with the Cu_A-containing COXII subunit of CcO (6).

Important insights on the function of this class of proteins also recently were obtained from a genome-wide search for all available prokaryotic genomes (12). This search showed the presence of several Sco paralogs adjacent to copper and/or redox proteins, thus suggesting that Sco proteins can have multifunctional properties involved in different physiological processes.

The structure of Sco proteins is characterized by a thioredoxin fold (13–15), and, from the first structural characterization (13), it was suggested that the protein also may fulfill a redox function. Recently, we have solved the solution structures of the demetallated, the copper(I), and the nickel(II) derivatives of human Sco1 (HSco1 hereafter) as well as the crystal structure of a nickel(II) derivative (16). The structural analysis showed that Cu(I) is coordinated by ligands located in two distant protein regions: Cys-169 and Cys-173 of the CXXXC conserved motif in loop 3 and His-260 in loop 8. In the structure of the apo protein, the latter loop is highly disordered and mobile in solution (16), suggesting that the metal binding is able to "freeze" this loop in a more rigid conformation, thus representing an important step in the metal-binding process of HSco1. In the crystal structure of oxidized Ni(II)HSco1, the two metal-binding cysteines are oxidized and form a disulfide bond, still with the metal ion interacting with the S-S moiety. This metal environment showed that the protein can have a peculiar mode of interaction with a metal ion, suggesting that cysteine oxidation of HSco1 also might play a role in the metal release to Cu_A site of CcO (16). These structural data further support our initial suggestion that Sco1 can act both as a copper chaperone and a thioredoxin (13).

Human *SCO1* and *SCO2* genes can experience pathogenic mutations that produce respiratory chain deficiency associated with CcO assembly defects (17). The missense mutation in human Sco1 gene of a proline into a leucine, P174L, is associated with a fatal neonatal hepatopathy when the second allele also is nonfunctional (18). This finding implies that the pathology is caused by a loss of normal Sco1 function rather than gain of some aberrant action of the mutant protein. This proline, adjacent to the conserved CXXXC domain of HSco1, is completely conserved in eukaryotes. Introduction of the P174L mutant chimeric HSco1 protein in Sco1-null yeast mutants impaired CcO assembly and induced loss of CcO activity (19). WT protein and P174L mutant chimera are present in comparable concentrations in mitochondrial extracts, thus indicating that the pathogenicity of the mutant does not result from its instability but rather from an impaired function (19). During the preparation of our work, a paper on the same P174L-HSco1 mutant came out indicating that the mutation compromises Cox17-dependent metalation

Author contributions: L.B., I.B., S.C.-B., and P.P. designed research; S.C.-B., I.L., M.M., P.P., and S.W. performed research; R.S. contributed new reagents/analytic tools; S.C.-B., M.M., P.P., and S.W. analyzed data; and L.B., I.B., S.C.-B., and P.P. wrote the paper.

The authors declare no conflict of interest.

This article is a PNAS direct submission.

Abbreviations: CcO, cytochrome *c* oxidase; HSQC, heteronuclear single quantum correlation; ESI, electrospray ionization; GSH, reduced glutathione; GSSG, oxidized glutathione.

Data deposition: The atomic coordinates and structural restraints for human Cu(I)P174LSco1 structure have been deposited in the Protein Data Bank, www.pdb.org (PDB ID code 2HRN).

‡To whom correspondence should be addressed. E-mail: bertini@cerm.unifi.it.

This article contains supporting information online at www.pnas.org/cgi/content/full/0606189103/DC1.

without impairing copper binding (20). In the present research, we have explored at the molecular level the effect of the mutation on the Sco1 function by solving the solution structure of the P174L-HSco1 mutant, characterizing the metal-binding and redox properties of the P174L-HSco1 mutant with respect to WT HSco1 (WT-HSco1 hereafter), and investigating the role of Cox17 in the copper transfer to both WT and mutant HSco1 proteins. Our work demonstrates that the P174L mutation alters hydrophobic interactions around the metal-binding site, thus affecting both the copper-binding and the redox properties of HSco1 and, therefore, determining a reduction of the copper transfer efficiency from Cox17 to HSco1. We also learned that the partially oxidized $Cu_1(I)Cox17_{2S\text{-}S}$ and not the fully reduced $Cu_4(I)Cox17$ are the preferential species delivering copper to HSco1.

Results

Structural Properties of the Pathogenic Mutant P174L-HSco1. ApoP174L-HSco1 at millimolar concentration is a well folded protein as it appears from the ^1H-^{15}N heteronuclear single quantum correlation (HSQC) spectrum [see supporting information (SI) Fig. 5], which also is similar to that of apoWT-HSco1. Accordingly, the mutant maintains the same fold of WT-HSco1, featuring indeed the same content of β-strands (21%) and α-helices (26%) as derived from circular dichroism spectra. Fluorimetric thermal unfolding assay (SI Fig. 5) shows that the thermal stability of apoP174L-HSco1 also is the same as that of apoWT-HSco1, both having a melting temperature of ≈54°C. These data show that the pathogenic nature of the mutation does not originate from fold and/or stability differences of apoP174L-HSco1 with respect to the WT protein. This conclusion also is consistent with *in vivo* results, which showed that comparable concentrations of either WT or P174L mutant protein are present in mitochondrial extracts (19).

ApoP174L-HSco1, as apoWT-HSco1, is able to bind Cu(I) ions, when the latter is provided as Cu(I) acetonitrile complex. The metalation of both proteins, followed through ^1H-^{15}N HSQC spectra in the presence of 1 mM DTT (SI Fig. 6), however, shows meaningful differences. Indeed, although 1 eq of Cu(I) fully metallates WT-HSco1, complete metalation of P174L-HSco1 is not achieved even when 3 eq of Cu(I) are added, as ≈20% of P174L-HSco1 is still in the apo form (SI Fig. 6). In the latter experiment, Cu(I) thus competes between the mutant and the DTT chelator, allowing us to determine the dissociation constant (K_D) of the Cu(I)P174L-HSco1 complex. Following the relative ratio of apo and copper(I) forms, as obtained from the ^1H-^{15}N HSQC spectra of the mixture during the titration steps [the interaction between the protein and Cu(I)DTT complex is slow on the chemical-shift time scale], K_D of the Cu(I)P174L-HSco1 complex is estimated to be $3.2 \pm 0.6 \times 10^{-13}$ M. This value is much higher than the $K_D \approx 10^{-17}$ of the WT protein (see *Transfer of Copper from Cox17 to HSco1*). When copper(I) is added in the absence of DTT, 1.5 eq are enough to fully metallate the mutant.

Copper binding to WT-HSco1 induces major conformational changes to the protein, which passes from an open state in the apo form to a closed, compact one upon copper binding (16). This change clearly is evident from the solution structures of these two states of WT-HSco1 and also can readily be assessed from the charge state analysis of electrospray ionization (ESI)-MS spectra. Conformational analysis by ESI-MS is based on observation that, during the ESI, tightly compact proteins acquire only a narrow range of low-charge values, whereas open conformations produce a more heterogeneous and highly charged population (21). Charge-state distribution of Cu(I)P174L-HSco1 ($Int_{+9}/Int_{+10} = 1.6$; Fig. 1) is similar to that of apoP174L-HSco1 ($Int_{+9}/Int_{+10} = 1.7$) and apoWT-HSco1 ($Int_{+9}/Int_{+10} = 1.4$), indicating that all these systems have a more

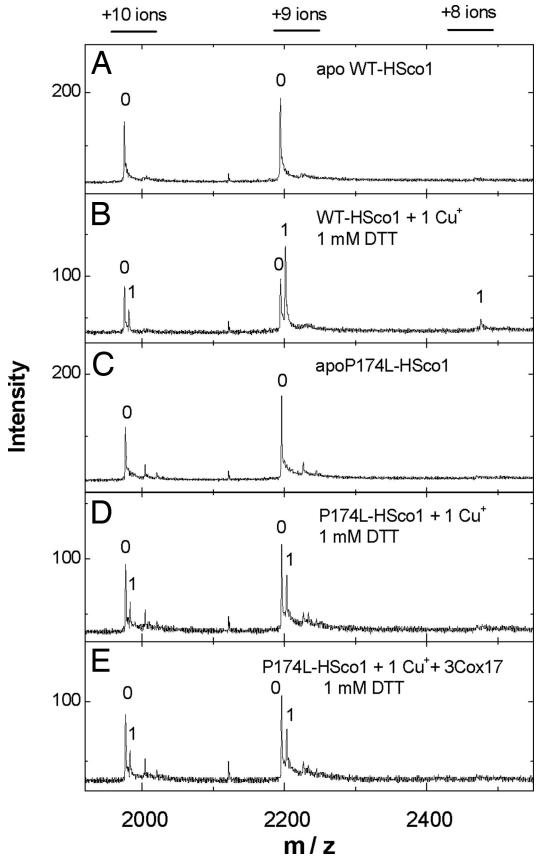

Fig. 1. Binding of copper ions to human Sco1 and mutant P174LSco1. ESI-TOF mass spectra of WT-HSco1 (0.8 μM) and P174L-HSco1 (1.2 μM) reconstituted with Cu(I)DTT complex in 50 mM ammonium acetate, pH 7.5. (*A*) apoWT-HSco1. (*B*) WT-HSco1 + 1 eq of Cu(I) in the presence of 1.0 mM DTT. (*C*) apoP174L-HSco1. (*D*) P174L-HSco1 + 1 eq of Cu(I) in the presence of 1.0 mM DTT. (*E*) P174L-HSco1 + 1 eq of Cu(I) + 3 eq of $Cox17_{2S\text{-}S}$ in the presence of 1.0 mM DTT. Charge state +8, +9, and +10 ions are presented and numbers on the peaks denote the metal stoichiometry of the complex.

open conformation than Cu(I)WT-HSco1, in which the lower +9 state was more populated ($Int_{+9}/Int_{+10} = 3.8$; Fig. 1). These data therefore show that Cu(I) binding to apoP174L-HSco1 is unable to induce the compact conformation as it occurs in the WT protein.

In the ^1H-^{15}N HSQC spectrum of the fully metallated P174L-HSco1 ($Cu_1(I)$P174L-HSco1), 34 residues show a splitting in two or, in a few cases, three NH cross-peaks, indicating the occurrence of structural heterogeneity, which is absent in $Cu_1(I)$WT-HSco1. The two major species are present in a ratio of 60:40. The relative intensity of the resonances of the two species is temperature-dependent, indicating that there is an equilibrium between the two. The solution structure of $Cu_1(I)$P174L-HSco1 (determined from the more abundant species) shows the same thioredoxin-like fold of the WT protein (Fig. 2) with an average backbone rmsd of 1.30 Å. The only significant structural difference is in loop 8, which contains the His copper ligand. In the mutant, this loop does not have the short β-hairpin (Fig. 2), similarly to what occurs in the apoWT-HSco1 solution structure but at variance with the $Cu_1(I)$WT-HSco1 structure (16). Because no apo form of the mutant is present in the NMR sample (see *Methods*), the latter less defined secondary structure could be the consequence of the structural heterogeneity in this region, which in turn could induce a weaker copper-affinity in the mutant. Several residues with double conformations are located in helix α2, which is in contact with the metal-binding CXXXC

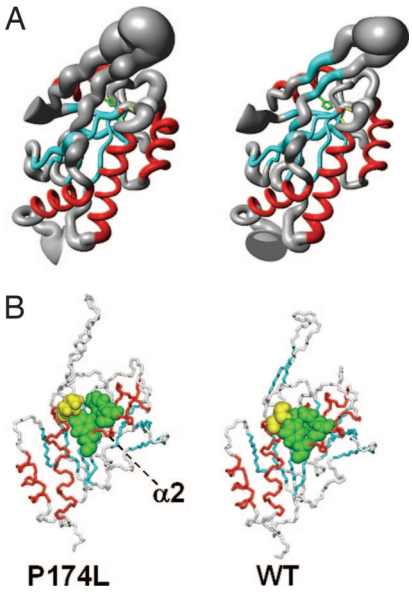

Fig. 2. Solution structure of Cu_1(I)P174L-HSco1 mutant. (*A*) Backbone atoms are represented as a tube with variable radius, proportional to the backbone rmsd value of each residue for Cu_1(I)P174L-HSco1 and Cu_1(I)WT-HSco1. The side chains of Cys-169, Cys-173, His-260, and the copper(I) ions are shown in yellow, green, and orange, respectively. The secondary structure elements also are indicated: β-strands are in cyan and α-helices in red. (*B*) Side-chain packing involving Pro-174 or Leu-174 (in yellow) and Tyr-216 and Phe-220 (in green) is shown on the WT and P174L mean minimized solution structures. The mutant protein was copper-saturated resulting in a 1:1 copper:protein complex.

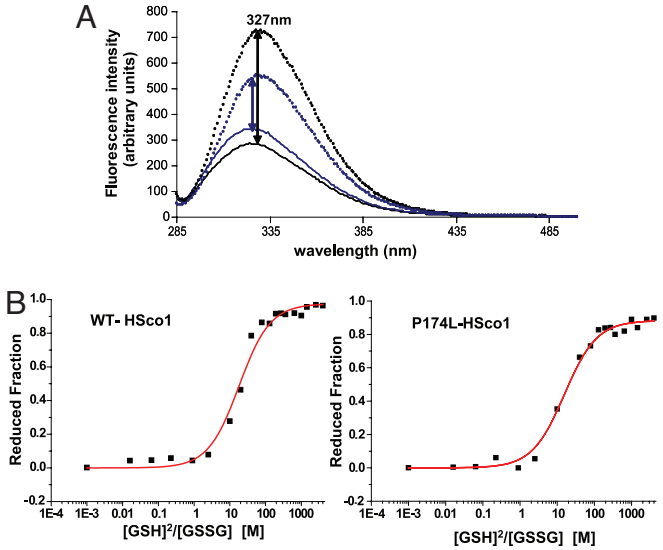

Fig. 3. Redox properties of WT-HSco1 and P174L-HSco1. (*A*) Fluorescence emission spectra of 5 μM WT-HSco1 (black) and P174L-HSco1 (blue) recorded under native conditions of the oxidized (50 mM phosphate buffer, pH 7.0, 0.01 mM GSSG; dotted lines) and the reduced (50 mM phosphate buffer, pH 7.0, 200 mM GSH; solid lines) protein after excitation at 280 nm. (*B*) Redox equilibrium of WT-HSco1 and P174L-HSco1 with different $[GSH]^2$/GSSG ratios as followed by measuring fluorescence emission at 327 nm. After nonlinear regression, values of K_{eq} = 17.70 ± 2.23 mM and of 15.66 ± 1.86 mM (correlation coefficient: 0.986 and 0.996) were obtained for the WT-HSco1 and P174L-HSco1/glutathione systems, corresponding to a redox potentials of −0.277 ± 0.030 V and −0.275 ± 0.028 V, respectively, by using the glutathione standard potential of −0.240 V at pH 7.0 and 298 K.

region through hydrophobic interactions involving Leu-174 or Pro-174 and Leu-177 (helix α1), and Tyr-216 and Phe-220 (helix α2). Although Pro-174 has extensive hydrophobic contacts with both Tyr-216 and Phe-220 in Cu_1(I)WT-HSco1, thus forming a compact hydrophobic patch, in the mutant, the bulkier Leu side chain prevents the optimal packing with the two aromatic side chains (Fig. 2), which indeed display double conformation. Leu-174 essentially interacts only with Phe-220 (Fig. 2) and is more solvent-exposed (25%) than Pro-174 is (12%). The lack of a well organized hydrophobic core on this side of the metal-binding region also causes the presence of a double conformation for His-260, located in loop 8. Two patterns for the aromatic ring of this His are observed in the $^2J_{NH}$ coupling-based ^1H-^{15}N HSQC spectra (SI Fig. 7). One pattern, belonging to the minor species, fully matches the shifts of His-260 in Cu_1(I)WT-HSco1, whereas the other has different shifts but still is indicative of copper(I) coordination through Nε2 as in the WT protein. In the major species, His-260 lacks NOEs contacts with the CXXXC metal-binding region that are present in the WT form. A decreased number of NOEs with respect to WT protein also is observed in the metal-binding loop 3 and in the surrounding loops 5, 7, and 8, likely reflecting the effect of the observed conformational disorder. From this structural investigation, we thus can conclude that the mutation (*i*) perturbs the hydrophobic interactions and (*ii*) induces conformational heterogeneity around the copper-binding site, with both effects overall reducing the affinity of the protein for copper(I).

Redox Properties of the Pathogenic Mutant P174L-HSco1. Based on its thioredoxin fold, it has been suggested that the two Cys residues of the CXXXC conserved motif in Sco protein family can be involved in redox reactions (13–15), perhaps in the reduction of the oxidized cysteines in Cu_A site of CcO (16). Oxidized and reduced forms of apoHSco1 are characterized by different fluorescence spectra (Fig. 3). Trp-159 and, to a lesser extent, Tyr-163 are the residues principally contributing to the difference of florescence intensity upon change of the oxidation state of the protein (see *SI Text* for details), as assessed by comparing the fluorescence spectra of W159F, W159F/Y163F, and Y216F mutants with that of WT-HSco1 (SI Fig. 8). Tyr-163 is close to the CXXXC motif, whereas Trp-159 is far but still belonging to the same β-strand of Tyr-163. From the difference in fluorescence of the two redox states of the protein, the reduction potential of the two cysteines for WT- and P174L-HSco1 in their apo forms can be determined. The measured reduction potentials at pH 7.2 are −0.277 ± 0.030 V and −0.275 ± 0.028 V for WT-HSco1 and P174L-HSco1, respectively (Fig. 3), falling in the standard state redox potentials range of the thioredoxin family of thiol-disulfide oxidoreductases (−124 to −270 mV) (22), consistently with a possible function of HSco1 as a thioredoxin. The similar reduction potentials of WT-HSco1 and P174L-HSco1 also indicate that the pathogenic mutation does not significantly affect the thermodynamic equilibrium between reduced and oxidized HSco1. However, the kinetic rates of disulfide bond formation and reduction are significantly different in WT-HSco1 and P174L-HSco1 forms. Air oxidation of cysteines in apoWT-HSco1 has an half-life time of ≈4 h. Oxidation of apoP174L-HSco1 is a much slower process, because ≈70% of the reduced form still is present after 4 h of air exposure (SI Fig. 9). Reduction of the disulfide bond in oxidized apoHSco1, by 1 mM DTT, also has different rates in the two proteins, being much faster in WT-HSco1 than in the mutant. In the former, the reduction of the disulfide bond is completed already after 1 min (SI Fig. 10); however, after the same period, only 20% of oxidized apoP174L-HSco1 is reduced, and, after 5 min, a reduction level of only 55% is reached (SI Fig. 10). In summary, P174L-HSco1 mutant has a similar redox potential as compared with WT protein but significantly slower reduction and oxidation rates.

Transfer of Copper from Cox17 to HSco1. After the characterization of the structural and redox properties of the P174L-HSco1 mutant, we also addressed and analyzed the mechanism of copper acquisition from the copper chaperone Cox17, which also could be affected by the mutation. For this analyses, we have used porcine Cox17, which differs from human Cox17 only in the first four amino acid residues. Cox17 could exist in three different oxidation states, which have different metal-binding properties (23). In oxidative environment, a completely oxidized form with three disulfide bonds ($Cox17_{3S\text{-}S}$ hereafter) is present that is unable to bind copper. In the presence of 1 mM DTT, Cox17 is partially oxidized with two disulfide bonds ($Cox17_{2S\text{-}S}$) and two reduced Cys residues, which bind one Cu(I) ion [$Cu_1(I)Cox17_{2S\text{-}S}$ hereafter]. In more reducing conditions, Cox17 exists in the fully reduced state, which binds cooperatively four Cu(I) ions forming a tetracopper-thiolate cluster [$Cu_4(I)Cox17$ hereafter] (23). In principle, both metallated forms of Cox17 could transfer metals to HSco1 protein.

To test which form of Cox17 can transfer Cu(I) to WT-HSco1, we have produced a mixture of $Cu_4(I)Cox17$ and $Cu_1(I)Cox17_{2S\text{-}S}$ forms and mixed it to reduced apoWT-HSco1. ESI-MS data of the Cox17 mixture showed metalation of apoWT-HSco1 with one Cu(I) ion and the concomitant decrease of the peak of $Cu_1(I)Cox17_{2S\text{-}S}$, whereas that of $Cu_4(I)Cox17$ remains unaltered (SI Fig. 11). This finding indicates that $Cu_1(I)Cox17_{2S\text{-}S}$ preferentially transfers Cu(I) to apoWT-HSco1. All of the subsequent NMR and ESI-MS experiments thus have been performed with the $Cu_1(I)Cox17_{2S\text{-}S}$ form.

Competition experiments for Cu(I) between the $Cox17_{2S\text{-}S}$ protein and the Cu(I) chelator DTT were carried out with ESI-MS technique as described in ref. 23. From these data, it results that $Cox17_{2S\text{-}S}$ bind one Cu(I) ion tightly with a K_D value of $6.4 \pm 0.6 \times 10^{-15}$ M (SI Fig. 12).

When ^{15}N-labeled apoWT-HSco1 is titrated with increasing amounts of unlabelled $Cu_1(I)Cox17_{2S\text{-}S}$ in the presence of 1 mM DTT, the intensity of some of its NH signals decreases in the ^{1}H-^{15}N HSQC spectra, and, concomitantly, NH signals of the Cu(I)WT-HSco1 species appeared with increasing intensities along the titration (SI Fig. 13). No additional signals from a possible (transiently populated) intermediate could be detected at any point of the titration. ApoWT-HSco1 reaches 90% of its metalation upon addition of 1 eq of $Cu_1(I)Cox17_{2S\text{-}S}$, indicating a lower limit of the equilibrium constant of 10^2. Considering the latter value and the K_D value of $Cu_1(I)Cox17_{2S\text{-}S}$ ($K_D = 6.4 \pm 0.6 \times 10^{-15}$ M), K_D of Cu(I)WT-HSco1 is estimated to be $\approx 10^{-17}$ or lower, thus WT protein displaying a higher affinity for Cu(I) compared with the mutant ($K_D = 3.2 \pm 0.6 \times 10^{-13}$ M). The rotational correlation time (13.2 ± 0.9 ns) of WT-HSco1 in the 1:1 mixture with $Cu_1(I)Cox17_{2S\text{-}S}$ is not higher than that of isolated apo or Cu(I)WT-HSco1 (13.8 ± 1.6 and 14.5 ± 1.1 ns, respectively), indicating that no complex is present at detectable concentrations. The copper(I) transfer process is slow on the chemical-shift time scale, setting a lower limit for the equilibration rate of $\approx 10^2\ s^{-1}$ [determined by the smallest chemical-shift difference between apoWT-HSco1 and Cu(I)WT-HSco1 that can be detected, i.e., $\approx$0.1 ppm at 800 MHz]. The comparison of the ^{1}H-^{15}N HSQC spectra of the Cu(I)WT-HSco1 metalated via $Cu_1(I)Cox17_{2S\text{-}S}$ with that of Cu(I)WT-HSco1 metallated via Cu(I) acetonitrile complex (SI Fig. 14) shows that a few NH resonances (residues 164, 243, 245, 258, and 260–262) close to the metal-binding site are missing, broader, or having two conformational states in the former spectrum, indicating that Cox17 is transiently interacting with this region of WT-HSco1 producing conformational exchange processes of these NH resonances.

ESI-MS spectrometry confirms the NMR data, showing that, by adding an excess of $apoCox17_{2S\text{-}S}$, the apoWT-HSco1/Cu(I)WT-HSco1 ratio does not change (SI Fig. 15 *C* versus *B*), indicating that Cu(I) ion is bound to WT-HSco1 with higher affinity than to $Cu_1(I)Cox17_{2S\text{-}S}$. According to the different metal-binding affinities, from ESI-MS experiments, we also established that even 10 mM DTT cannot extract Cu(I) from Cu(I)WT-HSco1, whereas already 5 mM DTT extracts $\approx$40% of copper from $Cu_1(I)Cox17_{2S\text{-}S}$. Therefore, $Cox17_{2S\text{-}S}$ does not compete with WT-HSco1 for Cu(I) ions, but vice versa, it contributes to metalation of WT-HSco1 protein as it follows from the fact that $Cox17_{2S\text{-}S}$ shifts the metalation equilibrium of HSco1 toward the Cu(I)WT-HSco1 form more than the Cu(I)DTT complex does (SI Fig. 15 *A* and *B*). These data are in agreement with the copper content of human Sco1, determined from the cytoplasm of yeast cells overexpressing human Sco1 in the presence and absence of co-overexpression of human Cox17 (9).

ESI-MS spectra also indicate that, in the absence of metal ion, WT-HSco1 and Cox17 proteins do not form any complex. However, in the presence of 1 eq of Cu(I) there are two minor twin-peaks in the ESI-MS spectra (SI Fig. 15*D*) whose deconvolution yields molecular masses of 26,497 and 26,562 Da, which correspond to WT-HSco1/$Cu_1(I)$/$Cox17_{2S\text{-}S}$ and WT-HSco1/$Cu_2(I)$/$Cox17_{2S\text{-}S}$ complexes (theoretical M_r 26,499.8 and 26,563.4 Da, respectively). These peaks have very low intensity, indicating that these complexes are transient and not highly populated states, in agreement with NMR results obtained at millimolar concentration. However, the relative intensity of these minor peaks increases at higher concentration of proteins, indicating that an equilibrium between free proteins and protein complexes is present. Moreover, at substoichiometric concentrations of Cu(I) ions, WT-HSco1/$Cu_1(I)$/$Cox17_{2S\text{-}S}$ is prevalent, whereas at higher Cu(I) concentrations, the WT-HSco1/$Cu_2(I)$/$Cox17_{2S\text{-}S}$ form prevails. This is another example of formation of a metal-mediated protein–protein complex, also observed in the case of other copper chaperones (24–26). As a whole, the ESI-MS results indicate that WT-HSco1/$Cu_1(I)$/$Cox17_{2S\text{-}S}$ is the transient intermediate involved in metal transfer from $Cu_1(I)Cox17_{2S\text{-}S}$ to WT-HSco1. At higher metal concentrations, WT-HSco1/$Cu_2(I)$/$Cox17_{2S\text{-}S}$ complex also exists, which suggests that the WT-HSco1/$Cox17_{2S\text{-}S}$ complex can accommodate two Cu(I) ions.

When $Cu_1(I)Cox17_{2S\text{-}S}$ is added to apoP174L-HSco1, differently from what happens for WT-HSco1, no copper transfer occurs at 1:1 $Cu_1(I)Cox17_{2S\text{-}S}$/P174L-HSco1 ratio, as judged by the ^{1}H-^{15}N HSQC spectrum of the mixture. By increasing the $Cu_1(I)Cox17_{2S\text{-}S}$/P174L-HSco1 ratio up to 2:1, copper transfer occurs slowly on the chemical-shift time scale, similarly to the WT protein, but only $\approx$20% of P174L-HSco1 is metallated, accordingly to the higher affinity of $Cox17_{2S\text{-}S}$ for copper(I) [$K_D = 6.4 \pm 0.6 \times 10^{-15}$ M for $Cu_1(I)Cox17_{2S\text{-}S}$; $K_D = 3.2 \pm 0.6 \times 10^{-13}$ M for Cu(I)P174L-HSco1]. ESI-MS spectra also show that the addition of $Cox17_{2S\text{-}S}$ up to 3 eq does not improve the metalation of P174L-HSco1 (Fig. 1 *E* versus *D*), which is different from what occurs with the WT protein. Addition of $Cox17_{2S\text{-}S}$ also does not change the charge-state distribution of Cu(I)P174L-HSco1 (SI Fig. 16), which remains similar to that of apoP174L-HSco1 (Fig. 1*E*). Similarly to WT-HSco1, no protein–protein complexes are observed in ESI-MS spectra in the absence of metal, and a minor twin peak, corresponding to P174L-HSco1/$Cu_1(I)$/$Cox17_{2S\text{-}S}$ and P174L-HSco1/$Cu_2(I)$/$Cox17_{2S\text{-}S}$ complexes, is detected in ESI-MS spectrum in presence of Cu(I) ions (SI Fig. 16), which indicates that transient protein–protein complexes with 1 and 2 Cu(I) ions also do exist in case of the mutant protein. All of the data indicate that, even if Cox17 is still capable of interacting and exchanging copper(I) with the P174L-HSco1 mutant, the latter is not efficiently metallated into a compact copper(I) form, at variance with what occurs in WT protein.

Discussion

Copper incorporation into CcO is biologically crucial; it is, however, an extremely complex process, which is tightly regulated and requires a large array of proteins, each of them with

a specific, in most of the cases, nonreplaceable role. The comprehension and description of these processes are still in their infancy, and only now knowledge about the structure and functional role of the assisting proteins has begun to become available. Many lines of evidence show that copper insertion into Cu_A site of COXII subunit is not a simple, passive copper transfer from Cox17 to Sco1/2 proteins and finally to COXII, but redox reactions are interlinked with the process of copper transfer (12, 15, 16, 27).

In this work, we have shown that the P174L mutation in HSco1 significantly affects the redox and metal-binding properties of this protein. Structurally, the mutation produces the lack of well organized hydrophobic contacts and a structural heterogeneity in the vicinity of the metal-binding region. The local structural changes induced by the point mutation decrease the copper(I) affinity of the mutant, thus negatively affecting the cometallochaperone function of HSco1 in the Cu_A assembly. The mutation also determines that the oxidation and reduction rates of the disulphide bond of the mutant are much slower than those of the WT protein. It is likely that introduction of the bulky Leu-174 disturbs the mutual orientation of cysteines and slows down the local conformational changes necessary for disulfide bond formation and disruption. The thioredoxin role of HSco1, proposed for maintaining the receiving Cu_A site in the suitable reduced state (15, 16), therefore is significantly perturbed because the mutation could slow down the reduction of the copper-binding cysteines in Cu_A site of CcO. Overall, these alterations induced by the mutation on copper-binding and redox properties of HSco1 can sizably decrease the efficiency of the copper transfer from Cu(I)HSco1 to the Cu_A site of CcO.

Our results also provide a detailed understanding of the metalation process of HSco1 by Cox17 and show how the mutation at position 174 of HSco1 affects this process. ESI-MS data demonstrate that $Cu_1(I)Cox17_{2S\text{-}S}$, but not $Cu_4(I)Cox17$, is capable of transferring Cu(I) to apoWT-HSco1 and that minor amounts of the metal-bridged species, WT-HSco1/$Cu_1(I)$/$Cox17_{2S\text{-}S}$ and WT-HSco1/$Cu_2(I)$/$Cox17_{2S\text{-}S}$, do occur, which are probably the transient intermediates involved in the metal transfer from $Cu_1(I)Cox17_{2S\text{-}S}$ to apoWT-HSco1. Such transient interaction with $Cox17_{2S\text{-}S}$ assists WT-HSco1 to pass from the open to the closed state, which binds Cu(I) ions extremely strongly (Fig. 4). The mutant P174L-HSco1 behaves differently: the conformational disorder experienced by Cu(I)P174L-HSco1 indeed is associated with a weakly bound metal (Fig. 4), and $Cox17_{2S\text{-}S}$ is not able to assist the mutant P174L-HSco1 to form the more compact state as it happens with WT-HSco1.

In conclusion, the P174L mutation in HSco1 decreases the efficiency of both metal-binding and redox properties of HSco1, which both are potentially involved in HSco1-mediated transfer of the copper and electrons from Cox17 to the Cu_A site of COXII (16).

Methods

Protein Expression and Characterization. The pathogenic mutation at the gene position C520T, corresponding to P174L amino acid change, was made by using QuikChange mutagenesis kit (Stratagene, La Jolla, CA). WT-HSco1 protein and P174L-HSco1 pathogenic mutant were produced in *E. coli* BL21-Gold(DE3) (Stratagene) following an already reported protocol (16). Porcine Cox17 was isolated from porcine intestine as fully oxidized apo protein ($Cox17_{3S\text{-}S}$) and lyophilized (23).

The oxidation state of the cysteines of the WT- and P174L-HSco1 proteins was evaluated through the selective reaction of the free thiol groups with 4-acetamido-4-maleimidylstilbene-2,2-disulfonic acid, which adds ≈500 Da per reactive thiol to the total mass, thus shifting the mobility of the protein on a SDS/PAGE denaturing gel. The metal content was determined by inductively coupled plasma mass spectrometry. Far-UV CD spectra (185–260 nm) were recorded on a Jasco J-810 spectropolarimeter on 10 μM protein solutions in 20 mM phosphate buffer, pH 7.2, at 298 K.

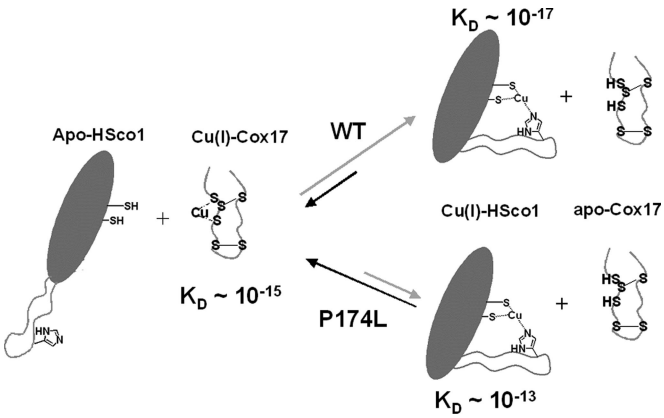

Fig. 4. The effect of the P174L-Sco1 mutation in the copper transfer with Cox17. The pathogenic human Sco1 mutation P174L, next to the copper-binding motif, determines a reduction of the efficiency of the copper transfer from the mitochondrial metallochaperone Cox17 to Sco1.

The melting temperatures of WT- and P174L-HSco1 proteins in the apo state were determined through the fluorescence-based thermal-shift assay (28). Fluorescence intensity was measured at different temperatures with excitation/emission wavelengths of 490 and 575 nm, respectively.

Redox equilibration between WT- or P174L-HSco1 and glutathione was followed through the change of fluorescence monitored on 5 μM concentrations of protein samples previously incubated for at least 6 h under an N_2 atmosphere, with different reduced/oxidized glutathione (GSH/GSSG) ratios (0.01 mM GSSG and varying concentrations of GSH, 0.1–200 mM) in 50 mM phosphate buffer, pH 7.2. The collection and data analysis was performed by following a protocol previously described for thioredoxins (29).

Preparation of Cox17, HSco1, and P174L-HSco1 Samples for MS Measurements. For MS experiments, purified WT- and P174L-HSco1 proteins containing one disulfide bond were brought into 50 mM ammonium acetate, pH 7.5, by using HiPrep26/10 desalting column (Amersham Biosciences, Uppsala, Sweden). Lyophilized $Cox17_{3S\text{-}S}$ was dissolved in argon-saturated 50 mM ammonium acetate, pH 7.5, at 75 μM concentration, and this stock solution was used for further experiments. $Cox17_{2S\text{-}S}$ was produced by reduction of $Cox17_{3S\text{-}S}$ with 1 mM DTT at 298 K (incubation time 2 min), which leads to reduction of one most labile disulfide bond in $Cox17_{3S\text{-}S}$. Fully reduced Cox17 was prepared by incubation of $Cox17_{3S\text{-}S}$ with 1 mM DTT at 45°C for 100 min.

MALDI-TOF and ESI-MS Protein Characterization. In MALDI-TOF experiments, reduction of oxidized apoWT-HSco1 and apoP174L-HSco1 (2 μM protein concentration) by 1 mM DTT was followed in 50 mM ammonium acetate buffer, pH 7.5, by stopping the reduction with 5 mM iodoacetamide. Protein adducts were identified by MALDI-TOF MS on a Voyager STR instrument (Applied Biosystems, Foster City, CA).

In ESI-MS experiments, 0.8–4.8 μM concentrations of protein samples or mixtures were infused by a syringe pump at 15 μl/min into an Ettan API ESI-TOF mass spectrometer (Amersham Biosciences). Mass spectra were recorded during 2 to 3 min at a capillary exit voltage of 150 V. HSco1 and P174L-HSco1 were reduced with 1.0 mM DTT at 298 K. ESI-MS spectrum of P174L-HSco1 also exposed two minor peaks corresponding to incorrectly cleaved protein forms, which did not disturb measurements. Reconstitution of HSco1 and Cox17 forms with

copper was conducted as follows. First, Cu(II) acetate was dissolved at 150 μM concentration in argon-saturated 50 mM ammonium acetate, pH 7.5, and Cu(II) was reduced to Cu(I) by addition of 1.0 mM DTT. Different equivalents of freshly prepared Cu(I)DTT complex were added to HSco1 or Cox17 and incubated in buffer with 1.0 mM DTT, and the mixture was incubated for additional 1 min at 25°C, and ESI-MS spectra were recorded as described above. In Cox17/HSco1 titration experiments, $Cu_1(I)Cox17_{2S\text{-}S}$ was prepared by addition of Cu(I) to $Cox17_{2S\text{-}S}$, which subsequently was mixed with a sample of HSco1 protein. All buffers contained 1 mM DTT. The dissociation constant of $Cu_1(I)Cox17_{2S\text{-}S}$ complex has been calculated as previously reported (23).

NMR Protein Characterization. The fully copper-loaded state of the $Cu_1(I)$P174L-HSco1 NMR sample used for structure determination has been produced by adding 1.5 eq of $[Cu(I)(CH_3CN)_4]PF_6$ complex to reduced apo protein in 50 mM phosphate buffer at pH 7.2 and in the absence of DTT. NMR spectral assignment and structure determination of $Cu_1(I)$P174L-HSco1 were obtained through the experiments listed in SI Table 1. The ^1H, ^{13}C, and ^{15}N resonance assignments of the $Cu_1(I)$P174L-HSco1 are reported in SI Table 2. After conversion of the NMR data in structural restraints, the structure was calculated by using the program DYANA. The relative intensity of the split resonances was taken into account when converting NOE volumes into distances. The best 30 conformers of the DYANA family were subjected to restrained energy minimization (REM) with AMBER 8.0, by using the metal force field already applied for WT-HSco1 (16). The statistical analysis of the REM family of $Cu_1(I)$P174L-HSco1 structures is reported in SI Table 3. The programs PROCHECK, PROCHECK-NMR (30, 31), and WHATIF (32) were used in the evaluation of the quality of the structures. More than 90% of residues were located in the allowed regions of the Ramachandran plot.

Titrations of ^{15}N-labeled apoHSco1 (0.1 mM) and apoP174L-HSco1 (0.1 mM) with unlabelled $Cu_1(I)Cox17_{2S\text{-}S}$ or $[Cu(I)(CH_3CN)_4]PF_6$ were performed with NMR spectroscopy following the ^1H-^{15}N spectral changes in HSQC spectra upon addition of increasing amounts of the unlabelled protein partner or copper(I) complex in the presence of 1 mM DTT. Aliquots were added in a Coy chamber under nitrogen atmosphere at 298 K. The metalation state of WT-HSco1 and P174L-HSco1 proteins was monitored along the NMR titration through a few residues that are next to the copper(I) binding motif CXXXC and therefore are experiencing chemical shifts sensitive to the metalation state. In addition, their NHs are not overlapped in the ^1H-^{15}N HSQC maps, thus they are easily integrated during the titration steps to estimate the relative population of apo and copper(I) loaded forms, which allows the estimation of the metal affinity. The dissociation constant K_D of Cu(I)P174L-HSco1 is obtained according to the following scheme:

$$\text{Cu(I)P174L-HScol} + \text{DTT} \Leftrightarrow \text{apoP174L-HScol} + \text{Cu(I)DTT}. \quad [1]$$

The conditional dissociation constant for the Cu(I)DTT complex, necessary for the above K_D estimation, is 6.31×10^{-12} M at pH = 7.4 and T = 298 K (33).

R_1 and R_2 ^{15}N relaxation rates on 1:1 $Cu_1(I)Cox17$/WT-HSco1 mixture were measured at 298 K on a Bruker (Billerica, MA) Avance 500 spectrometer and then analyzed by using a standard procedure (34). An estimate of the overall rotational correlation time was derived from the measured R_2/R_1 ratio.

This work was supported by Marie Curie Host fellowships for early stage research training ("NMR in Inorganic Structural Biology" Fellowship MEST-CT-2004-504391), the European Community (EU-NMR Contract 026145), Estonian Science Foundation Grant 5635, and a grant from Ente Cassa di Risparmio di Firenze (to FiorGen Foundation).

1. Carr HS, Winge DR (2003) *Acc Chem Res* 36:309–316.
2. Nobrega MP, Bandeira SCB, Beers J, Tzagoloff A (2002) *J Biol Chem* 277:40206–40211.
3. Barros MH, Johnson A, Tzagoloff A (2004) *J Biol Chem* 279:31943–31947.
4. Glerum DM, Shtanko A, Tzagoloff A (1996) *J Biol Chem* 271:20531–20535.
5. Beers J, Glerum DM, Tzagoloff A (2002) *J Biol Chem* 277:22185–22190.
6. Lode A, Kuschel M, Paret C, Rodel G (2000) *FEBS Lett* 485:19–24.
7. Mattatall NR, Jazairi J, Hill BC (2000) *J Biol Chem* 275:28802–28809.
8. Andruzzi L, Nakano M, Nilges MJ, Blackburn NJ (2005) *J Am Chem Soc* 127:16548–16558.
9. Horng YC, Leary SC, Cobine PA, Young FB, George GN, Shoubridge EA, Winge DR (2005) *J Biol Chem* 280:34113–34122.
10. Nittis T, George GN, Winge DR (2001) *J Biol Chem* 276:42520–42526.
11. Horng YC, Cobine PA, Maxfield AB, Carr HS, Winge DR (2004) *J Biol Chem* 279:35334–35340.
12. Arnesano F, Banci L, Bertini I, Martinelli M (2005) *J Proteome Res* 4:63–70.
13. Balatri E, Banci L, Bertini I, Cantini F, Ciofi-Baffoni S (2003) *Structure (London)* 11:1431–1443.
14. Williams JC, Sue C, Banting GS, Yang H, Glerum DM, Hendrickson WA, Schon EA (2005) *J Biol Chem* 280:15202–15211.
15. Ye Q, Imriskova-Sosova I, Hill BC, Jia Z (2005) *Biochemistry* 44:2934–2942.
16. Banci L, Bertini I, Calderone V, Ciofi-Baffoni S, Mangani S, Martinelli M, Palumaa P, Wang S (2006) *Proc Natl Acad Sci USA* 103:8595–8600.
17. Shoubridge EA (2001) *Am J Med Genet* 106:46–52.
18. Valnot I, Osmond S, Gigarel N, Mehaye B, Amiel J, Cormier-Daire V, Munnich A, Bonnefont JP, Rustin P, Rotig A (2000) *Am J Hum Genet* 67:1104–1109.
19. Paret C, Lode A, Krause-Buchholz U, Rodel G (2000) *Biochem Biophys Res Commun* 279:341–347.
20. Cobine PA, Pierrel F, Leary SC, Sasarman F, Horng YC, Shoubridge EA, Winge DR (2006) *J Biol Chem* 281:12270–12276.
21. Eyles SJ, Kalatshov IA (2004) *Methods* 34:88–99.
22. Aslund F, Berndt KD, Holmgren A (1997) *J Biol Chem* 272:30780–30786.
23. Palumaa P, Kangur L, Voronova A, Sillard R (2004) *Biochem J* 382:307–314.
24. van Dongen EM, Klomp LW, Merkx M (2004) *Biochem Biophys Res Commun* 323:789–795.
25. Banci L, Bertini I, Cantini F, Felli IC, Gonnelli L, Hadjiliadis N, Pierattelli R, Rosato A, Voulgaris P (2006) *Nat Chem Biol* 2:367–368.
26. Strausak D, Howie MK, Firth SD, Schlicksupp A, Pipkorn R, Multhaup G, Mercer JF (2003) *J Biol Chem* 278:20821–20827.
27. Imriskova-Sosova I, Andrews D, Yam K, Davidson D, Yachnin Y, Hill BC (2006) *Biochemistry* 44:16949–16956.
28. Lo MC, Aulabaugh A, Jin G, Cowling, R, Bard J, Malamas M, Ellestad G (2004) *Anal Biochem* 332:153–159.
29. Haugstetter J, Blicher T, Ellgaar L (2005) *J Biol Chem* 280:8371–8380.
30. Laskowski RA, Rullmann JAC, MacArthur MW, Kaptein R, Thornton JM (1996) *J Biomol NMR* 8:477–486.
31. Laskowski RA, MacArthur MW, Moss DS, Thornton JM (1993) *J Appl Crystallogr* 26:283–291.
32. Vriend G (1990) *J Mol Graphics* 8:52–56.
33. Krezel A, Lesniak W, Jezowska-Bojczuc M, Mlynarz P, Brasun J, Kozlowski H, Bal W (2001) *J Inorg Biochem* 84:77–88.
34. Peng JW, Wagner G (1992) *J Magn Reson* 98:308–332.

Structure
Article

A Structural Characterization of Human SCO2

Lucia Banci,[1] Ivano Bertini,[1,*] Simone Ciofi-Baffoni,[1] Ioannis P. Gerothanassis,[2] Iliana Leontari,[1] Manuele Martinelli,[1] and Shenlin Wang[1]
[1]Magnetic Resonance Center (CERM) and Department of Chemistry, University of Florence, Via Luigi Sacconi 6, 50019, Sesto Fiorentino, Florence, Italy
[2]Section of Organic Chemistry and Biochemistry, Department of Chemistry, University of Ioannina, 45110, Ioannina, Greece
*Correspondence: bertini@cerm.unifi.it
DOI 10.1016/j.str.2007.07.011

SUMMARY

Human Sco2 is a mitochondrial membrane-bound protein involved in copper supply for the assembly of cytochrome *c* oxidase in eukaryotes. Its precise action is not yet understood. We report here a structural and dynamic characterization by NMR of the apo and copper(I) forms of the soluble fragment. The structural and metal binding features of human Cu(I)Sco2 are similar to the more often studied Sco1 homolog, although the dynamic properties and the conformational disorder are quite different when the apo forms and the copper(I)-loaded forms of the two proteins are compared separately. Such differences are accounted for in terms of the different physicochemical properties in strategic protein locations. The misfunction of the known pathogenic mutations is discussed on the basis of the obtained structure.

INTRODUCTION

Cytochrome *c* oxidase (CcO) is the terminal enzyme of the energy transducing respiratory chain in eukaryotes and certain prokaryotes. The enzyme is embedded within the inner membrane of the mitochondrion with a portion of the molecule protruding into the intermembrane space and a separate portion extending into the matrix (Tsukihara et al., 1996). It catalyzes the reduction of molecular oxygen and couples this reduction with proton translocation across the inner membrane (Ramirez et al., 1995; Branden et al., 2006; Richter and Ludwig, 2003). In eukaryotes, it consists of 12–13 subunits, with the three subunits (Cox1–Cox3) that form the enzyme core being encoded by the mitochondrial genome (Capaldi, 1990). The remaining subunits are encoded by the nuclear genome and consist of small polypeptides (ranging from 6 to 15 kDa) that surround the catalytic core. Catalytic cofactors in CcO include copper ions and heme moieties (Tsukihara et al., 1995). In particular, two copper ions exist in a cysteine-bridged, binuclear, mixed valent center, designated Cu_A, located in Cox2. The domain of Cox2 containing the Cu_A site protrudes into the inner membrane space with the Cu_A site 8 Å outside the membrane surface (Tsukihara et al., 1995). In addition to the two copper ions present in the Cu_A site, a mononuclear copper site interacts with a heme moiety forming a heterobimetallic site in Cox1. This metal center, designated heme a3-Cu_B, is buried 13 Å below the membrane surface (Tsukihara et al., 1995). Copper insertion into nascent Cox1 and Cox2 chains is likely to occur in the intermembrane space, as all of the thus far identified copper donor molecules, Cox17, Sco1, Sco2, and Cox11, are localized within this mitochondrial compartment (Khalimonchuk and Rodel, 2005; Cobine et al., 2006). Cox11 and Sco1 were proposed to be the cometallochaperones assisting Cox17 in the metallation of the Cu_B and the Cu_A sites of CcO, respectively (Carr and Winge, 2003). It has been shown that Cox17 is capable of donating Cu(I) to both Sco1 and Cox11 (Horng et al., 2004; Banci et al., 2007) and that the Sco1 protein forms a transient complex with Cox2 in yeast (Lode et al., 2000). Sco2 is a protein highly similar to Sco1 (Smits et al., 1994); indeed, both are tethered to the inner membrane by a single transmembrane helix, have a globular metal binding domain that protrudes into the intermembrane space (Buchwald et al., 1991), and are capable of binding copper ions in vitro and in vivo (Beers et al., 2002; Nittis et al., 2001; Horng et al., 2005). These features thus suggest the same or a very similar function. Accordingly, both are proposed to be involved in copper incorporation in the Cu_A site. However, whereas sco1Δ yeast cells are respiratory deficient and are devoid of CcO activity, sco2Δ yeast cells lack an obvious phenotype associated with respiration (Glerum et al., 1996). Moreover, at variance with Sco2, Sco1 overexpression fully restores respiratory growth in cox17Δ yeast cells, whereas high levels of Sco2 fail to overcome the respiratory defects of sco1Δ yeast cells (Glerum et al., 1996). In humans, patients with mutations in the *Sco2* gene have a clinical presentation distinct from that of *Sco1* patients, even if *Sco1* and *Sco2* are ubiquitously expressed and exhibit a similar expression pattern in different human tissues (Shoubridge, 2001). Studies with immortalized fibroblasts from Sco1 and Sco2 patients suggest that human Sco1 and Sco2 have nonoverlapping but cooperative functions in CcO assembly (Leary et al., 2004). Recently, it was shown that human Sco2 is also the downstream mediator of the balance between the utilization of respiratory and glycolytic pathways (Matoba et al., 2006) and has a regulatory role in the maintenance of cellular

copper homeostasis (Leary et al., 2007). In particular, the latter study suggests that both Sco1 and Sco2 might have a role in regulating the cellular copper level, which is a further phenotype independent from that of CcO assembly. They are also proposing that Sco2 has a copper-level signaling role and acts in conjunction with but upstream of Sco1. Therefore, the role of the two distinct Sco molecules in mammals is still debated, and the experimental evidence available has not fully settled their functional aspect.

In this work, we report a solution NMR investigation of both the apo and metallated forms of human Sco2 (hereafter HSco2). The solution structure of Cu(I)HSco2 shows that the protein has a thioredoxin fold, with one copper(I) ion bound through a conserved CXXXC motif and a conserved His, similar to what occurs in human Cu(I)Sco1 (hereafter Cu(I)HSco1). However, in Cu(I)HSco2, some regions are more disordered than in Cu(I)HSco1, as a consequence of the lack of long-range hydrogen bond/salt bridge interactions. We also show that copper(I) binding dramatically affects the dynamic properties of HSco2, the apo form having a global dynamic tertiary structure whereas copper(I) binding makes the protein more rigid, even if a certain degree of global conformational motion is still present in Cu(I)HSco2. Some changes from a disordered apo protein to a compact metallated form upon copper binding were also observed for HSco1 but, at variance with HSco2, in HSco1 this effect is only restricted to the metal binding region.

RESULTS AND DISCUSSION

Two truncated forms of the human *Sco2* gene were engineered, both lacking the N-terminal mitochondrial targeting sequence and the single transmembrane helix (see Figure S1 in the Supplemental Data available with this article online). The two truncated forms differ by a 21 amino acid segment at the N terminus, which is predicted to be unstructured, similar to what occurs in HSco1 (Banci et al., 2006). Size-exclusion chromatography equipped with multiangle light scattering showed that both apoHSco2 constructs eluted in fractions corresponding to a monomeric state for the protein (Figure S2). This behavior differs from the corresponding constructs of HSco1, being the longer HSco1 in a dimeric state and the shorter HSco1 in a monomeric state (Banci et al., 2006). In vivo studies have shown that this N-terminal region is crucial for yeast Sco1 function and cannot be replaced even by its Sco2 counterpart (Lode et al., 2002). Our data support the hypothesis proposed by Lode et al. (2002) that this N-terminal region is important for the spatial orientation of the C-terminal soluble domain and/or for modulating the aggregation state of the proteins.

To investigate the structural and metal binding properties of HSco2, the shorter construct of 166 amino acids was used (plus four residues corresponding to the TEV protease recognition site [GSFT]; Figure S1), the first residue being Gly100.

Reduced apoHSco2 is able to bind one equivalent of either copper(I) or copper(II), similar to HSco1 (Horng et al., 2005; Banci et al., 2006). UV/VIS and electron paramagnetic resonance (EPR) spectra of Cu(II)HSco2 (Figure S3) are also similar to those recently reported for HSco1 (Horng et al., 2005; Banci et al., 2006) as well as those of bacterial Sco homologs (Balatri et al., 2003; Andruzzi et al., 2005), suggesting that the copper(II) binding site is formed by the same ligands in both HSco1 and HSco2 proteins.

The ^{1}H-^{15}N and ^{1}H-^{13}C heteronuclear single quantum correlation (HSQC) spectra of apo and Cu(I)HSco2 show well-dispersed resonances indicative essentially of a folded protein in both states, according to similar circular dichroism spectra of the metallated and apo forms (data not shown). However, only 84 out of the expected 160 ^{15}N backbone amide resonances were detected in the ^{1}H-^{15}N HSQC spectrum of apoHSco2, whereas only 2 NHs are absent in the spectrum of Cu(I)HSco2 (Tables S1 and S2). In apoHSco2, the backbone amide resonances are missing for the regions containing the CXXXC metal binding motif and the conserved His, and for their closest surroundings (Figure 1). The signals detected in the ^{1}H-^{15}N HSQC spectra of Cu(I)HSco2 and apoHSco2 have very similar chemical shifts (Figure S4), the $\Delta\delta_{NH}$ differences being smaller than 0.10 ppm. This indicates that the observed region in apoHSco2 is not largely affected by metal binding. Accordingly, chemical shift index analysis of the residues detected in both apo and copper(I) forms indicates the presence of the same secondary-structure elements. Finally, a number of residues located at the borderline between the regions of detected and undetected NH resonances show double or multiple resonances in the NMR spectra of the apo form (Figure 1), whereas only a set of signals is present in Cu(I)HSco2.

In conclusion, the inability to detect many backbone NH signals as well as the presence of double-backbone NH resonances indicate that apoHSco2 in solution samples multiple local conformational states exchanging with each other on the intermediate or slow NMR timescale. At variance with apoHSco1, the conformational heterogeneity involves not only the metal binding region but also the β sheet and the surrounding α helices, which constitute the protein core of HSco2 (Figure 1). Copper(I) binding is, however, able to "freeze" the above regions in an ordered, more rigid conformation, thus allowing its structure determination. The latter can, however, be determined only at 308K, as the majority of the NH signals were too broad at lower temperatures to achieve a high-resolution structure. Consistently, the number of observed nuclear Overhauser effects (NOEs) is much larger than at 298K.

The overall fold of Cu(I)HSco2 contains four α helices and nine β strands forming a central β sheet and two β hairpins, organized into a thioredoxin fold as found in the Cu(I)HSco1 structure (Banci et al., 2006) (Figure 2). Copper(I) is coordinated by the two cysteines of the CXXXC conserved motif, located in loop 3 and helix α1, and by the conserved His224 (Figure 2), located in a β hairpin.

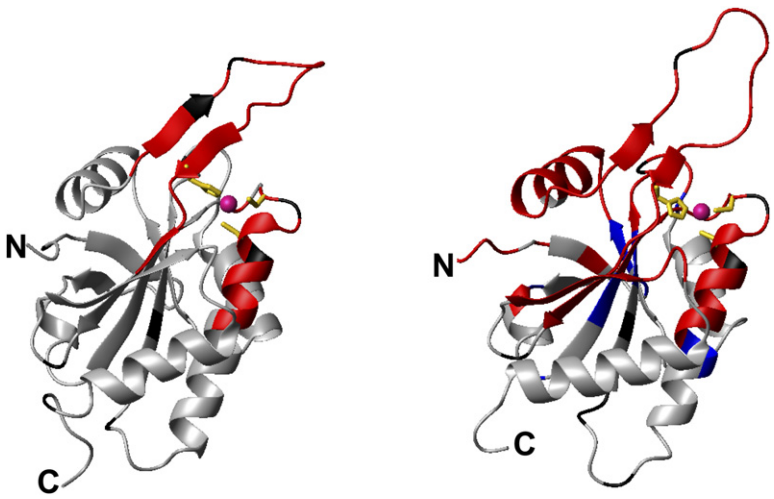

Figure 1. Detectability of the NMR Backbone NH Resonances between ApoHSco1 and ApoHSco2

Backbone NH resonances not detected in apoHSco1 or apoHSco2 are mapped in red on Cu(I)HSco1 (left) and Cu(I)HSco2 (right) solution structures. In apoHSco2, the backbone amide resonances are missing for residues located in the N terminus (100, 101, 102, 103), strand β1 (105, 107), 3_{10}-helix (116), strand β3, loop 3, and helix α1 (127–144), loop 5 (166–171), loop 7, helix α3, loop 8, and strand β6 (193–200, 202–231), and strand β7 and loop 10 (237–244), according to the secondary-structure elements observed in Cu(I)HSco2. In apoHSco1, 36 backbone amide resonances in strand β3 (164), loop 3 (166–173), helix α1 (175–180), loop 5 (202–204), and loop 8 (244–264) are missing. Residues showing double or multiple conformations in NMR spectra of apoHSco2, located in loop 1 (109), strand β2 (115), loop 2 (121), strand β3 (125, 126), helix α1 (145, 146), strand β4 (164, 165), loop 5 (172), and strand β5 (191 and 192), are mapped in blue. Copper(I) ions, metal ligands, and proline residues are shown in pink, yellow, and black, respectively.

From ^{2}J NH coupling-based ^{1}H-^{15}N HSQC experiments (Figure 3), it appears that His224 binds copper(I) through Nε2, whereas Nδ1 is protonated. Copper(I) coordination in HSco2 is the same as in Cu(I)HSco1 (Banci et al., 2006). The Cu(I)HSco2 structure is also very close to that of Cu(I)HSco1, the global root-mean-square deviation (rmsd) between Cu(I)HSco1 and Cu(I)HSco2 being 1.27 Å for backbone atoms. No regions with rmsd's between the two mean minimized structures larger than the sum of the rmsd's of each family are found, indicating no substantial structural differences within solution structure resolution.

The dynamic properties were mapped over the backbone of the copper(I)-bound protein based on ^{15}N relaxation rates and heteronuclear ^{1}H-^{15}N NOEs. R_1 and R_2 values measured at two different protein concentrations are similar, indicating that the aggregation state is not changing upon dilution (Figure S5). Accordingly, upon change of concentration, no meaningful variation in the ^{15}N chemical shift ($\geq$0.05 ppm) is observed for any residue of the protein. R_1 values (Figure S5) measured at 500 MHz (0.2 mM protein) and 600 MHz (0.6 mM protein) indicate that the protein reorients in solution as a monomer. Indeed, these values at 298K (1.32 ± 0.17 s^{-1}) compare well with those of proteins of similar size (human Sco1, 1.38 ± 0.11 s^{-1}; *Bacillus subtilis* Sco, 1.40 ± 0.06 s^{-1}; monomeric superoxide dismutase (SOD), 1.41 ± 0.29 s^{-1}) (Balatri et al., 2003; Banci et al., 2000). Moreover, R_1 values of dimeric SOD (MW 32 kDa) (Banci et al., 2000) are less than half of our data, confirming that Cu(I)HSco2 is

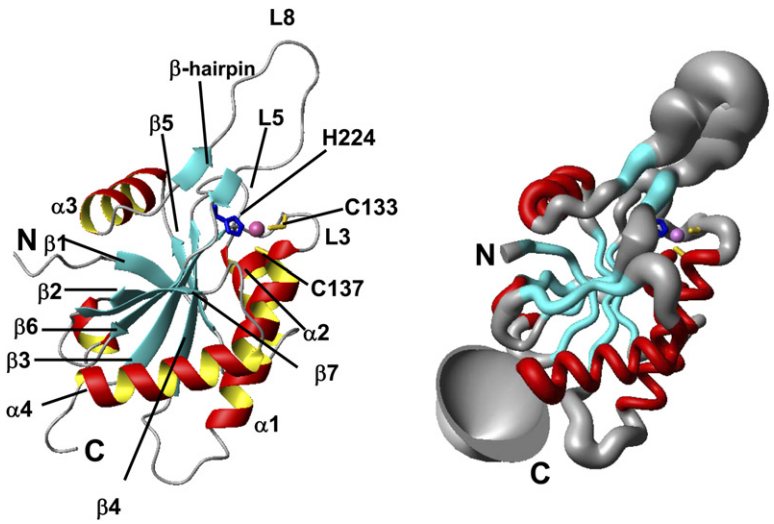

Figure 2. Solution Structure of Cu(I)HSco2

On the left side, the average structure of the lowest-energy ensemble is shown. The secondary-structure elements are also reported. The metal binding residues Cys133 and Cys137 are shown in yellow, and His224 is shown in blue. The copper(I) ion is depicted as a pink sphere. On the right, the superimposition of 30 lower-energy structures of Cu(I)HSco2 is represented as a tube whose radius is proportional to backbone rmsd. α helices and β strands are colored in red and cyan, respectively.

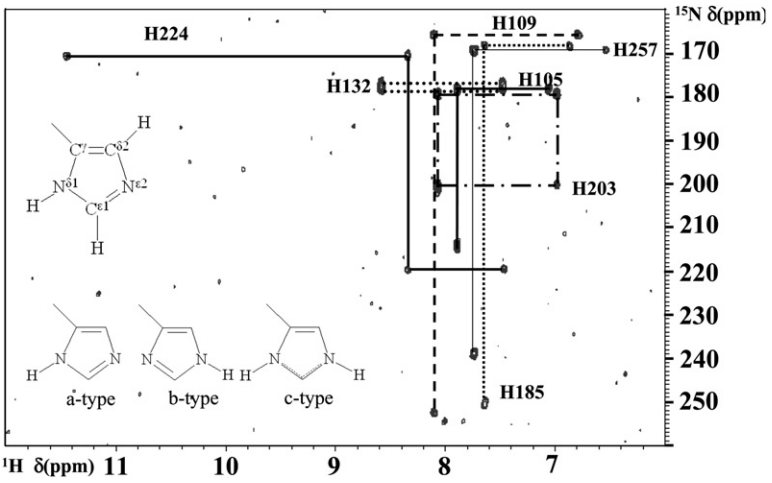

Figure 3. ^{1}H-^{15}N HSQC Spectrum Optimized for the Detection of ^{2}J NH of His Rings, Recorded on Cu(I)HSco2

The spectra were collected at 308K and pH 7.2 on a spectrometer equipped with a cryoprobe and operating at 500 MHz. A schematic diagram showing the nomenclature used to describe the imidazole atoms and the three possible protonation states of the histidine ring is presented. From ^{2}J patterns, His224 has an a-type tautomeric state, His105, His109, His185, and His257 have b-type tautomeric states, and His132 and His203 have c-type tautomeric states.

reorienting in solution as a monomer. The ^{1}H-^{15}N NOEs indicate that there are no regions with local fluctuations on the ps-ns timescale. However, the R_2 mean value (25.9 ± 4.5 s^{-1} at 500 MHz and 298K on a 0.2 mM sample) of Cu(I)HSco2 (Figure S5) is much higher than expected (17.3 ± 0.7 s^{-1} at 500 MHz as obtained from the HYDRONMR program [Garcia de la Torre et al., 2000] for the monomeric Cu(I)HSco2 structure). The unexpected values of R_2 can be ascribed to some degree of backbone conformational fluctuations of the protein occurring along the whole amino acid sequence on the NMR timescale (~10^{-3} s). Transverse crosscorrelated relaxation rates, η_{xy}, which are not affected by slow conformational exchange (Tjandra et al., 1996), were measured to evaluate whether exchange contributions are operative in transverse relaxation rates. The average η_{xy} value is 11.0 ± 1.8 s^{-1} at 308K (Figure S6), which is significantly lower than the average R_2 value measured under the same experimental conditions (26.4 ± 5.8 s^{-1}). From the average η_{xy} value, the effective τ_c was estimated (Lee et al., 2006) assuming a uniform chemical shift anisotropy of −160 ppm, $\theta = 17°$, and r_{HN} = 1.02 Å. The effective τ_c is 10.7 ± 1.8 ns, equal to the overall tumbling time calculated through HYDRONMR, which is 10.9 ns, thus confirming the monomeric state of Cu(I)HSco2. The value of 10.7 ± 1.8 ns at 308K is also in agreement with that estimated for HSco1 (having the same MW of 19.7 kDa), 14.5 ± 1.1 ns at 298K. If the values are extrapolated at the same temperature they are the same within experimental uncertainty, indicating the same monomeric state for both proteins. According to the Redfield relaxation matrix approach (Palmer, 2004), R_2 values of a ^{15}N nucleus of an isolated ^{1}H-^{15}N dipole not affected by exchange contributions for a protein tumbling at 10.7 ns should be in the range of 14–15 s^{-1}. However, the average R_2 of Cu(I)HSco2 is much higher than that value, indicating there is an exchange contribution to R_2 (Akerud et al., 2002). Therefore, HSco2 behaves in both apo and copper(I) forms as a protein with a dramatic backbone fluxionality, though to different extents in the two forms, which is distinct from HSco1. This property can, therefore, play a role in distinguishing the molecular functions of the two human paralogs.

Comparison between the Structural and Dynamic Properties of HSco1 and HSco2

In order to understand the factors determining the different behavior in solution between apoHSco1 and apoHSco2, we analyzed the sequences of the solvent-soluble domain of the two proteins. Only 51 residues are different or weakly similar (Figure 4; sequence identity 51%; sequence homology 73%). By displaying them on the structures of Cu(I)HSco2 and Cu(I)HSco1, the result is that 29 residues are located in the secondary-structure elements, while 22 are in loop regions. These residues are mainly located on the protein surface, with the exception of three residues which are largely buried in both proteins. In HSco2 they are Ala201, Ala227, and Thr238, which are replaced by longer hydrophobic side-chain residues in HSco1 (Val237, Ile263, and Leu274, respectively). The shorter side chains in these positions could determine less compact hydrophobic contacts and therefore a less tight hydrophobic core in apoHSco2 with respect to apoHSco1, thus allowing the protein to sample multiple local conformations. A similar correlation has indeed been previously observed in the ferredoxin βαββαβ fold, where a mutation from a short residue (Ser or Ala) to a longer hydrophobic residue (Val) in the hydrophobic core stabilizes the tertiary structure of the protein in a single conformation (Banci et al., 2003). According to this hypothesis, position 201 (HSco2 numbering) (Figure 4) is structurally important for orienting helix α3 with respect to the β sheet, through hydrophobic interactions with several hydrophobic residues conserved in both HSco1 and HSco2 proteins (Phe104, Leu106, Phe128, and Ile165 in HSco2): the shorter Ala201 chain present in HSco2 cannot optimize the protein core packing as Val237 in HSco1 can do. This single amino acid substitution could thus represent the structural basis for the conformational disorder of helix α3 reflected in the undetectability of its backbone NHs in apoHSco2 (Figure 1). Similarly, positions 227 and 238 (HSco2 numbering) (Figure 4) are involved in

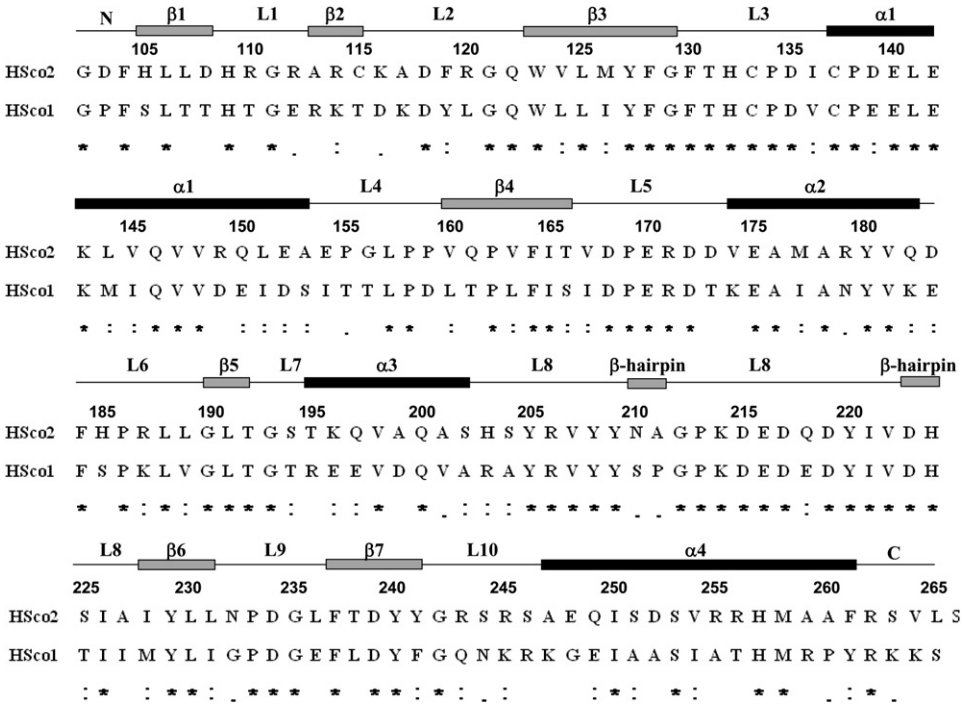

Figure 4. Sequence Alignment of HSco1 and HSco2

Residues that are conserved, highly similar, or weakly similar are indicated, respectively, by *, :, and · below the sequences. Secondary-structure elements are also depicted at the top according to the Cu(I)HSco2 structure.

hydrophobic interactions between strands β6, β7, and β3 interacting with residues conserved in both HSco1 and HSco2 proteins (Trp123, Phe128, Tyr229, Leu230, and Tyr240 in HSco2). The shorter Ala227 and Thr238 side chains in HSco2 with respect to the Ile263 and Leu274 side chains in HSco1 could contribute to the conformational destabilization of strands β6 and β7, whose backbone NHs are indeed not detected in apoHSco2 as a consequence of a less tight hydrophobic packing. Backbone NHs of loop 8, which contains the His ligand, are also missing in the ^{1}H-^{15}N HSQC map. Loop 8 is the junction between helix α3 and strand β6, and the undetectability of its signals is in agreement with the presence of local conformational heterogeneity in this region of apoHSco2. In conclusion, a single amino acid variation in key positions of the sequence could significantly affect the dynamic behavior of apoHSco2 with respect to apoHSco1.

Upon copper(I) binding, all the unobserved backbone NH signals of apoHSco2 (except for residues 196 and 237) become detectable, indicating that the metal ion is capable of freezing one of the possible conformations present in the apo form, that is, the one which appropriately orients the ligands, Cys and His, to bind copper(I). Still, the disorder in helices α3 and α4 and three loop regions (loops 5, 8, and 10; Figure S7) in Cu(I)HSco2 (as estimated from the backbone rmsd among the conformers of the family) is higher than that found in the corresponding regions of Cu(I)HSco1. Loops 5 and 8 show the most striking differences in this conformational disorder. In the Cu(I)HSco2 structure, loop 8 is highly disordered in the solvent-exposed region, from residue 211 to 222, as medium- and long-range NOEs cannot be detected for this stretch. On the contrary, in Cu(I)HSco1, long-range NOEs are present between loop 8 and loop 5 involving the side chains of Tyr256 (loop 8) and Glu206 (loop 5), which are indeed hydrogen bonded. These interactions are absent in Cu(I)HSco2, despite the residues in those positions being conserved on both sides. Also, helix α3 shows an overall decreased number of long-range NOEs with respect to those found in Cu(I)HSco1 (five against eight long-range NOEs per residue), thus determining a slight increase in backbone rmsd in Cu(I)HSco2 (Figure S7). Positions 195 and 199 of this helix (Figure 4) are not involved in salt bridge and hydrogen bond interactions, respectively, in HSco2, at variance with what occurs for the corresponding residues in HSco1 (Figure 5) (Banci et al., 2006; Williams et al., 2005). Indeed, the residues in these positions change from Arg to Thr and from Asp to Ala, respectively, thus making impossible the salt bridge between Arg231 (helix α3) and Glu206 (loop 5) and the hydrogen bond between Asp235 (helix α3) and Tyr245 (loop 8) observed in HSco1 (Figure 5). In conclusion, the result is that some hydrogen bonds and charged interactions connecting helix α3 and loops 5 and 8 in HSco1 are not conserved in HSco2, accounting for the lower rigidity of Cu(I)HSco2 with respect to Cu(I)HSco1.

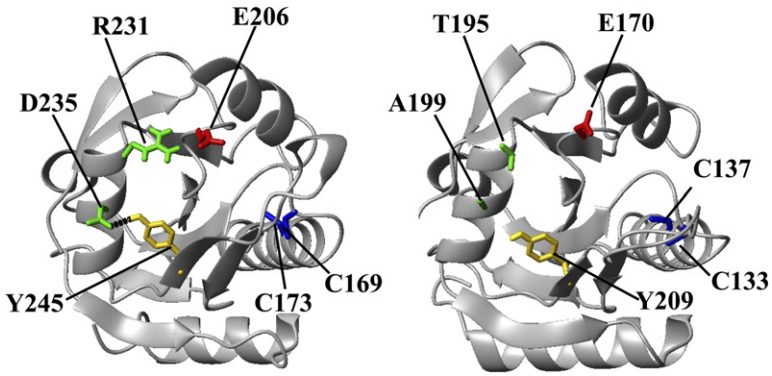

Figure 5. Network of Hydrogen Bond and Salt Bridge Interactions in the Case of HSco1 and HSco2

The salt bridge between Glu206 (in loop 5) and Arg231 (in helix α3) is present in HSco1 (left) but absent in HSco2 (right), where Arg231 is replaced by Thr195. Similarly, the hydrogen bond between Oδ of Asp235 (in helix α3) and OH of Tyr245 (in loop 8) is present in HSco1 (left) but missing in HSco2 (right), where Asp235 is replaced by Ala199.

Sco2 Point Mutations Causing Human Mitochondrial Disease

Five known pathogenic missense mutations in the human *Sco2* gene have so far been identified: Cys133Ser (Tarnopolsky et al., 2004), Glu140Lys (Papadopoulou et al., 1999), Leu151Pro (Sacconi et al., 2003), Arg171Trp (Jaksch et al., 2000), and Ser225Phe (Papadopoulou et al., 1999). The Cys133Ser mutation eliminates the first cysteine in the conserved metal binding CXXXC motif, thus making the protein unable to bind copper and likely determining a nonfunctional HSco2 protein. In the Cu(I)HSco2 structure, Glu140, located in helix α1 and essentially not solvent exposed, is involved in a salt bridge with Lys143, which is disrupted in the Glu140Lys mutant. In addition, the introduction of a longer side chain in a buried region could locally destabilize side-chain packing between helix α1 and the facing β sheet. Because Glu140 is relatively close to the copper binding Cys137, the possible structural rearrangements induced by the mutation could affect both the copper binding properties and protein stability, factors which both influence protein function, thus possibly rationalizing at the molecular level the mutant misfunction. Similarly, the mutation of Ser225 to Phe could affect the copper binding properties of HSco2, destabilizing the copper(I) coordination of the proximal His224 ligand. As copper(I) binding induces a transition from an open apoHSco2 state to a compact Cu(I)HSco2 state where His is metal coordinated, the mutation could alter this conformational transition determining a weaker metal affinity, similar to what we recently found for the Pro174Leu mutation in the HSco1 protein, the mutated residue being similarly next to the Cys ligand (Banci et al., 2007).

The mutation of Arg171Trp produces the loss of salt bridges between Arg171 and the conserved charged residues Asp168 and Glu170 in loop 5, whereas the mutation of Leu151Pro could affect the hydrophobic packing, as indeed Leu151 in helix α1 is involved in hydrophobic interactions with Leu157 (loop 4), Val147 (helix α1), Val160 (strand β4), and Val254 (helix α4). Therefore, both pathogenic mutations could likely destabilize the protein fold, rendering the protein more susceptible to aggregation and/or degradation, that is, increasing the turnover rate of the protein.

Comparison between the Redox Properties of ApoHSco1 and ApoHSco2

Similar to what occurs in apoHSco1 (Banci et al., 2006), oxidized and reduced forms of apoHSco2 are characterized by different fluorescence spectra. The reduction potential of the two cysteines in apoHSco2 at pH 7.2 is lower than −0.3 V, which compares with −0.28 V in HSco1 (Banci et al., 2007). Higher concentrations of glutathione (GSH) (50 mM) are needed to reduce 90% of the disulfide bond in apoHSco2, whereas in apoHSco1 the complete reduction was obtained with 30 mM GSH. This shows that the reduction potential is slightly lower for HSco2 than for HSco1. In any case, the negative reduction potential values of apoHSco2 and apoHSco1 suggest that both need a reductant capable of reducing disulfide bonds in order to bind the copper(I) ion. Mitochondrial inner membrane space is indeed suggested to be more oxidizing than cytosol, which has a redox potential of −0.29 V (Koehler et al., 2006).

Biological Implications

Human Scos have essential, nonoverlapping functions in the biogenesis of the Cu_A site that depend on their capability to bind Cu(I) and/or Cu(II) and to interact in the protein cascade of copper transfer (Horng et al., 2005; Leary et al., 2004). Other additional molecular functions have been suggested. Recently, both proteins have been suggested to be involved in the maintenance of cell copper homeostasis (Leary et al., 2007) or, limited to HSco2, as a downstream mediator of the Warburg effect, as its expression is regulated by p53 (Matoba et al., 2006). No other specific functions for HSco1 and HSco2 have been proposed. We have shown here that (1) HSco2 has a thioredoxin fold similar to its human paralog HSco1 and that (2) the metal binding and redox properties are similar. HSco2, however, has an internal dynamic and conformational disorder higher than that of HSco1, especially pronounced in its apo form, where it samples more than one conformation. Despite the same overall structure, some key interactions, whether hydrophobic or hydrogen bonds or salt bridges, are dramatically different in the two proteins, being less numerous in HSco2. The different dynamic properties of HSco2 with respect to HSco1 can play an important role in molecular recognition with different

protein partners. In particular, as HSco2, with respect to HSco1, has been proposed to act upstream in the maintenance of cellular copper homeostasis (Leary et al., 2007) and is in addition involved in the p53-linked pathway (Matoba et al., 2006), we can propose that the structural malleability of HSco2, especially in its apo form, is an essential requirement for taking part in various protein pathway recognition. Indeed, a molecular feature commonly associated with protein interaction sites is structural disorder, even if local (Ishima and Torchia, 2000).

EXPERIMENTAL PROCEDURES

Protein Preparation and Characterization

Long and short soluble domains of HSco2 (lacking the first 234 and 297 bp, respectively, corresponding to residues 1–78 and 1–99) were amplified by polymerase chain reaction (PCR), cloned into the Gateway entry vector pENTR-tobacco etch virus-D-TOPO (Invitrogen), and subcloned into pETG-30A (European Molecular Biology Laboratory Protein Expression and Purification Facility) by a Gateway LR reaction to generate N-terminal, His-GST-fused proteins.

The proteins were expressed in *Escherichia coli* BL21-codon$^+$ cells (Stratagene), which were grown in Luria Bertani and minimal medium ($[^{15}NH_4]_2SO_4$ and/or [^{13}C]glucose) for the production of labeled samples. Protein expression was induced by adding 0.7 mM IPTG for 16 hr at 30°C. Purification was performed by using a HiTrap chelating HP column (Amersham Pharmacia Biosciences) charged with Zn(II). The His-GST tag was cleaved with AcTEV protease (Invitrogen), and separated from the C-terminal domain with a second purification step. After this purification, the protein preparations showed a single component by SDS-PAGE with <5% of copper bound to the protein, as checked by inductively coupled plasma mass spectrometry (MS).

To investigate the aggregation state of HSco2, 0.5–1 mM protein samples were run on a Superdex 75 HR-10/30 size-exclusion column on an AKTA-FPLC system (Amersham Pharmacia Biosciences) connected to a multiangle light-scattering system (DAWN-EOS; Wyatt Technologies) equipped with quasielastic light-scattering detectors. A mixture of protein standards (a, b, c, and d in Figure S2) of various size were loaded to obtain a calibration line for the Supedex 75 column. Blue dextran was used in each mixture to determine the void volume.

Dithiothreitol (DTT) was added to the apo protein at 10 mM concentration to reduce the Cys residues of the CPXXCP motif before metal reconstitution. Then, in the case of Cu(II) metallation, DTT was completely removed through a PD-10 desalting column (Amersham Pharmacia Biosciences) in an N_2 atmosphere chamber, whereas 1 mM DTT was present in the case of Cu(I) metallation. The Cu(I) and Cu(II) metallated forms were obtained by addition of stoichiometric amounts of the metal ions, as $(Cu[I][CH_3CN]_4)PF_6$ or $CuSO_4$, to diluted protein solutions in 50 mM phosphate buffer (pH 7.2), which were then concentrated under nitrogen atmosphere. The metal content was then determined by inductively coupled plasma MS.

Electronic spectra on Cu(II) derivatives were recorded on a Cary 50 spectrophotometer (Varian) at 298K. EPR spectra on Cu(II)HSco2 were recorded at 180K on an Elexsys E500 spectrometer (Bruker) equipped with an X-band microwave bridge (microwave frequency, 9.45 GHz) and an ER 4131 VT unit for temperature control.

Redox equilibration between apoHSco2 and GSH was followed through the change of fluorescence monitored on 5 μM protein samples previously incubated, for at least 6 hr under an N_2 atmosphere, with different GSH/GSSG (glutathione disulfide) ratios (0.1 mM GSSG and varying concentrations of GSH, 10–200 mM) in 50 mM phosphate buffer (pH 7.2). The collection and data analysis were performed following a protocol previously described for HSco1 (Banci et al., 2007).

NMR Experiments and Structure Calculations

NMR spectral assignment and structure determination of Cu(I)HSco2 were obtained through the experiments listed in Table S3, which also indicates the magnetic fields at which they were collected. All NMR spectra were acquired at 308K. Overall, the resonances of 96% of carbon atoms, 98% of nitrogen atoms, and 95% of protons were assigned in Cu(I)HSco2 (Table S1; deposited in the BioMagResBank database). For the apo form, backbone assignment was performed collecting triple-resonance experiments HNCA, HN(CO)CA, and HNCO. The His ring protons of Cu(I)HSco2 were assigned through a ^{1}H-^{15}N HSQC experiment tailored to the detection of ^2J ^{1}H-^{15}N couplings and from the analysis of ^{13}C-NOESY-HSQC spectra. In Cu(I)HSco2, all nonexchangeable protons of all His rings were assigned. The exchangeable proton of the metal binding ligand, His224, is also detected in Cu(I)HSco2. Proton-proton distance constraints were derived from the analysis of 2D-NOESY (nuclear Overhauser enhancement spectroscopy), ^{15}N-NOESY-HSQC, ^{13}C-NOESY-HSQC, and ^{13}C-NOESY-HSQC recorded on a D_2O-exchanged sample. In total, 2296 meaningful proton-proton distance constraints together with 87 ϕ and 89 ψ torsion angle constraints, derived from chemical shift index analysis, were used in the structure calculation of Cu(I)HSco2. The structure was calculated using the program DYANA (Güntert et al., 1997). The copper ion was included in the structure calculations by adding a new residue in the amino acid sequence, following an approach used for similar systems (Banci et al., 2004). The sulfur atoms of the Cys ligands (Cys133 and Cys137) and Nε2 of His224 were linked to the metal ion through upper distance limits of 2.3 and 2.1 Å, respectively. The best 30 structures of the DYANA family were then subjected to restrained energy minimization (REM) with AMBER 8.0 (Case et al., 2004). The force field parameters for the metal ion were adapted from similar systems (Poger et al., 2005; Banci et al., 1994). The statistical analysis of the REM family of the Cu(I)HSco2 structure is reported in Table S4. The programs PROCHECK, PROCHECK-NMR (Laskowski et al., 1993, 1996), and WHAT IF (Vriend, 1990) were used in the evaluation of the quality of the structures, and the results of this analysis are reported in Table S4. More than 90% of residues were located in the allowed regions of the Ramachandran plot.

Relaxation Measurements and Analysis of Cu(I)HSco2

^{15}N R_1, R_2, and steady-state heteronuclear ^{1}H-^{15}N NOEs were measured on 0.6 mM Cu(I)HSco2 at 600 MHz (308K) and on 0.2 mM or 0.6 mM Cu(I)HSco2 at 500 MHz (298K and 308K) equipped with a cryoprobe using standard pulse sequences (Table S3). Relaxation rates R_1 and R_2 were determined by fitting the crosspeak heights, obtained through the standard routine of the Sparky program (T.D. Goddard and D.G. Kneller, SPARKY 3, University of California, San Francisco), measured as a function of the delay within the pulse sequence to a single-exponential decay. The heteronuclear NOE values were obtained from the ratio of the peak height for ^{1}H-saturated and unsaturated spectra. The heteronuclear NOE values and their errors were estimated by calculating the mean ratio and the standard error from the available data sets. Reliable ^{15}N R_1, R_2, and ^{1}H-^{15}N NOE values were obtained for 107 out of the 160 assigned backbone NH resonances. The others were too weak, or were overlapped, to be accurately analyzed. Transverse crosscorrelated relaxation rates, η_{xy}, were measured on a 0.6 mM sample at 600 MHz (308K) using the pulse sequences of Tjandra et al. (1996) with a dephasing period $2\Delta = 14$ ms. The effective τ_c value was estimated using the equations described in Lee et al. (2006).

HYDRONMR Calculations

Theoretical prediction of the rotational properties of Cu(I)HSco2 was calculated by using the "shell modeling" strategy implemented in HYDRONMR software (Garcia de la Torre et al., 2000). The calculation was performed by using a viscosity of water at 308K of 0.71 Ns/m^2. The value of the atomic element radius was set to 3.2 Å according to the

average value determined previously on a set of different proteins (Garcia de la Torre, 2001).

Supplemental Data

Supplemental Data include seven figures and four tables and can be found with this article online at http://www.structure.org/cgi/content/full/15/9/1132/DC1/.

ACKNOWLEDGMENTS

This work was supported by the European Community (SPINE2 n°QLG2-CT-2002-00988, Structural Proteomics in Europe), by Marie Curie Host Fellowships for early-stage research training (n°MEST-CT-2004-504391, NMR in Inorganic Structural Biology), and by Ente Cassa Risparmio di Firenze.

Received: February 21, 2007
Revised: July 12, 2007
Accepted: July 16, 2007
Published: September 11, 2007

REFERENCES

Akerud, T., Thulin, E., Van Etten, R.L., and Akke, M. (2002). Intramolecular dynamics of low molecular weight protein tyrosine phosphatase in monomer-dimer equilibrium studied by NMR: a model for changes in dynamics upon target binding. J. Mol. Biol. *322*, 137–152.

Andruzzi, L., Nakano, M., Nilges, M.J., and Blackburn, N.J. (2005). Spectroscopic studies of metal binding and metal selectivity in *Bacillus subtilis* BSco, a homologue of the yeast mitochondrial protein Sco1p. J. Am. Chem. Soc. *127*, 16548–16558.

Balatri, E., Banci, L., Bertini, I., Cantini, F., and Ciofi-Baffoni, S. (2003). Solution structure of Sco1: a thioredoxin-like protein involved in cytochrome *c* oxidase assembly. Structure *11*, 1431–1443.

Banci, L., Bertini, I., Bruni, B., Carloni, P., Luchinat, C., Mangani, S., Orioli, P.L., Piccioli, M., Ripniewski, W., and Wilson, K.S. (1994). X-ray, NMR and molecular dynamics studies on reduced bovine superoxide dismutase: implications for the mechanism. Biochem. Biophys. Res. Commun. *202*, 1088–1095.

Banci, L., Bertini, I., Cramaro, F., Del Conte, R., Rosato, A., and Viezzoli, M.S. (2000). Backbone dynamics of human Cu, Zn superoxide dismutase and of its monomeric F50/EG51E/E133Q mutant: the influence of dimerization on mobility and function. Biochemistry *39*, 9108–9118.

Banci, L., Bertini, I., Ciofi-Baffoni, S., Gonnelli, L., and Su, X.C. (2003). A core mutation affecting the folding properties of a soluble domain of the ATPase protein CopA from *Bacillus subtilis*. J. Mol. Biol. *331*, 473–484.

Banci, L., Bertini, I., Borrelly, G.P.M., Ciofi-Baffoni, S., Robinson, N.J., and Su, X.C. (2004). Solution structures of a cyanobacterial metallochaperone: insight into an atypical copper binding motif. J. Biol. Chem. *279*, 27502–27510.

Banci, L., Bertini, I., Calderone, V., Ciofi-Baffoni, S., Mangani, S., Martinelli, M., Palumaa, P., and Wang, S. (2006). A hint for the function of human Sco1 from different structures. Proc. Natl. Acad. Sci. USA *103*, 8595–8600, Erratum: Proc. Natl. Acad. Sci. USA *103*, 11814.

Banci, L., Bertini, I., Ciofi-Baffoni, S., Leontari, I., Martinelli, M., Palumaa, P., Sillard, R., and Wang, S. (2007). Human Sco1 functional studies and pathological implications of the P174L mutant. Proc. Natl. Acad. Sci. USA *104*, 15–20.

Beers, J., Glerum, D.M., and Tzagoloff, A. (2002). Purification and characterization of yeast Sco1p, a mitochondrial copper protein. J. Biol. Chem. *277*, 22185–22190.

Branden, G., Gennis, R.B., and Brzezinski, P. (2006). Transmembrane proton translocation by cytochrome *c* oxidase. Biochim. Biophys. Acta *1757*, 1052–1063.

Buchwald, P., Krummeck, G., and Rodel, G. (1991). Immunological identification of yeast SCO1 protein as a component of the inner mitochondrial membrane. Mol. Gen. Genet. *229*, 413–420.

Capaldi, R.A. (1990). Structure and function of cytochrome *c* oxidase. Annu. Rev. Biochem. *59*, 569–596.

Carr, H.S., and Winge, D.R. (2003). Assembly of cytochrome *c* oxidase within the mitochondrion. Acc. Chem. Res. *36*, 309–316.

Case, D.A., Darden, T.A., Cheatham, T.E., Simmerling, C.L., Wang, J., Duke, R.E., Luo, R., Merz, K.M., Wang, B., Pearlman, D.A., et al. (2004). AMBER 8 (computer program). University of California, San Francisco.

Cobine, P.A., Pierrel, F., and Winge, D.R. (2006). Copper trafficking to the mitochondrion and assembly of copper metalloenzymes. Biochim. Biophys. Acta *1763*, 759–772.

Garcia de la Torre, J.G. (2001). Hydration from hydrodynamics. General considerations and applications of bead modelling to globular proteins. Biophys. Chem. *93*, 159–170.

Garcia de la Torre, J.G., Huertas, M.L., and Carrasco, B. (2000). HYDRONMR: prediction of NMR relaxation of globular proteins from atomic-level structures and hydrodynamic calculations. J. Magn. Reson. *147*, 138–146.

Glerum, D.M., Shtanko, A., and Tzagoloff, A. (1996). SCO1 and SCO2 act as high copy suppressors of a mitochondrial copper recruitment defect in *Saccharomyces cerevisiae*. J. Biol. Chem. *271*, 20531–20535.

Güntert, P., Mumenthaler, C., and Wüthrich, K. (1997). Torsion angle dynamics for NMR structure calculation with the new program DYANA. J. Mol. Biol. *273*, 283–298.

Horng, Y.C., Cobine, P.A., Maxfield, A.B., Carr, H.S., and Winge, D.R. (2004). Specific copper transfer from the Cox17 metallochaperone to both Sco1 and Cox11 in the assembly of yeast cytochrome *c* oxidase. J. Biol. Chem. *279*, 35334–35340.

Horng, Y.C., Leary, S.C., Cobine, P.A., Young, F.B., George, G.N., Shoubridge, E.A., and Winge, D.R. (2005). Human Sco1 and Sco2 function as copper-binding proteins. J. Biol. Chem. *280*, 34113–34122.

Ishima, R., and Torchia, D.A. (2000). Protein dynamics from NMR. Nat. Struct. Biol. *7*, 740–743.

Jaksch, M., Ogilvie, I., Yao, J., Kortenhaus, G., Bresser, H.G., Gerbitz, K.D., and Shoubridge, E.A. (2000). Mutations in SCO2 are associated with a distinct form of hypertrophic cardiomyopathy and cytochrome *c* oxidase deficiency. Hum. Mol. Genet. *9*, 795–801.

Khalimonchuk, O., and Rodel, G. (2005). Biogenesis of cytochrome *c* oxidase. Mitochondrion *5*, 363–388.

Koehler, C.M., Beverly, K.N., and Leverich, E.P. (2006). Redox pathways of the mitochondrion. Antioxid. Redox Signal. *8*, 813–822.

Laskowski, R.A., MacArthur, M.W., Moss, D.S., and Thornton, J.M. (1993). PROCHECK: a program to check the stereochemical quality of protein structures. J. Appl. Cryst. *26*, 283–291.

Laskowski, R.A., Rullmann, J.A.C., MacArthur, M.W., Kaptein, R., and Thornton, J.M. (1996). AQUA and PROCHECK-NMR: programs for checking the quality of protein structures solved by NMR. J. Biomol. NMR *8*, 477–486.

Leary, S.C., Kaufman, B.A., Pellecchia, G., Guercin, G.H., Mattman, A., Jaksch, M., and Shoubridge, E.A. (2004). Human SCO1 and SCO2 have independent, cooperative functions in copper delivery to cytochrome *c* oxidase. Hum. Mol. Genet. *13*, 1839–1848.

Leary, S.C., Cobine, P.A., Kaufman, B.A., Guercin, G.H., Mattman, A., Palaty, J., Lockitch, G., Winge, D.R., Rustin, P., Horvath, R., and Shoubridge, E.A. (2007). The human cytochrome *c* oxidase assembly factors SCO1 and SCO2 have regulatory roles in the maintenance of cellular copper homeostasis. Cell Metab. *5*, 9–20.

Lee, D., Hilty, C., Wider, G., and Wuthrich, K. (2006). Effective rotational correlation times of proteins from NMR relaxation interference. J. Magn. Reson. *178*, 72–76.

Lode, A., Kuschel, M., Paret, C., and Rodel, G. (2000). Mitochondrial copper metabolism in yeast: interaction between Sco1p and Cox2p. FEBS Lett. *485*, 19–24.

Lode, A., Paret, C., and Rodel, G. (2002). Molecular characterization of *Saccharomyces cerevisiae* Sco2p reveals a high degree of redundancy with Sco1p. Yeast *19*, 909–922.

Matoba, S., Kang, J.G., Patino, W.D., Wragg, A., Boehm, M., Gavrilova, O., Hurley, P.J., Bunz, F., and Hwang, P.M. (2006). p53 regulates mitochondrial respiration. Science *312*, 1650–1653.

Nittis, T., George, G.N., and Winge, D.R. (2001). Yeast Sco1, a protein essential for cytochrome *c* oxidase function is a Cu(I)-binding protein. J. Biol. Chem. *276*, 42520–42526.

Palmer, A.G., III. (2004). NMR characterization of the dynamics of biomacromolecules. Chem. Rev. *104*, 3623–3640.

Papadopoulou, L.C., Sue, C.M., Davidson, M.M., Tanji, K., Nishino, I., Sadlock, J.E., Krishna, S., Walker, W., Selby, J., Glerum, D.M., et al. (1999). Fatal infantile cardioencephalomyopathy with COX deficiency and mutations in SCO2, a COX assembly gene. Nat. Genet. *23*, 333–337.

Poger, D., Fuchs, H.J.R., Nedev, H., Ferrand, M., and Crouzy, S. (2005). Molecular dynamics study of the metallochaperone Hah1 in its apo and Cu(I)-loaded states: role of the conserved residue M10. FEBS Lett. *579*, 5287–5292.

Ramirez, B.E., Malmström, B.G., Winkler, J.R., and Gray, H.B. (1995). The currents of life: the terminal electron-transfer complex of respiration. Proc. Natl. Acad. Sci. USA *92*, 11949–11951.

Richter, O.M., and Ludwig, B. (2003). Cytochrome *c* oxidase—structure, function, and physiology of a redox-driven molecular machine. Rev. Physiol. Biochem. Pharmacol. *147*, 47–74.

Sacconi, S., Salviati, L., Sue, C.M., Shanske, S., Davidson, M.M., Bonilla, E., Naini, A.B., De Vivo, D.C., and DiMauro, S. (2003). Mutation screening in patients with isolated cytochrome *c* oxidase deficiency. Pediatr. Res. *53*, 224–230.

Shoubridge, E.A. (2001). Cytochrome *c* oxidase deficiency. Am. J. Med. Genet. *106*, 46–52.

Smits, P.H., de Hann, M., Maat, C., and Grivell, L.A. (1994). The complete sequence of a 33 kb fragment on the right arm of chromosome II from *Saccharomyces cerevisiae* reveals 16 open reading frames, including ten new open reading frames, five previously identified genes and a homologue of the SCO1 gene. Yeast *10*, 75–80.

Tarnopolsky, M.A., Bourgeois, J.M., Fu, M.H., Kataeva, G., Shah, J., Simon, D.K., Mahoney, D., Johns, D., MacKay, N., and Robinson, B.H. (2004). Novel SCO2 mutation (G1521A) presenting as a spinal muscular atrophy type I phenotype. Am. J. Med. Genet. A *125*, 310–314.

Tjandra, N., Szabo, A., and Bax, A. (1996). Protein backbone dynamics and N-15 chemical shift anisotropy from quantitative measurement of relaxation interference effects. J. Am. Chem. Soc. *118*, 6886–6891.

Tsukihara, T., Aoyama, H., Yamashita, E., Tomizaki, T., Yamaguchi, H., Shinzawa-Itoh, K., Nakashima, R., Yaono, R., and Yoshikawa, S. (1995). Structures of metal sites of oxidized bovine heart cytochrome *c* oxidase at 2.8 Å. Science *269*, 1069–1074.

Tsukihara, T., Aoyama, H., Yamashita, E., Tomizaki, T., Yamaguchi, H., Shinzawa-Itoh, K., Nakashima, R., Yaono, R., and Yoshikawa, S. (1996). The whole structure of the 13-subunit oxidized cytochrome *c* oxidase at 2.8 Å. Science *272*, 1136–1144.

Vriend, G. (1990). WHAT IF: a molecular modeling and drug design program. J. Mol. Graph. *8*, 52–56.

Williams, J.C., Sue, C., Banting, G.S., Yang, H., Glerum, D.M., Hendrickson, W.A., and Schon, E.A. (2005). Crystal structure of human SCO1: implications for redox signaling by a mitochondrial cytochrome *c* oxidase "assembly" protein. J. Biol. Chem. *280*, 15202–15211.

Accession Numbers

Atomic coordinates, structural restraints, and resonance assignments for Cu(I)HSco2 have been deposited in the Protein Data Bank under ID code 2rli and the BioMagResBank under accession number 11001.

3.5

A Structure Characterization of Hyp1 protein from *Thermus Thermophillus*

Luciano Arbiata, Lucia Banci, Ivano Bertini, Simone Ciofi-Baffoni, Petros Gkazonis, Manuele Martinelli, Shenlin Wang

In preparation

Introduction

Hyp1 protein has been suggested to have a role of copper trafficking in prokaryotes, as predicted from genomic contexts analysis [1]. The latter is a soluble protein mostly occurring in the periplasm of Gram-negative bacteria, and consisting of about 150 amino acids. Recently, the first structure of Hyp1 protein from *Deinococcus radiodurans* (DR1885) showed that the fold of this class of proteins organizes in cupredoxin-like fold [2], which is similar to more studied protein CopC, involved in copper homeostasis. All Hyp1 sequences share a conserved $Hx_{14}Mx_{21}HxM$ consensus motif, which could bind copper(I) ion. By analyzing the neighborhood of Hyp1 gene, it is suggested that Hyp1 protein has a possible relationship with Sco protein, which is proposed to be involved in copper ion delivery to the Cu_A center of cytochrome c oxidase (CcO) complex[1]. Although a large number of data have already established that Sco proteins are involved the assembly of CcO, precise function of these proteins are still unknown and, indeed, might be different from organism to organism [3-5] . Based on the previous observations, three basic models are widely proposed: 1) Sco is a copper(I) chaperone, which transfer copper(I) ion to Cu_A site; 2) recent resolved structures of Sco proteins in different organisms show that Sco proteins adopt a thioredoxin-like fold, thus Sco could reduce the cysteines in the Cu_A center for copper binding; 3) on the basis of extreme sensitivity to hydrogen peroxide, the Sco proteins have also been proposed to function as copper-dependent redox switches in signaling. In this model, bound copper(I) ion is oxidized to copper(II) and released. Based on our investigation on hSco1, it was indicated that Sco protein could have a dual function role of combination of two of the three above points.

Since Sco proteins show great variance, it is likely that Hyp1 proteins have different functions in different organisms, i.e., Hyp1 proteins could be copper(I) donor upstream of Sco protein or Hyp1 transfer copper(I) directly to Cu_A site.

In order to understand the function of Hyp1 protein in different organisms, the solution structures of Hyp1 protein in *T. Thermophillus*, the gene product of TTHA1943, were solved by NMR in both apo and copper(I) binding forms. Copper binding affinity was also determined by competition experiments, showing a dissociation constant of K_D=2.2 ± 0.6×$10^{-13}M^{-1}$. Protein-protein interactions with Sco protein of *T. Thermophillus* (TTSco hereafter) and CoxII have been also performed. From the structure, dynamic and protein-protein interaction data, a possible copper transfer mechanism for copper assembly of Cu_A site was suggested for this bacterium. Instead of being copper donor to TTSco, TTHA1943 is more likely a protein transferring Cu(I) ion directly to Cu_A site of CcO. The functional role of TTSco is either a copper(II) translocation protein or thioredoxin or the combination of the two.

Result

Assignment and structural heterogeneity of TTHA1943 ---- TTHA1943 Protein was expressed according to the description in materials and methods section. NMR samples were 1.0 mM in protein concentration in 50 mM potassium phosphate buffer (pH 7.2) containing 10% D2O. Copper(I) metalation was followed by using NMR: ^{1}H-^{15}N HSQC spectra were acquired at increasing copper(I) ion concentrations and no more spectra change were observed when copper(I)/TTHA1943 ratio was beyond 1:1. The ^{1}H-^{15}N and ^{1}H-^{13}C HSQC spectra of apoTTHA1943 and Cu(I)TTHA1943 show well-dispersed resonances indicative of an essentially folded protein in both states. The backbone and side chain assignments were performed by using standard triple resonance experiments. All the resonances are detected through the whole peptide sequence except for the residues 80 and 107 in both apo and Cu(I) form. 23 and 24 residues show two sets of amide resonaces in apoTTHA1943 and Cu(I)TTHA1943, respectively. The two species are present in a molar ratio of 65:35 in both apo and Cu(I) form. Since MS spectra shows one species with the correct molecular weight, the heterogeneity should arise from

conformational variability of the protein backbone. The chemical shift difference between Cβ and Cγ of P14 and NOE's patterns of P14 and G13 indicate that structure heterogeneity is originated from *trans*/*cis* isomerization of peptide bond preceding P14 (Xaa-P14). The major species belong to the *cis* conformation.

Structures of apoTTHA1943 and Cu(I)TTHA1943 ---- The solution structures of apoTTHA1943 and Cu(I)TTHA1943 were determined by using distance and angle restraints as obtained from 2D and 3D heteronuclear NMR experiments. *Trans* and *cis* conformations were considered separately according to different short and long range NOE partterns. Therefore, four conformations were totally obtained from structure calculations (apoTTHA1943 with *trans* form Xaa-P14, apoTTHA1943 with *cis* form Xaa-P14, Cu(I)TTHA1943 with *trans* form Xaa-P14 and Cu(I)TTHA1943 with *cis* form Xaa-P14). **Fig 1.** shows the structure of Cu(I) TTHA1943 with *trans* form Xaa-P14 as an example of the four structures. About 1700 restraints are used in the calculation of each of the four conformations. Backbone RMSD values were in all cases around 0.70 ± 0.10 Å. The structure difference induced by *trans*/*cis* isomerization is only localized at loop 1 and loop 8. No regions with RMSD between the mean minimized structures of apo and Cu(I) forms larger than the sum of the RMSDs of each family are indeed found, indicating no substantial structural differences between apo and copper forms.

The overall structure of TTHA1943 contains the cupredoxin-like fold, constituted by two β sheets forming a Greek key β-barral motif that involves ten β strands, two of which is parallel and the others are anti-parallel. Different from a typical cupredoxin-like fold, strand β4 and strand β5 form an extended and solvent exposed β heparin. Cu(I) ion is bound to two Met and two His of the conserved $Hx_{14}Mx_{21}HxM$ motif, also confirming by combined chemical shift variation. The copper ion coordinated in a tetrahedral arrangement and the metal ligand atoms are sulfur atoms of Met 61 and Met 85, $N^{\delta 1}$ of His 46 and $N^{\varepsilon 2}$ of His 85.

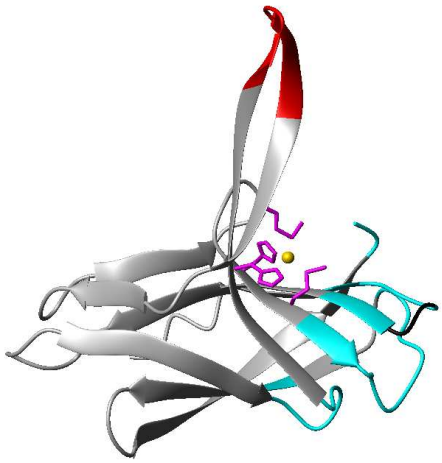

Fig 1. The minimized mean structure of Cu(I)TTHA1943 with trans form Xaa-P14 Copper(I) binding ligands are shown in pink color; copper(I) sphere is shown in yellow; Xaa-P14 is shown in black; Residues showing fast motion and double conformation are shown in red and cyan, respectively.

Measuring Cu(I) binding affinity ---- The copper binding affinity of Cu(I)TTHA1943 was investigated by titrating the ^{15}N Cu(I)TTHA1943 with DTT. The process was followed through ^{1}H-^{15}N HSQC spectra. No variation in the chemical shifts of the amide signals in Cu(I)TTHA1943 could be observed at any stage of the titration. Instead, the intensities of Cu(I) protein signals decreased with increasing DTT concentration. Thus the equilibrium constant between Cu(I)TTHA1943 and DTT was detected by the relative intensity of peaks of apo and Cu(I) species **(Fig 2)**. The molar fraction of apo and Cu(I)-TTHA1943, when plotted as a function of the DTT:TTHA1943 molar ratio, can be fitted with an equilibrium constant of $(3.45 \pm 0.18) \times 10^{-2}$ for the transfer of copper(I) ion from TTHA1943 to DTT. Thus the dissociation constant for Cu(I)TTHA1943 can be obtained as $K_D = (2.17 \pm 0.10) \times 10^{-13}$ M, considering K_D of DTT is 6.31×10^{-12} M.

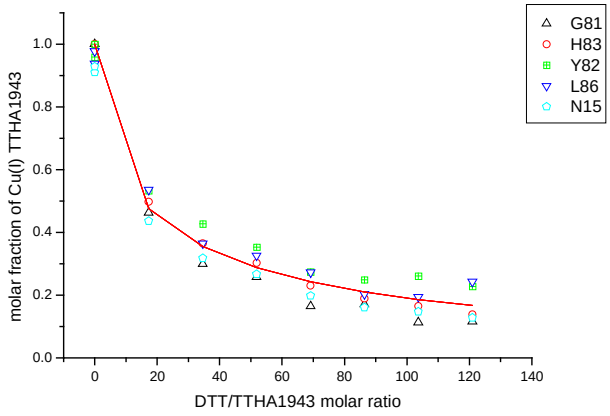

Fig 2. Fitting curve of measuring K_D value of Cu(I)TTHA1943

Protein dynamics ---- The ^{15}N relaxation parameters of apoTTHA and Cu(I)TTHA were measured as described in materials and methods section. The correlation times for molecule reorientation of apo- and Cu(I)TTHA1943 is 9.0 ± 0.2 and 9.2 ± 0.3 ns, respectively, as expected for a protein of this size in a monomeric state[2]. Although these values are consistent with a molecule of 120 amino acids, use of an isotropic rotational diffusion model is statistically rejected in TENSOR2 program. This is not surprising in view of the anisotropic nature of the inertia tensor. A fully analysis of the diffusion tensor was therefore undertanken. The rotational diffusion tensor of Cu(I)TTHA1943 has axes D_{xx} = (1.545±0.033) × 10^{-7} s^{-1}, D_{yy} = (1.765±0.035) × 10^{-7} s^{-1} and D_{zz}= (2.109±0.033) × 10^{-7} s^{-1}, suggesting a significantly rhombic tensor. The angles between inertia tensor and diffusion tensor were also calculated and three main axes are almost collinear with the values no more than 20^0. The anisotropic rotational diffusion tensors were then used to determine the internal mobility of the TTHA1943 molecules in solution, according to model-free approach.

Overall, the TTHA1943 molecules are rather rigid as shown by the average order parameter S^2 values are 0.84±0.10 and 0.83±0.12 for the residues without splitting on ^1H-^{15}N HSQC. ^1H-^{15}N NOE values of residues 53-58, located in the solvent exposed β strands and the according β-turn, are lower than 0.55 and, as a consequence, S^2 values of those residues are much lower than overall average values, showing the presence of fast motion in ps-ns time scale. Residue 22, located in the link between β2a and β2b, and residue 109, located in the turn of β9 and β10 are also tumbling faster than overall tumbling rate. Residues 7 and 112 show motion in us-ms time scale with exchange rate around $5s^{-1}$ and $1s^{-1}$, respectively.

The relaxation parameters for the residues showing double conformation are quite different. For the resonances belong to the *trans* form of Xaa-14, relaxation data of residues 11, 91 and 120 suggest fast motion. Residues 86 and 119 show slow motion. Residue 13 has both a very fast and very slow motion. The rest of residues showing double conformations are rigid. In the *cis* conformation, on the contrary, residues 11 and 13 are rigid, as shown by the ^{1}H-^{15}N NOEs and S^2 data. This data suggested that in addition to the structure variations, *trans*/*cis* isomerition of peptide bond preceding P14 (Xaa-P14) induce different local dynamic properties between *trans* and *cis* conformation. The *trans* conformation is overall rigid but with a flexible loop 1, while the *cis* conformation forms a rigid loop1**.**

Temperature dependent HSQC ---- Considering that the optimal growth of *T. Thermophillus* is 65^{o}C, the ^{1}H-^{15}N HSQC spectra were collected stepwise up to 70 ^{o}C. The spectra are still well dispersed in high temperature (70 ^{o}C), suggesting that the overall fold of TTHA1943 doesn't alter significantly in different temperature. The equilibrium between *trans* and *cis* Xaa-P14 is not significantly changing as well, indicating that structure heterogeneity of TTHA1943 is still present in physiological condition. No collapse of two forms at higher temperature was detected, indicating a very slow process on the exchange rate between the two states (k_{ex} > 500 ms). The majority of resonances shifted along the same direction with increasing of temperature, with exception of residues 52-58, 119, 120, which are detected fast motion in 25 ^{o}C. The line widths of latter residues also turn boarder at temperature higher than 60 ^{o}C. Thus, it is reasonable to believe that the solvent exposed and extended β–heparin, composed by strands β4 and strands β5, could be highly flexible in the physiological conditions. Moreover, one of the copper binding ligands, sulfur atom of Met 61, is also located on β4. Thus, it is also predictable that, at physiological

conditions, this residue is flexible and can easily adapt to structural changes induced by the presence of the Cu(I) ion.

Interaction with Sco and CuA ---- Previous studies has already suggested that proteins of Hyp1 family are potential copper transporter in prokaryotes. Moreover, genes of *Hyp1* are close to genes of *Sco*, the product of which are known to be involved in the copper assembly of Cu_A site of CcO. Thus Hyp1 proteins could have potential roles in copper trafficking to CcO. In order to investigate these points, the interaction of Sco and Cu_A with TTHA1943 is also studied by titrating the ^{15}N-Cu(I)TTHA1943 with unlabelled apoSco and unlabelled apoCuA, respectively. The process was followed through ^{1}H-^{15}N HSQC spectra and 1mM acrobatic acid was added into the mixture to keep the copper(I) in the reduced state. In the titration between ^{15}N-Cu(I)TTHA1943 and apoTTSco, no copper transfer occurs from Cu(I)TTHA1943 to apoTTSco, even when more than two equivalents of apoTTSco were added. This data suggested that TTHA1943 has much higher affinity than TTSco. Indeed, TTSco is unable to bind copper(I) ion in the presence of equal equivalent DTT, differently from human Sco1 (data not shown). Considering that K_D value of Cu(I)DTT is 6.31×10^{-12} M, K_D value of Cu(I)Sco could be estimated higher than 10^{-10} M.

Differently, when 0.5 equivalent apoCu_A is added to Cu(I)TTHA1943 solution, 100% copper(I) has already been transferred from TTHA1943 to Cu_A. In this process, no variation in the chemical shifts of the amide signals in TTHA1943 could be observed at any stage of the titration. Instead, the intensities of Cu(I)TTHA1943 signals decreased with increasing apoCu_A concentration and, concomitantly, apoTTHA1943 signals appeared with increasing intensities along the titration. This data indicated that one apoCu_A is capable of receiving two copper(I) ions from two Cu(I)TTHA1943 molecules, forming the binuclear center. A constant of 10^2 can be estimated as lower limit for the following equilibrium.

$$2\text{Cu(I)TTHA1943} + \text{apoCu}_\text{A} \rightleftharpoons \text{Cu(I)}_2\text{Cu}_\text{A} + 2\text{apoTTHA1943}$$

Discussion:

Potential function role of TTHA1943 — The overall fold of TTHA1943 is organized into cupredoxin fold. Similar fold is shared by other proteins with different functions, i.e., immunoglobulin receptors (PDB ID codes 1IAR and 1F42), cellular adhesion molecules (1ZXQ and 1VCA), blue oxidases (1BGL and 1AOZ), plastocyanin (1PLC), hemocyanin (1LLA), cytochrome f (1HCZ), and the superoxide dismutase copper chaperone (1QUP). Notably, the Cu_A domain of CcO in *T. Thermophillus* also adopts similar fold[6]. Different from other proteins sharing similar cupredoxin fold, a solvent exposed and extended β-heparin was detected at 25 ^{0}C. When temperature is increasing to the physiological condition of *T. thermopiles*, the resonances of residues located on this β-heparin (residues 52-58) turn melting, indicating a conversion into a highly flexible loop at high temperature. One of the binding ligands is close to this region, suggesting the possibility of a partner protein to access the metal site by means of conformational changes and coordination of an incoming side chain. More than twenty residues show double conformations, which are induced by *trans*/*cis* isomerization of Xaa-P14. Interestingly, a similar behavior was also detected in Cu_A site of *T. Thermophillus*. Moreover, interaction studies between Cu(I)TTHA1943 and apoCu_A showed that copper could be quantitatively transferred from TTHA1943 to Cu_A. On the basis of these finding, we can propose the copper chaperone role of TTHA1943, involved the supply of the copper cargo to the Cu_A site of CcO.

Potential function role of Sco protein of *T. Thermophillus* ---- The Sco proteins have been proposed to function as thiol:disulfide oxidoreductases, redox signaling proteins, copper trafficking proteins, or some combination thereof. Genomic analysis reveals a co-expression relationship of TTSco and TTHA1943, indicating that two proteins are

functional related. Based on our finding, TTSco has much lower affinity to copper(I) ion compared to TTHA1943 (K_D value of Cu(I)TTHA1943 is $(2.17\pm 0.10) \times 10^{-13}\ M^{-1}$ and that value of Cu(I)TTSco is estimated as ~ $10^{-10} M^{-1}$). Assuming a similar expression level and turn over rates of these two proteins, TTSco is unlikely to bind copper(I) ion in the presence of TTHA1943. Thus the functional role of copper(I) chaperone for Cu_A site can not be supported. To the same reason, redox signaling protein role of TTSco could be also ruled out.

Therefore, the TTSco function as a reductase seems reasonable, which reduces Cu_A Cys residues prior to copper insertion. The overall fold of Sco family is organized into thioredoxin fold, as shown by solution and crystal structures of resolved homologies. In particular, from crystal structure of BS Sco, a disulphide switch was detected, thus supporting the thioredoxin functional role of bacterie Sco proteins[7]. In addition to the three typical function roles, TTSco might also be a copper(II) chaperone. A number of studies have already shown that Sco proteins, in both eukaryotic and prokaryotic organisms, are able to specificly bind copper(II) ion in a 1:1 stoichiometry. And copper(II) ion is also available in the periplasm, being much oxidizing environment than cytoplasm of prokaryotic cell. In our study, it was found that TTSco binds copper(II) ions stronger than copper(I) and it is able to interact with CuA, exchanging copper(II) ions (data not shown).

According to our observations, two potential mechanisms of copper supply to Cu_A site of *T. Thermophillus* could be proposed. 1) TTSco is a solely thioredoxin function, which reduces the Cys residues of Cu_A site. Cu(I)TTHA1943 supply two copper(I) ions to Cu_A site after reduction. 2) TTSco has a dual function as thioredoxin and copper(II) chaperone. Reduced TTSco receives one copper(II) ion from other proteins; Cu(II)TTSco reduces the Cys residues of Cu_A site, at that stage, copper(II) ion is still bound by oxidized TTSco; Cu(I)TTHA1943 and Cu(II)TTSco transfer copper(I) and copper(II) simultaneously to Cu_A site, forming a mixed-valence [Cu(1.5)... Cu(1.5)] center; oxidized TTSco is reduced by

other proteins, such as other thioredoxin proteins or cytochrome c, to be ready for next metal transfer.

Materials and Method:

Sample preparation ---- STRING program (http://string.embl.de) was used to identify the *Thermus Thermophillus* Sco neighboring genes. TTHA1943 was expressed in *E. coli* BL21-Gold (DE3) cells (Stratagene), which were grown in LB and minimal medium [$(^{15}NH_4)_2SO_4$ and/or [^{13}C]-glucose] for the production of labeled samples. Purification was performed by using a HiTrap chelating HP column (Amersham Pharmacia Biosciences) charged with Ni(II). His-GST tag was cleaved with AcTEV, and separated from the C-terminal domain with a second purification step. After this purification, the protein preparations showed a single component by SDS-PAGE, as checked through ESI-MS spectrometry.

The Cu(I) metallated form was obtained by addition of stoichiometric amounts of the metal ion, $(Cu(I)(CH_3CN)_4)PF_6$) to diluted protein solutions in 50mMphosphate buffer at pH 7.2, followed by protein concentration under nitrogen atmosphere.

Solution structure determination

NMR spectral assignment and structure determination were obtained through the classical triple resonance experiments. Back bone assignments were done through HNCA, HN(CO)CA, CBCA(CO)NH, HNCACB and HNCO spectra. Side chain were assigned through 3D (h)CCH-TOCSY together with ^{13}C-NOESY-HSQC and ^{15}N-NOESY HSQC. The His ring protons were assigned through a ^{1}H-^{15}N HSQC experiment tailored to the detection of ^{2}J ^{1}H-^{15}N couplings and from the analysis of the ^{13}C-NOESY-HSQC spectra. Proton-proton distance constrains were derived from the analysis of ^{2}D-NOESY, ^{15}N-NOESY-HSQC and ^{13}C-NOESY-HSQC. The relative intensity of the split resonances was taken into account when converting NOE volumes into distances. The secondary structure

elements were predicted from the chemical shift index and angle constrains were derived accordingly. *Trans* and *cis* conformation of peptide bonds preceding Prolines are identified according to chemical shift difference between Cβ and Cγ as described in Schubert et al [8]. The structures were calculated using the program CYANA-2.0. The best 30 structures of the CYANA family were then subjected to restrained energy minimization (REM) with AMBER 8.0[9]. The force field parameters were adapted from similar systems[10]. The programs PROCHECK, PROCHECK-NMR[11] and WHATIF[12] were used in the evaluation of the quality of the structures. More than 90% of residues were located in the allowed regions of the Ramachandran plot for solved structures.

Relaxation parameters measurement and data analysis

^{15}N R_1, R_2, and steady-state heteronuclear $^{1}H–^{15}N$ NOEs were measured on at 400 MHz 298K using standard pulse sequences. Relaxation rates R_1 and R_2 were determined by fitting the cross-peak heights, obtained through the standard routine of Sparky program, measured as a function of the delay within the pulse sequence, to a single-exponential decay. The heteronuclear NOE values were obtained from the ratio of the peak height for ^{1}H-saturated and unsaturated spectra. The heteronuclear NOE values and their errors were estimated by calculating the mean ratio and the standard error from the available data sets.

Measuring dissociation constant of Cu(I)TTHA1943

Titrations of ^{15}N-labeled Cu(I)TTHA1943 (0.2 mM) and DTT were performed with NMR spectroscopy following the $^{1}H–^{15}N$ spectral changes in HSQC spectra upon addition of increasing amounts of DTT. The metalation state of Cu(I)TTHA1943 was monitored along the NMR titration through a few residues that are next to the copper(I) binding motif. In addition, the NHs of these resonances are not overlapped in the $^{1}H–^{15}N$ HSQC maps, thus they are easily integrated during the titration steps to estimate the relative population of apo and copper(I) loaded forms, which allows the estimation of the metal affinity. The dissociation constant K_D of Cu(I)TTHA1943 is obtained according to the following scheme:

$$Cu(I)TTHA1943 + DTT \rightleftharpoons apoTTHA1943 + Cu(I)DTT$$

The conditional dissociation constant for the Cu(I)DTT complex, necessary for the above K_D estimation, is 6.31×10^{-12} M[13] at pH 7.4 and T 298 K.

Reference lists

(1) Arnesano, F.; Banci, L.; Bertini, I.; Martinelli, M.; (2005) *J. Proteome Res.*, 4 , 63 –70.

(2) Banci, L.; Bertini, I.; Ciofi-Baffoni, S.; Katsari, E.; Katsaros, N.; Kubicek, K.; Mangani, S.; (2005) *Proc Natl Acad Sci* U S A. 102 3994-9

(3) Banci, L.; Bertini, I.; Cavallaro, G.; Rosato, A.; (2005) *J. Proteome Res.*, 6 , 1568-79

(4) Glerum, D. M.; Shtanko, A.; Tzagoloff, A.; (1996) *J. Biol. Chem.* 271 20531–20535

(5) Lode, A.; Kuschel, M.; Paret, C.; Rodel, G. (2000) *FEBS Lett* 485, 19-24

(6) Williams, PA.; Blackburn, NJ.; Sanders D.; Bellamy, H.; Stura1, EA.; Fee JA.; McRee DE.; (1999) *Nature* 6, 509-516

(7) Ye, Q., Imriskova-Sosova, I., Hill, B. C. & Jia, Z. (2005) *Biochemistry* 44, 2934–2942.

(8) Schuberta, M.; Labuddea, D.; Oschkinata, H.; Schmiedera P.; (2002) *J. Biomol. NMR* 24,149-154

(9) Case, D.A.; Darden, T.A.; Cheatham, T.E.; Simmerling, C.L.; Wang, J.; Duke, R.E.; Luo, R.; Merz, K.M.; Wang, B.; Pearlman, D.A.; et al. (2004). AMBER 8 (computer program). University of California, San Francisco.

(10) Banci, L., Bertini, I., Bruni, B., Carloni, P., Luchinat, C., Mangani, S., Orioli, P.L., Piccioli, M., Ripniewski, W., and Wilson, K.S. (1994).*Biochem. Biophys. Res. Commun*. 202, 1088–1095.

(11) Laskowski, R.A., Rullmann, J.A.C., MacArthur, M.W., Kaptein, R., Thornton, J.M. (1996). *J. Biomol. NMR* 8, 477–486.

(12) Vriend, G. (1990). *J. Mol. Graph*. 8, 52–56.

(13) Krezel, A.; Lesniak, W.; Jezowska-Bojczuk, M.; Mlynarz, P.; Brasun, J.; Kozlowski, H.; and Bal, W. (2001) *J. Inorg. Biochem.* 84, 77–88

4

CONCLUSIONS AND PERSPECTIVE

Structural biology provides a detailed analysis of the structure of biological macromolecules at atomic level. From solved structures, the relationship between structure and function could be investigated. Metalloproteins, which comprise a significant share of the proteome, contain biologically relevant metal ions which can have one or more accessible oxidation states. In recent years, the investigation of mechanisms how metals are transported and inserted into diverse protein locations is an emerging field in the scientific world. Therefore structural characterization of metalloproteins is an important aspect of post-genomic research. Our activity is integrated into this framework and intends to contribute to the coverage of metalloprotein structures and to pursue functional studies aiming to elucidate the role of metal cofactors, their redox properties, and implications in protein-protein interactions.

Moreover, several metalloproteins are involved in diseases, and often they contain copper. The alteration of copper homeostasis leads to errors of metabolism and damage to cells, resulting in pathological conditions. Among the factors required to achieve copper ion homeostasis are the metallochaperones, which specifically traffic copper to cuproenzymes. During the PhD course my attention was focused on the structure determination of three copper proteins, MNK6, HSco1 and HSco2.

MNK6 is the sixth copper(I) binding domain of Menkes protein, where the disease causing A629P mutation occurs. On the basis of our investigation on protein structures, dynamic properties, and interaction with its copper donor, HAH1, it was unraveled that protein structures don't alter significantly but the dynamic properties are affected by the mutation. Comparing H/D exchange rates between wild type and mutant MNK6, it can be concluded that for the mutant protein the equilibria between folded and unfolded conformations are shifted towards the unfolded state(s), i.e. the β-sheet is more often transiently exposed to the bulk solvent, being more susceptible to degradation. This proposal could agree also with some other pathogenic mutation detected from Wilson and Menkes disease, i.e. H1069Q and Y532H in Wilson disease. Next step, we will characterize the Y532H localized on the copper(I) binding domain 5 of Wilson protein.

Many experimental evidences support the hypothesis that HSco1 and HSco2 are involved in the copper insertion into Cu_A site of Cox2 subunit. However, the precise function of these two proteins is not clear yet. In order to understand the mechanism of

Sco-mediated copper insertion into CcO, we have determined the solution structures of apoHSco1, Cu(I)HSco1, Ni(II)HSco1 and Cu(I)HSco2. The structures indicate that the metal ion is bound by two Cys residues of CXXXCP motif and one highly conserved His residue. Upon metal binding, proteins pass from an open and flexible state to a close and rigid state, as confirmed also by ESI-MS studies. We obtained crystals of Ni(II)HSco1, and the relative X-ray structure suggest the binding of the metal ion to the oxidized form of HSco1. The species, described from the above mentioned structure, may be represent a transition state of the copper transfer from HSco1 to the Cu_A site of Cox2. It may represent a missing link, which integrates the metal transfer and thioredoxin functions already proposed for this fascinating protein.

Structure of HSco2 is similar to HSco1. But the dynamic properties are quite different between two proteins in both apo and copper(I) loaded form. In apo form, 84 out of 160 HN signals are missing in HSco2 protein, while only 20 in HSco1 protein. This indicates that HSco2 are more flexible than HSco1 in apo form. Although, upon copper binding, HSco2 protein turns more rigid and only 2 of the missing signals are still undetected, some degree of flexibility is still present among the whole peptide sequence. Since the function roles are quite relevant to the dynamic properties of protein, it is reasonable to believe that the partners of these two proteins are different.

The solution structure of P174L-HSco1 mutant showed that the mutation significantly affects the metal binding properties of HSco1 protein. Structurally, the mutation produces the lack of well-organized hydrophobic contacts and a structural heterogenity in the vicinity of the metal binding region. The local structural changes induced by the point mutation decrease the copper(I) affinity of the mutant, thus negatively affecting the metallochaperone function of HSco1. ESI-MS and NMR interaction studies between HSco1 and HCox17 demonstrate that Cu_1(I)-HCox17$2_{S\text{-}S}$, is capable of transferring efficiently Cu(I) to apoWT-HSco1, but not to apoP174L-HSco1.

Although we have got some hints for the function of HSco1 and HSco2 and the pathological mechanism by which P174L mutant induces severe CcO deficiency disease has been proposed, a number of questions are still open for this topic and will be investigated. For example, 1) HSco1 and HSco2 are membrane bound protein, and indeed, are homodimer in physiological conditions. However, the proteins we expressed here were only soluble domains. In result section 3.2, we reported another HSco1 construct, called long HSco1, where 14 more residues were expressed on N-terminal. From gel filtration

data, it is indicated this long HSco1 construct could form a dimmer or the monomer-dimmer equilbra is present in this system. Therefore, the next step will be the investigation of interface of homodimer. 2) From the crystal structure of Ni(II)HSco1, it is indicated that the two Cys residues of CXXXCP conserved motif are oxidized when copper(I) is transferred to Cu_A site. But nothing is known at the moment about how the two cysteines of CXXXC conserved motif of HSco1/2 are reduced prior to copper transfer from Cox17. Therefore interaction studies between HSco1/HSco2 and HCox17 in both reducing and oxidizing environment will be performed.